IMPROVED MODIS AEROSOL RETRIEVAL USING MODIFIED VIS/SWIR SURFACE ALBEDO RATIOS OVER URBAN SCENES

BY

MIN MIN OO

A dissertation submitted to the Graduate Faculty in Electrical Engineering in partial fulfillment of the requirements for the degree of Doctor of Philosophy, The City University of New York

2009

This manuscript has been read and accepted for the Graduate Faculty in Engineering in satisfaction of the dissertation requirement for the degree of Doctor of Philosophy

Professor Barry M. Gross

Chair of Examining Committee **Date**

Professor Mumtaz K. Kassir

Executive Officer **Date**

Supervisory Committee:

Professor Fred Moshary – Electrical Engineering Department in the City College

Professor Samir Ahmed – Electrical Engineering Department in the City College

Professor Alex Gilerson – Electrical Engineering Department in the City College

Dr. Jacek Chowdhary – NASA/GISS & Columbia University

THE CITY UNIVERSITY OF NEW YORK

To My Parents and Wife

Acknowledgements

First and foremost, I would like to thank my direct supervisor Prof. Barry Gross who taught me programming languages starting from the basic level and introduced me into the filed of remote sensing. Prof Barry Gross is the major motivational and inspirational figure who made me interested in this area of research. Moreover, his thoughtful insights into the problems and numerous supportive discussions had helped me accomplish my research. I have been under his supervision since 2003 when I was in Master degree program. I gratefully acknowledge his graceful patience and relentless support for my career development.

After joining the Ph.D. program I was fortunate enough to be a part of a scientifically inspiring group headed by Prof Fred Moshary, Prof Samir Ahmed and Prof Barry Gross. As a mentor, Prof Barry Gross always cares about me and my career and gave me the guidance and kind help for my future job. Without his enthusiastic support and inspiring mentorship, I would not have achieved my thesis today.

Moreover, I owe special thanks to Prof Fred Moshary along with Prof Barry Gross. Both of them provided me with the opportunity to pursue my graduate studies in CUNY with full finical support. Prof Fred Moshary also helped me to clarify and organize the concept presented here. I am also indebted to Dr Jacek Chowdhary for his invaluable teaching on radiative transfer theory and calculation. His explicit teaching and intelligent explanation inspired me to become a research scientist.

Furthermore, I would like to express my sincere gratitude to the other members of my Ph.D. committee: Professor Samir Ahmed and Prof Alex Gilerson who took time and effort in reading despite of their busy schedules and provided me with valuable comment on my research.

Most importantly, I wish to thank my beloved wife, Tin Nwe Oo who sincerely believes and shares my dreams with me. Tin always provided tireless dedication and devoted love to me while we had to stay apart because of our demanding work schedules during my Ph.D. program. Without a doubt, Tin is the most important woman in my life and I love most.

Last but not the least, I dedicated this thesis to my parents who believed in me and instilled my life with vision, love and joy. They supported me financially and spiritually throughout my whole life to pursue my dreams. They let me come to the United States to widen my horizon even though they were in dire need of my filial support during the twilight of their lives. Especially, I would like to salute my father, U Soe Nyunt, for his heroic sacrifice for me and our family. No word can express my appreciation for what he had given me.

Abstract

IMPROVED MODIS AEROSOL RETRIEVAL USING MODIFIED VIS/SWIR SURFACE ALBEDO RATIOS OVER URBAN SCENES

by

Min Min Oo

Adviser: Professor Barry M. Gross

Determination of Aerosol Optical Depth (AOD) by satellite remote sensing measurements over land is complicated by the fact that the Top of Atmosphere (TOA) reflectance is a combination of the desired atmospheric path reflectance as well as the ground reflectance. Unfortunately, inaccurate surface modeling results in inaccurate AOD retrieval as well as reducing spatial resolution. In this thesis, the primarily focus is on the use of simultaneous MODIS and AERONET sky radiometer data to refine the surface albedo models regionally and improve on the current AOD operational retrieval. In particular, it is shown that the correlation coefficient assumption used in the MODIS Collection (5) model between the VIS and SWIR channels used for surface reflection parameterization in urban areas such as New York and Mexico City is severely underestimated. This is demonstrated both directly using high spatial imagery data from Hyperion and

indirectly by constraining MODIS TOA reflection data with AERONET Sky radiometer AOD retrievals. Especially, the combining of the satellite and radiometer measurements allows to generate a regional VIS/SWIR surface reflectance correlation coefficient map at spatial resolutions up to 1.5km is shown. Application of the regional VIS/SWIR surface reflectance ratio model is shown to completely remove the bias and reduce uncertainty at the operational resolution of 10km as well as at higher resolutions to 1.5km resolution. Finally, spatial AOD retrievals using the surface albedo model are developed within the MODIS operational software showing the reduction in artificial AOD hotspots. Moreover, validation of MODIS derived AOD over vegetated area, located at Billerica-Massachusetts in this experiment, is discussed. We found that there is also slight error in MODIS surface reflectance assumption over the vegetated area. We suggest a new MVI-VIS/SWIR surface model for both urban and vegetated area and show improvement in AOD retrieval. In addition, the angular dependence of the surface albedo is explored. In particular, it is found that the correlation coefficients are insensitive to scattering angle as expected MODIS and errors in using a Lambertian assumption are shown to be less than the errors associated in the albedo variability.

Table of Contents

List of Tables

List of Figures

Chapter 1

Chapter 2

Chapter 3

Chapter 5

Chapter 6

CHAPTER 1

INTRODUCTION

1.1. What are aerosols and why are they so important to measure?

Aerosols are tiny particles suspended in the air. Some occur naturally, originating from volcanoes, dust storms, forest and grassland fires, living vegetation, and sea spray. Human activities, such as the burning of fossil fuels and the alteration of natural surface cover, also generate aerosols. Averaged over the globe, aerosols made by human activities currently account for about 10 percent of the total amount of aerosols in our atmosphere [1]. Aerosol particles may be solid or liquid; they range in size from 0.01 microns to several tens of microns. Under normal circumstances, the majority of aerosols form a thin haze in the lower atmosphere (troposphere), where they are washed out of the air by rain within about a week. Aerosols are also found in a part of the atmosphere just above the troposphere (called the "stratosphere") [2].

Aerosols are an important but uncertain agent of climate change. Aerosols alter atmospheric temperatures by absorbing and scattering radiation. Aerosols can both warm or cool the troposphere, depending on their type and location. Therefore, aerosols also modify clouds and affect precipitation. Sulfate aerosols can reduce cloud droplet size, making clouds brighter so that they reflect more

solar energy. Black carbon aerosols strongly absorb solar radiation, warming the mid-troposphere and reducing cloud formation. Poor knowledge of the global distribution of aerosols contributes to a large uncertainty in climate prediction.

The following are two important reasons why do we care about aerosol and why are they so important.

1.1.1 Direct and Indirect Effect of Aerosol on Global Climate

Aerosols play major role within Earth's climate system [3] (Intergovernmental Panel on Climate Change (IPCC), 2001), and affect the radiation budget, cloud processes, and surface air quality [4]. Aerosols tend to cause cooling of the Earth's surface unless they are black carbon aerosol. Because most aerosols reflect sunlight back into space, they have a "direct" cooling effect by reducing the amount of solar radiation that reaches the surface. The magnitude of this cooling effect depends on the size and composition of the aerosol particles, as well as the reflective properties of the underlying surface. It is thought that aerosol cooling may partially offset expected global warming that is attributed to increases in the amount of carbon dioxide from human activity.

Aerosols are also believed to have an "indirect" effect on climate by changing the properties of clouds (Figures 1a and 1b). Indeed, if there were no aerosols in the atmosphere, there would be no clouds. It is very difficult to form cloud droplets without small aerosol particles acting as "seeds" to start the formation of cloud

droplets. As aerosol concentration increases within a cloud, the water in the cloud gets spread over many more particles, each of which is correspondingly smaller. Smaller particles fall more slowly in the atmosphere and decrease the amount of rainfall. In this way, changing aerosols in the atmosphere can change the frequency of cloud occurrence, cloud thickness, and rainfall amounts.

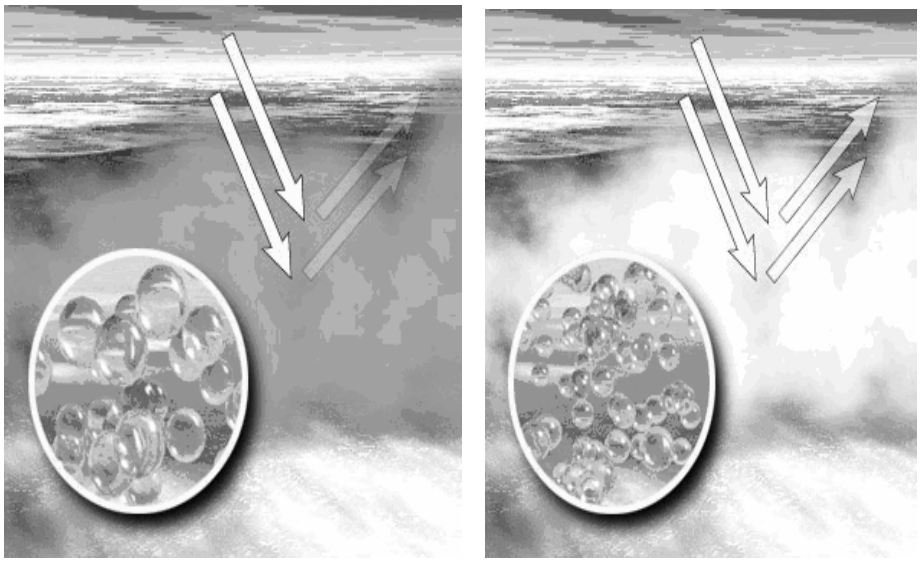

Figure 1 (a) Clouds with low aerosol concentration and a few large droplets do not scatter light well, and allow much of the Sun's light to pass through and reach the surface (b) the high aerosol concentrations in these clouds provide the nucleation points necessary for the formation of many small liquid water droplets. Up to 90% of visible radiation (light) is reflected back to space by such clouds without reaching Earth's surface. http://terra.nasa.gov

1.1.2 Effect of Aerosol on Human Health over Urban Area

Aerosols, also known as particulate matter (PM), are defined by three general categories commonly used by the U.S. Environmental Protection Agency (U.S. EPA): coarse (10 to 2.5 μm), fine (2.5 μm or smaller), and ultra fine (0.1 μm or smaller). Research suggests that particle size is an important factor that influences how particles deposit in the respiratory tract and affect human health [5-6]. Coarse particles are deposited almost exclusively in the nose and throat; whereas, fine and ultra fine particles generally are able to penetrate to deep areas of the lung. Fine and ultra fine particles are present in greater numbers and have greater surface area than larger particles of the same mass, and they are generally considered to be more toxic. Because these particles, PM2.5 (fine particles with 2.5 micrometer in diameter or smaller) are so small, they are able to penetrate to the deepest parts of the lungs. Scientific studies have suggested links between fine particulate matter and numerous health problems. In particular, it has been well documented that adverse health effects from breathing air with a high PM2.5 concentration include premature death, increased respiratory symptoms and disease, chronic bronchitis, and decreased lung function particularly for individuals with asthma [7].

The health effects of particulates matter are also heavily dependent on composition, and the concentrations and lifetime. In an effort to improve Air Quality Forecasting, the EPA has implemented an ambient air quality-monitoring

program to determine the composition of airborne PM2.5 in urban air. There is also growing interest in using satellite retrievals of AOD (Aerosol Optical Depth) as a means to improve Air Quality Forecasts of PM2.5 and PM10 measurements [5-8]. Systems such as IDEA (Infusing satellite Data into Environmental Applications) [9] routinely use MODIS (Moderate Resolution Imaging Spectroradiometer) AOD retrievals along with lagrangian models to provide 24 hour predictions of PM2.5. This system works by using static estimators which attempt to connect AOD remote sensing measurements directly to surface PM2.5 concentrations [5-8]. Further systems at research level are already endeavoring to assimilate AOD from satellites into air transport models [8].

1.2 Measurement Approaches for Aerosols

Tropospheric aerosols are produced by both natural and anthropogenic process. As their lifetimes are on the order of days, aerosols are inhomogeneous in time and in space, with much higher concentrations near sources. Also, they vary in size by orders of magnitude and their properties change as they age and interact within the atmosphere. Thus it is extremely difficult to characterize aerosols on a global scale. The following methods provide the quantitative analysis of tropospheric aerosol optical properties, especially aerosol optical thickness.

a) Insitu (point) sensors

Physical, chemical, and optical properties of aerosols are routinely measured in the laboratory and in situ from all types of instruments, both from the ground and from aircraft. Unfortunately, these measurements perturb the aerosol field during collection and they are only measured at discrete points in space.

b) Radiometer measurements from ground

Passive ground-based and airborne radiometers and Sun photometers provide measurements of the optical properties of ambient (nonperturbed) aerosol properties but also only at discrete locations. Few of these measurements offer insight into aerosol characteristics at remote locations [3].

c) Space based techniques.

However, with the advent of calibrated, sophisticated satellite-borne radiometers; the aerosol community has been offered an observational dataset to bridge spatial gaps. These satellite radiometers (passive remote sensing) offer a much wider spatial view than traditional in situ or radiometric observations. Therefore, coordination between surface based network observations and satellite measurements will be required to develop a long term monitoring system of the Earth's aerosol environment [11].

Some of the current satellites sensor , such as (National Oceanic and Atmospheric Administration) NOAA's polar orbiting satellite sensor AVHRR3 (Advanced Very High Resolution Radiometer), NOAA's GOES (Geostationary Operational Environmental Satellite), POLDER-2 (POLarization and Directionality of the Earth's Reflectances), MERIS (Medium Resolution Imaging Spectrometer) on the European ENVISAT (ENVIronment SATellite), (National Aeronautics and Space Administration) NASA's MODIS and MISR (Multi-angle Imaging SpectroRadiometer) onboard Terra/Aqua platform can derive aerosol optical properties, such as aerosol optical thickness and aerosol size distribution. Moreover the future sensor like Glory APS (Aerosol Polarimetry Sensor) can provide additional information on single scattering albedo, and refractive index.

While the above sensors have been used for aerosol retrieval, currently the most important (and work horse) sensor for aerosols continues to be the NASA MODIS sensor. This sensor is on board both *Terra* launched in late 1999 and *Aqua* which was launched in early 2002. Terra's orbit around the Earth is timed so that it

passes from north to south across the equator in the morning, while Aqua passes south to north over the equator in the afternoon. The MODIS instrument access is the most commonly used instrument because Terra (EOS AM) MODIS and Aqua (EOS PM) MODIS view the entire Earth's surface every 1 to 2 days, due to it's large swath, acquiring data in 36 spectral bands (from 0.4 to 14.4 μm) for atmosphere, land, and ocean imaging in a single instrument with 1,000-m, 500-m, and 250-m resolution. There are six Level-2 (Orbital Swath) MODIS Atmosphere products collected from Terra platform and is assigned an 8-character Earth Science Data Type (ESDT) name, which is used in cataloging and archiving the datasets. The Level-2 MODIS Atmosphere products are: 1. Aerosol Product 2. Water Vapor Product 3. Cloud Product 4. Atmosphere Profile Product 5. Cloud Mask Product and 6. Post-launch Joint Atmosphere Product [12].

The MODIS instrument obtains spectral reflectance observations from land band (7 wavelength bands: 0.47μm, 0.55μm, 0.66μm, 0.85μm, 1.24μm, 1.65μm and 2.12μm). While all these channels are used for aerosol retrieval over water, difficulties in obtaining estimates of the ground reflection make it impractical the use all of the channels in aerosol over land retrieval have been dedicated to aerosol retrieval over land.. In particular, the retrieval over land uses only (0.47μm, 0.66μm and 2.12μm) and uses assumptions for aerosol type based on geographical climatology [13] as well as assumptions on the surface albedo for the VIS channels. Based on optimal fitting of the appropriate TOA reflectance to appropriate radiative transfer Look Up Tables (LUT), the MODIS operational

algorithm retrieves both the Aerosol Optical Depth τ and the mixture between fine and coarse mode (i.e. fine mode weighting FW or η).

Naturally, the operational algorithms have gone through many improvements. For example, the previous version of the operational algorithm over land is known as Collection 004 (C004) algorithm [14]. However, when the MODIS C004 aerosol product was validated by comparison with AERONET derived aerosol product, over the U.S. East coast, of the retrievals tended to overestimate AOD (or τ) in clean conditions (i.e. low aerosol optical depth conditions), and underestimate in more hazy conditions[13] . Furthermore, an AOD measurement over urban areas was often overestimated [15]. When studied more carefully, weaknesses in the C004 approach included incomplete aerosol model capabilities, an assumption that the aerosol reflectance at 2.12um is negligible which invalidates cases where coarse mode aerosols are significant and surface models most associated with vegetation. To address these issues, modifications were built into the most recent operational algorithm Collection 005 (or C005) [16]. However, as is reasonable for operational global algorithms, modeling over urban regions was not a major focus and even with new algorithms which apply a more robust surface model based on a modified vegetation index, the MODIS derived AOD over urban regions is still significantly overestimated when compared to AERONET derived AOD.

1.3 Outline of the Thesis and Background for Aerosol Retrieval from MODIS

The main focus of this thesis is to refine the surface models appropriately so that more accurate aerosol retrieval is possible. In addition to accuracy, the use of accurate surface models also results in better spatial resolution since less pixels need to be discarded in a reflectance filter which tries to work only with vegetation pixels. The principle behind aerosol retrieval over land is based on the fact that the Top of Atmosphere (TOA) reflectance is the combination of the desired atmospheric path reflectance as well as the ground reflectance. Historically, algorithm for AOD retrieval over land required "dark" pixels as described in the Collection (4) algorithm [14]. Since many land covers such as vegetation and some soils has very low surface reflectance in the red (0.60-0.68 μm) and blue (0.4-0.48 μm) wavelengths, it is reasonable to use the darkest pixels in the image to explore the aerosol optical properties. For example, dense dark vegetation in an image can be considered as "dark" pixel and the aerosol contribution can be isolated. Isolating dark targets in the aerosol retrieval algorithm [17] was based on the detection of green forests as dark pixels combining Normalized Difference Vegetation Index (NDVI) and the magnitude of the near IR reflectance. In particular, dark vegetation was determined by a combination of high NDVI and low reflectance in the near IR.

However, even moderately dark vegetation scenes have a residual reflectance that cannot be realistically ignored unless the aerosol optical depth is high. Therefore, some estimate of the ground reflectance is essential. To this end, it was noticed

that the surface reflectance across the solar spectrum is correlated to some extent. Soils usually have an increasing reflectance as a function of the wavelength with correlation between the reflectances slowly decreasing with an increase of the wavelength span. Parallel physical processes affect the reflectance in the 0.47 and 0.66 μm channels and in the 2.1 and 3.8 μm channels. For example, the presence of vegetation decreases the reflectivity in the visible channels due to chlorophyll absorption and in the MIR (middle infrared) channels due to absorption by liquid water associated with the plant [18]. In particular, wet soil has a lower reflectance in the visible channels due to light trapping, and in the 2.1 and 3.8 μm channels due to the liquid water absorption.

To utilize this correlation, it is necessary to observe that in the 2.1 and 3.8 μm channels, the aerosol signature is negligible and the TOA reflectance in the MIR can be taken as the ground reflectance. Using correlations based on a-priori estimates of land cover type, the 0.47 and 0.66 μm ground reflectances can be estimated thereby allowing an improved estimate of atmospheric reflectance [19]. Finally, as pointed out in [20], the 3.8 μm channel is often contaminated by significant thermal emission and is therefore not used in the operational MODIS aerosol retrieval over land un less it is expected that large aerosol modes such as Saharan dust and/or smoke are present. However, these ground correlations would be useless if the 2.12μm reflectance which we normally assume to be ground reflection has a significant aerosol contribution. Unlike the C004 algorithm, as we will discuss, the C005 algorithm is capable of isolating out the aerosol contribution.

Finally, it is necessary to point out that even with accurate atmospheric path reflectance values, aerosol retrieval is hardly straightforward. In order to derive the optical thickness from the atmospheric reflection, the aerosol size distribution, single scattering albedo and refractive index have to be assumed Sensitivity studies showed that in a general case these assumptions generate substantial errors in the derived aerosol optical thickness (~30%). To reduce the errors, a good model of the aerosol properties based on measurements is required [19] [21]. In regions where the model is most applicable, we can expect the remote sensing procedure to be more accurate.

The above approach has been shown to be useful over dark and fairly uniform land cover types [22]. Unfortunately, these conditions are not realistically met over large urban areas such as the New York City megalopolis. In fact, as pointed out in [14] and [21], the retrieval of MODIS AOD over the northeast coast of U.S. resulted in remarkably high overestimation when compared to sunphotometer derived data. It is quite reasonable that such overestimations was a result of poor land surface assumption. However, quite erroneously, the AOD overestimation results were attributed to high spatial inhomogeneity and sub pixel water contamination but no quantitative calculations were offered for this explanation.

To address the need for more realistic aerosols, the C005 algorithm was developed. Surface models which allowed for non vegetative scenes were developed based on global matchups of AERONET sky radiometer data and MODIS TOA reflectances. At the same time, in performing these comparisons, it

was found helpful to obtain more realistic global aerosol models based on cluster analysis techniques. Unlike the static aerosol models obtained by global cluster analysis used for Cloud-Aerosol Lidar and Infrared Pathfinder Satellite Observation (CALIPSO) analysis, an effort was made to modify the microphysical models for different AOD levels. Once these models were obtained and their climatology examined, aerosol models (depicting the fine mode aerosols) were chosen in the retrieval suitable for a specific geographic location. From these analysis, empirical relationships were found to describe the surface VIS-SWIR correlation functions which were shown to be functions of surface type (as defined by a SWIR vegetation index which is not sensitive to atmospheric uncertainty) and to a lesser extent on scattering angle. However, this approach, while suitable for a global analysis, is less than optimal for regional studies of urban regions.

Recently, there has been interest in modifying the surface model for urban areas using simultaneous measurements from sunphotometers and MODIS TOA reflectances. For example, in Mexico City, such an effort was performed using a set of distributed hand-held photometers as a means to explore different regions of the metropolitan area. In particular, when the data from the MILAGRO (Megacity Initiative: Local and Global Research Observation) [15] project was analyzed for AOD retrieval at 10×10 km^2 spatial resolution , it was found that the VIS-SWIR surface ratio between 660 and 2120 nm value was found to be best described by a numerical value of (0.73) However, when examined at higher resolutions (i.e.1.5x1.5 km^2), a high variability of the surface reflectance ratio of VIS

(660)/SWIR (2120) was found which is significant enough to increase the uncertainties in the AOD values retrieved from satellite at the higher spatial resolution. These values are clearly not accessible to the Collection (5) models which result in a maximum peak of approximately 0.59 for the 660 nm channel.

In this thesis, the efforts for the New York City (NYC) area are quite similar in spirit to the approach used in the MILAGRO [15] project. However, there are several differences in the methodology. To begin, there is only a single CIMEL sky radiometer is used because at present, the distributed ground AOD measurement is not available. Therefore, to obtain surface measurements over a large distributed area, the measurements need to be filtered so that the AOD measurements (and aerosol type) were sufficiently homogeneous over the entire day. This homogeneity (discussed in detail in section 4) allows developing full contiguous surface correlation ratio maps for the entire metropolitan. The validity of this approach is demonstrated in section 4 by observing the agreement of correlation coefficient map (in extended area) with scene (for example high vegetation area VIS/SWIR correlation coefficient closely agree to the old static model (C004) and C005 assumption). In addition, unlike the MILAGRO study, the variability of the correlation coefficients as a function of angle over a long time period is explored. The results show that there is no or any significant trends in the variability in correlation as a function of angle and these trends are less than the fluctuations in the surface variability around the trend line for all resolutions. Therefore, it is sufficient to use a Lambertian surface model with values changing depending on surface type.

The thesis is focused on showing that the MODIS Collection (5) model used to estimate the ground reflectance is not appropriate for heavily urban areas such as NYC. In Chapter 2, a comparison of the AERONET derived AOD with MODIS retrieved AOD is given for both the traditional Collection (4) (which used a simple static surface correlation model) and Collection (5) algorithm (using the modified surface albedo models which dynamically input the geometrical angles as well as the surface type via a SWIR vegetation index. In particular, the AOD bias of MODIS is not removed even in Collection (5) retrieval. In Chapter 3, calculation of the surface albedo is performed for HYPERION Imagery data to compare with surface reflectance retrieval using MODIS TOA reflectance and operational LUT. The two results match up very well and details are discussed. In Chapter 4, the calculation of correlation coefficients for MODIS using simultaneous comparison of AERONET including the preprocessing steps and filters used are described. In particular, significant changes in the correlation coefficient from the standard algorithms are obtained. Furthermore, significant differences in the correlation coefficient values for different spatial averaging are observed but shown to be an artifact due to the different levels of water contamination from the nearby Hudson river resulting in an apparent modification of the surface model to length scales. However, removing the water pixels directly results in correlation values which are not very sensitive to scale as expected. In Chapter 5, the modified surface models are applied to MODIS data at different resolution scales. It is shown that even for 1.5km resolution, AOD retrieval is significantly improved. Furthermore, the

method is applied over Mexico City where it is shown that the surface correlation coefficients are comparable to those from NYC suggesting a more robust model for the surface reflection correlations. Further investigations at Billerica, Massachusetts (near Boston) are also included. In Chapter 6, assessment of aerosol retrieval with Lambertian surface model and BEDF surface model is discussed. Moreover, theory of BRDF surface model, kernel parameters, and MODIS derived BRDF surface parameters is explained. In Chapter 7, the improvement of the AOD retrieval using local surface correlation coefficient maps are obtained and compared statistically to AERONET Time series retrievals.

In putting this thesis in better context, in recent years, several publications have appeared which show that refined surface albedos can account for errors in aerosol optical depth. For example, the technique use in reference [23] uses a regression approach which plots the TOA nadir corrected reflectances in the VIS channels against the TOA nadir corrected reflectances for cases within a comparatively short observation time where the surface is assumed constant. The idea is to identify the lower bound on the envelope as belonging to clean conditions and the slope of the curve than determines the VIS-SWIR correlation coefficient. However, the resulting regressions obtained for high resolution does not yield a sufficiently clean linear plot in which to identify the clean molecular signal. In addition, on theoretical ground, even small deviations in the observation geometry can prevent the lowest bound from being due only to molecular scattering.

On the other hand, more rigorous but highly complex approaches in determining the details of the surface (including BRDF) under more general conditions have been developed. For example, an algorithm called MAIAC (multi angle implementation of atmospheric correction) has been developed and is being considered for operational processing, [24]. This approach in analogy to our method attempts to solve for the regression parameters but attempts to simultaneously pull out the AOD together with the surface properties. However, unlike the approach used in this thesis which utilizes existing ground assets, and relies on simple estimates of the surface correlation which are assumed stable over time, this MAIAC method is extremely complex. Furthermore, to provide stability based on the small number of angular observations used, the resolution of the surface products is 25km. Clearly, it will be useful in future to compare the reflection output of MAIAC to the regional surface maps retrieved in this thesis.

References

[1] NASA Earth Observatory http://earthobservatory.nasa.gov/

[2] NASA: TERRA(EOS AM-1) http://terra.nasa.gov/

[3] Intergovernmental Panel on Climate Change (IPCC), 2001 web site info at http://www.ipcc.ch/

[4] R. J. Charlson, S. E. Schwartz, J. M. Hales, R. D. Cess, J. A. Coakley Jr., J. E. Hansen, and D. J. Hofmann, "Climate forcing by anthropogenic aerosols", *Science* Vol. 255. no. 5043, pp. 423 – 430 (1992)

[5] Al-Saadi, J., J. Szykman, R. B. Pierce, C. Kittaka, D. Neil, D. A. Chu, L. Remer, L. Gumley, E. Prins, L.Weinstock, C. MacDonald, R. Wayland, F. Dimmick and J. Fishman. "Improving National Air Quality Forecasts with Satellite Aerosol Observations", Bull. Am. Met. Soc. 86, 1249-1261, (2005)

[6] Y. Liu, M. Franklin, R. Kahn, P. Koutrakis, "Using aerosol optical thickness to predict ground-level PM2.5 concentrations in the St. Louis area: A comparison between MISR and MODIS", Remote Sensing of Environment 107, 33-44 (.2007)

[7] Department of Environmental Conservation,"PM2.5 Monitoring" http://www.dec.ny.gov

[8] C. Kittaka, J. Szykman; B. Pierce; Al-Sadi, J.; D. Neil; A. Chu; L. Remer; E. Prins, and J. Holdzkom, "Utilizing MODIS satellite observations to monitor and analyze fine particulate matter, PM2.5, transport event**"**. Conference on Atmospheric Chemistry, 6th: Air Quality in Megacities, Seattle, WA, 11-15 January 2004 (preprints). Boston, MA, American Meteorological Society, Paper 1.3 , (2004)

[9] Doreen Neil, James J. Szykman, Jack Fishman, R. Bradley Pierce, Jassim A. Al-Saadi, Chieko Kittaka, "A good IDEA" (Infusing satellite Data into Environmental Applications), American Meteorological Society, 13the Conference on Satellite Meteorology, Society, Norfolk, VA Sept. 21, 2004.

[10] Levy, Robert C., Remer, Lorraine A., and Dubovik, Oleg " Global aerosol optical properties and application to Moderate Resolution Imaging Spectroradiometer aerosol retrieval over land", . *J. Geophys. Res*., 112, D13,210, 2007

[11] Holben, B.N., D. Tanre, A. Smirnov, et al., An emerging ground-based aerosol climatology: Aerosol optical depth from AERONET. *J. Geophys. Res*., 106, 12,067- 12,097, 2001

[12] Level-2 MODIS atmosphere product,: http://modis-atmos.gsfc.nasa.gov

[13] Remer, L., A., R., Tanré, D., Kaufman, Y.,J., Levy, R., and Mattoo, S., "ALGORITHM FOR REMOTE SENSING OF TROPOSPHERIC AEROSOL FROM MODIS: Collection 005" ATBD document

[14] Kaufman, Y.J.; Tanre, D. "Algorithm for Remote Sensing of Tropospheric Aerosol from MODIS" Mod04 ATBD Document (1998)

[15] Castanho, A., A.D. de, Prinn, R., Martins, V., Herold, M., Ichoku, C. and Mollna, L. T., "Urban Visible/SWIR surface reflectance ratios from satellite and sun photometer measurements in Mexico City", Atmos. Chem. Phys, Discuss., 8113-8139, (2007)

[16] Levy, R. C., L. A. Remer, et al. (2005), Evaluation of the MODIS aerosol retrievals over ocean and land during CLAMS, *J. Atmos. Sci.,* 62(4), 974-992.

[17] Kaufman, Y. J. and C. Sendra,: 'Algorithm for atmospheric corrections', Int. J.Rem. Sens., 9 , 1357-1381 (1988)

[18] Kaufman, Y. J. and L. Remer: 'Remote Sensing of Vegetation in the mid-IR: the 3.75 µm channels', IEEE J. Geosc. and Rem. Sens. 32, 672-683 (1994)

[19] Martins, J., V., Tanre, D., Remer, L., Kaufman, Y.,J., Mattoo, S., Levy, R. , "MODIS cloud screening for remote sensing of aerosols over oceans using spatial variability "; Geophysical Research Letters .29, no.12 : MOD4-1-4, (2002)

[20] Kaufman, Y., J., Wald, A., E., Remer, L., A., Gao, B-C., Li, R-R., Flynn, L., "The MODIS 2.1- mu m channel-correlation with visible reflectance for use in remote sensing of aerosol"; IEEE Transactions on Geoscience and Remote Sensing 35 1286-98, (1997)

[21] Remer, L., A., Wald, A., E., Kaufman, Y., J., "Angular and seasonal variation of spectral surface reflectance ratios: implications for the remote sensing of aerosol over land" ; IEEE Transactions on Geoscience and Remote Sensing 39, 275-83, (2001)

[22] Wen, G., Tsay, S-C.; Calahan, R.F., Oreopoulos, L., "Path Radiance Technique for retrieving aerosol optical thickness over land", JGR 104 31321-31332 (1999).

[23] E. Drury, D. J. Jacob, J. Wang, R. J. D. Spurr, and K. Chance (2008), "Improved algorithm for MODIS satellite retrievals of aerosol optical depths over western North America", *J. Geophys. Res.*, 113, D16204, 2007JD009573

[24] A. Lyapustin and Y. Wang, “MAIAC: multi-angle implementation of atmospheric correction for MODIS” NASA, GFSC, ATBD (Feb, 2007)

CHAPTER 2

Comparison of MODIS derived AOD with AERONET retrieved AOD

In this section, Satellite retrieved AOD data is evaluated with situ measured data from the AERONET sky radiometer AOD data, which we take as "ground truth". In particular, comparison of MODIS (C004 and C005) retrieved AOD with AERONET (CIMEL) derived AOD dataset are discussed. In particular, by studying the MODIS retrieved AOD L2 (level 2) data in an 80km box (which include both vegetated and urban area) surrounding the New York City, it is possible to identify which regions of the domain result in accurate retrievals and which regions are biased. In particular, it is shown that the best correlations to the AOD occur in regions of highest vegetation illustrating that the over bias is a surface reflection effect.

2.1 DATASET Intercomparison

2.1.1 MODIS Datasets

The MODIS Aerosol Product provides aerosol optical depth data which are processed for every overpass. Every granule results in Level 2 AOD data which

are produced at 10km resolution [1]. In our comparisons, MODIS L2 data are downloaded from http://modis.gsfc.nasa.gov/data using filtering based on particular temporal selection (date) and spatial selection (latitude/ longitude). The MOD04_L2 product files are stored in Hierarchical Data Format (HDF) which is a convenient multi-object file format for sharing scientific data in multi-platform distributed environments. In each HDF file, under the Geo-location Fields folder, latitude and longitude information for each pixel are provided while in the Data Fields folder, all necessary data such as Solar Zenith, Sensor Zenith, Solar Azimuth, Sensor Azimuth, Scattering Angle and Corrected Optical Depth Land (AOD for 0.47, 0.55 and 0.66μm) are stored. In fact, the L2 dataset is ready to analysis since all cloud masks have been implemented and gas absorption and solar zenith corrections are applied. However, when discussing improved spatial resolution, we will need to re-implement these corrections at finer scale. For this reason in Chapter 4, the uncorrected MODIS L1 B dataset is and a modified cloud masking procedure, together with the operational gas absorption and solar zenith correction is applied .

2.1.2 AERONET Datasets

The sky radiometers making up AERONET are the most robust and most accurate instruments for obtaining local column aerosol properties. Retrievals based on AERONET result in spectral AOD measurements, microphysical aerosol inversion products, and precipitable water in diverse aerosol regimes. In particular, most relevant for us, these instruments measure AODs at 0.34, 0.38, 0.44, 0.50, 0.67, 0.87 and 1.02 μm with an uncertainty of ±0.01 [2] allowing us to

obtain interpolated AOD at 0.550μm. Aerosol optical depth data are computed for three data quality levels: Level 1.0 (unscreened), Level 1.5 (cloud-screened), and Level 2.0 (cloud-screened and quality-assured). For our purposes, both the spectral AOD and Level 1.5 Direct Sun and Inversion measurement datasets are downloaded from http://aeronet.gsfc.nasa.gov [3]. While the purpose of the AOD retrievals is obvious, the calculation of the angstrom coefficient also allows us to filter out cases where coarse mode aerosols are significant. In addition, time series data are used to assess homogeneity of aerosol conditions which are requires if consistent matchups with satellite products is attempted.

2.2 MODIS Collection (4) land AOD retrieval algorithm

As briefly mentioned earlier, The Collection (4) algorithm uses the low optical depth of aerosols in the SWIR (2.12 nm) and assumes the reflectance to be the ground surface reflection only. The dark (vegetative) pixels are identified using a correlation between the land reflectance in the SWIR and in the blue and red channels. For pixels that are identified to have low reflectance in the mid-IR, correlations between the SWIR and VIS channels are implemented to estimate the reflectance in to the VIS channels and thereby allow us to derive the optical thickness in these two channels. The transparency assumption in the SWIR is reasonable except for dust, which has a small angstrom coefficient. The importance of isolating dark pixels is reasonable since for dark surfaces, the scattering effect dominates while for brighter surfaces the effect is mixed.

Based on these principles, the basic approach for an operational and unsupervised aerosol remote sensing algorithm for the MODIS sensor is described within the ATBD document [4] as :

1. Determination of the presence of the dark pixels in the blue (0.47 μm) and red (0.66 μm) channels using their remotely sensed reflectance in the SWIR channels (2.12 μm). Note that Collection (4) assumption for surface reflectance ratios are $\rho_{0.47} / \rho_{2.12} = 0.25, \rho_{0.66} / \rho_{2.12} = 0.5$ for all surface types
2. Estimation of the surface reflectance of the dark pixels in the red and blue channels using the measurements in the mid-IR and information on surface type.
3. Determination of the aerosol type using information on the global aerosol distribution and the ratio between the aerosol path radiance in the red and blue channels.
4. Inversion of the measured radiance at TOA into the aerosol optical thickness, volume (or mass) concentration and spectral radiative forcing using radiative transfer look-up tables.

   In order to derive the optical thickness from the path radiance, the aerosol size distribution, single scattering albedo and refractive index have to be assumed. Spherical and homogeneous aerosol particles are also assumed in order to use the Mie theory in the calculations, unless non-sphericity is identified and modeled. Sensitivity studies [4] showed that in a general case these assumptions can generate substantial errors in the derived aerosol optical thickness (~30%). To

reduce the errors, a good model of the aerosol properties based on measurements is required.

The sensitivity studies indicate that the expected error for AOD over land is $\Delta\tau = \pm 0.05 \pm 0.15\tau$, for the 550nm MODIS channel. However, while in general the MODIS retrievals meet expected accuracy, under certain conditions they do not. For example, assuming constant surface correlations assumptions leads to overestimating AOD in clean conditions along the U.S. East Coast and errors (both positive and negative) in other regions [5-6]. The available choice of aerosol optical models over land can also lead to either positive or negative bias for large AOD in many regions (such as negative bias over the U.S. East Coast [7-8]). To improve AOD retrieval in Collection (4) algorithm, by addressing some of the avoidable assumptions, the new Collection (5) algorithm was developed and implemented operationally as discussed in the next section.

2.3 Improvement of MODIS land AOD retrieval algorithm from C004 to C005

The algorithm to retrieve the aerosol optical depth over land has been completely restructured to produce the Collection 005 products. A detailed documentation of the new algorithm and the changes from previous version is provided by Levy [7-8]. The new algorithm, C005, is based on a true inversion that uses three pieces of information: apparent reflectance at 470 nm, 660 nm and 2120 nm to derive three products: aerosol optical depth (AOD), fraction of AOD attributed to non-dust aerosol and the surface reflectance at 2120 nm. This structure deviates from C004 in the following ways:

1. No longer are the AODs in individual wavelengths derived independently. Now all wavelengths are linked through the choice of aerosol model. The look up table is indexed by AOD at 550 nm, even though the reflectance at 550 nm is not used as input to the retrieval.

2. Fitting error of inversion is output as a diagnostic SDS.

3. The Look Up Table is calculated with the MieV-RT3 radiative transfer code that accounts for the effects of polarization.

4. No longer does the algorithm assume that the reflectance at 2120 nm measured by satellite is the same as surface reflectance in that channel. There are still relationships between surface reflectance in the visible to surface reflectance at 2120 nm.

5. No longer does the algorithm use a cascade to choose the darkest pixels in a 20 by 20 pixel box. Now all pixels with 2120 nm reflectance 0.01 to 0.25 are included.

Other changes to the land algorithm include updated aerosol models with new geographic distribution, the inclusion of negative AODs, more sophisticated relationships between surface reflectance in the various wavelengths and improved snow and cloud masking. These improvements are described in [9] in greater detail. The net effect of these major changes to the over land algorithm is to reduce the biases previously noted in various validation studies [9] and also to introduce more realistic aerosol particle size information, both in terms of fine model fraction and fine model AOD (a new parameter introduced for Collection 005).

Five aerosol models are used in Collection 005 and described in Levy [7]. These are continental, dust, non-absorption, moderate absorption and heavy absorption. In C004, aerosol models were based on the work of D'Almeida and Remer in the 1990's [4, 10] whiles the C005 aerosol model are based on Dubovik's aerosol model [9]. The inversion chooses between dust and one of the fine mode dominated models, which are designated by geography and season. All fine mode dominated models are multimodal and contain both fine and coarse modes.

In previous versions of the algorithm, a fixed relationship between the visible surface reflectances (470 nm and 660 nm) and the 2120 nm reflectance measured at top of atmosphere is used. These were $\rho_{0.47} / \rho_{2.12} = 0.25$, $\rho_{0.66} / \rho_{2.12} = 0.5$. In Collection 005 these relationships are

$\rho_{660} = f_1(MVI, \Theta)\rho_{2120}$, $\rho_{470} = f_2(MVI, \Theta)\rho_{660}$ where the modified vegetation index $MVI = (\rho_{1240} - \rho_{2120})/(\rho_{1240} + \rho_{2120})$ which is sensitive to vegetation and is the scattering angle. The use of the MVI index instead of the conventional NDVI is due to the relative insensitivity of the MVI to aerosols. These new dependencies permit different relationships depending on the degree of vegetation of the surface. They also account for some of the scatter introduced by BRDF effects.

2.4 Preliminary validation result of MODIS derived AOD with AERONET retrieved AOD

In order to validate MODIS AOD retrieval using inter-comparisons of MODIS and AERONET data, it is very important that only spatially and temporally homogeneous datasets are used. Since the MODIS retrieval is often cloud contaminated, and the surface reflectance (albedo) itself is spatially variable, the spatial homogeneity of the CIMEL dataset was determined by using the condition that a 5 hour interval surrounding the MODIS inter-comparisons is stable within 10%. The retrievals of AERONET were then compared against two optical depth retrievals from MODIS using Collection (4).. The first value is the aerosol optical depth obtained closest to the sky radiometer position which would be sensitive to MODIS algorithm bias due to urban scenes while the second value is the minimum AOD measured by MODIS (in 2001) within an 80km box around the sky radiometer. It is reasonable to expect that the minimum AOD should be far

less sensitive to algorithm bias. The results of this inter-comparison are illustrated in Fig 2.1.

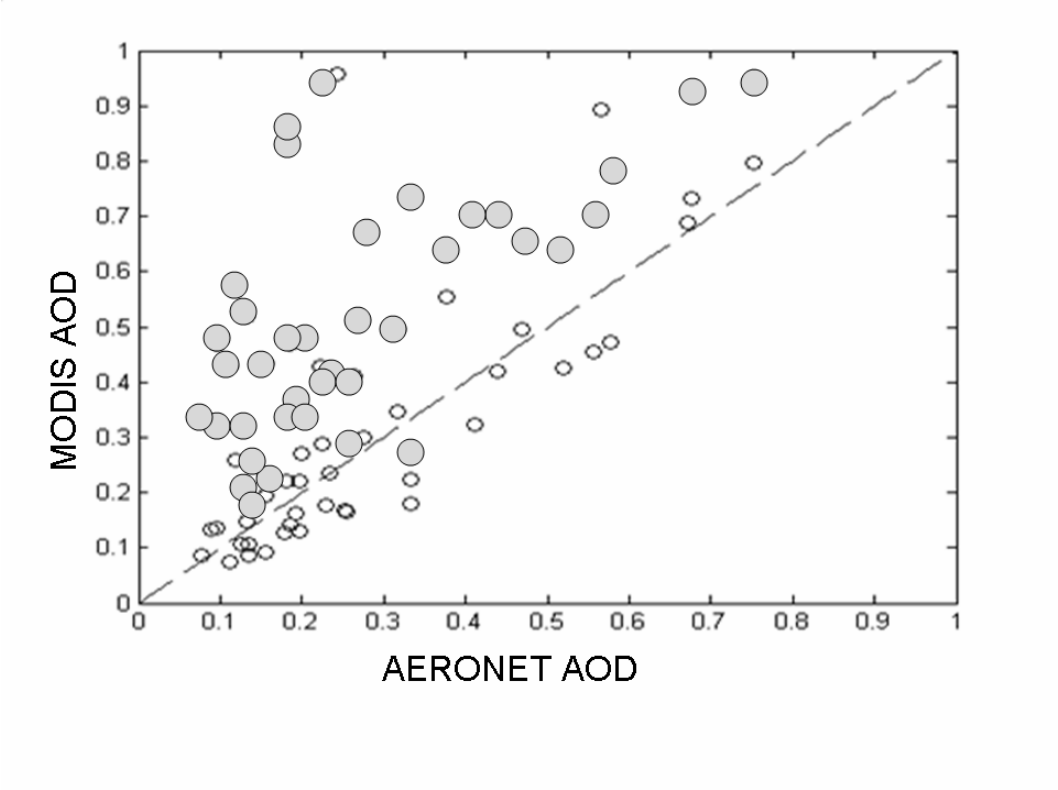

Figure 2.1 Minimum distance MODIS AOD (opaque) and minimum MODIS AOD (transparent) versus AERONET AOD

In particular, the MODIS retrievals for the nearest pixel measurements are strongly overestimated. On the other hand, the MODIS minimum AOD measurements are much more accurately correlated to the AERONET measurements. The reason for this is clearly deduced by determining the spatial locations within the 80km box where the minimum AOD is measured.

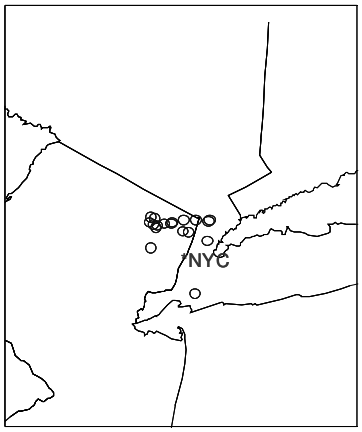

Figure 2.2 Location of AOD Minimum relative to NYC

The locations marked in Fig 2.2 shows the minimum AOD is most likely to occur in highly vegetated scenes which are mostly north of New York City and some area of New Jersey. Therefore the direct influence of the surface reflectance assumption is clearly correlated to the bias in the retrieval of AOD. Therefore, the need of a land surface reflectance model which is not static and connected to the surface type is crucial

.

2.5 Comparison of result from MODIS C004 and C005

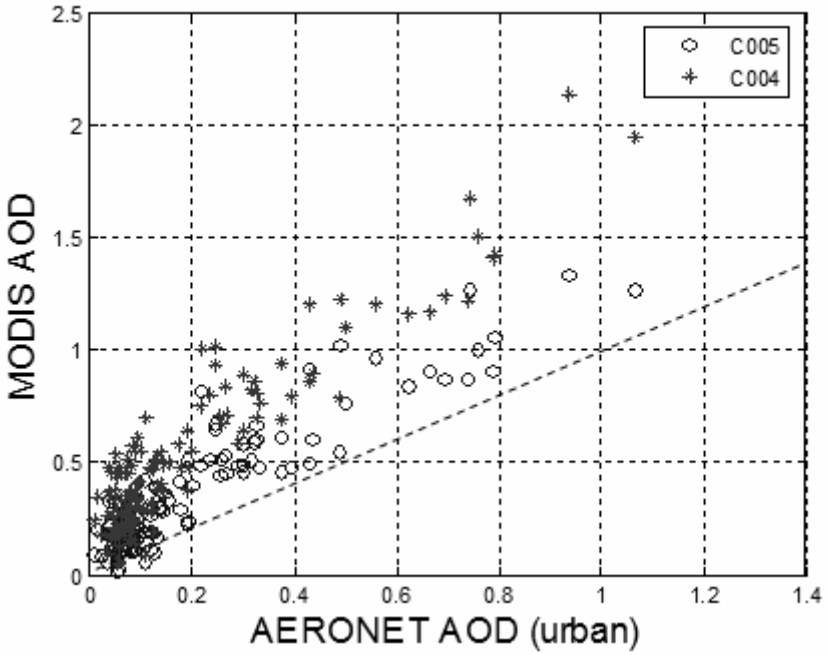

Figure 2.3 Comparison of MODIS retrieved AOD (C004 and C005) at 550nm with AERONET derived AOD (CIMEL sun-photometer data acquired in New York City (the City College of New York) from 2001 to 2007

The simplest assessment of the different algorithms is done by simple matchup based on the data filters described in section 2.1 and 2.4. In Fig 2.3, we compare the MODIS retrieved AOD in two algorithms, C004 and C005, against AERONET AOD derived from CCNY station. Clearly, even with C005 algorithm, significant positive bias can still be found. This is because C005 improvements obtained from global modeling is not accurate for regional urban area like New York City.

2.6 Comparison of MODIS Collection (5) derived AOD with AERONET retrieved AOD

MODIS Collection (5) Aerosol retrieval algorithm attempts to use a dynamic surface model based on surface classification using a modified vegetation index to improve the retrieval. The procedure and detail steps are described in Chapter 3. Since the application of dynamic surface reflection ratio is an improvement over the Collection (4) constant surface reflection ratio assumption, the comparison between retrieved aerosols data from MODIS and AERONET are generally improved [4]. However, as already shown in Fig 2.3, although the Collection (5) algorithm seems to partially improve the retrieval, there are still significant overestimating biases. To get some more insight into why the Collection (5) algorithm provides only partial improvement, the urban area reflection ratio obtained in the C005 algorithm for both vegetative and urban scenes is plotted in Fig 2.4. The urban surface reflection ratio of (660nm / 2120nm) derived by MODIS Collection (5) algorithm is approximately 0.55 (downloaded L2 dataset 2001 to 2007). That number is sometime higher than MODIS Collection (4) algorithm value, which is 0.5. However, as we will see in Chapter 3, it is significantly lower than the number retrieved using high resolution Hyperion Imagery [11]. In fact, the reason the C005 (un-tuned) algorithm is not that useful for urban retrieval is the fact that the correlations are only about 10% -20% higher than the static relationship used in the Collection (4) algorithm. In Chapter 3, the

true correlation values are dramatically larger than these VIS/SWIR ratios particularly in heavily urban scenes will be discussed.

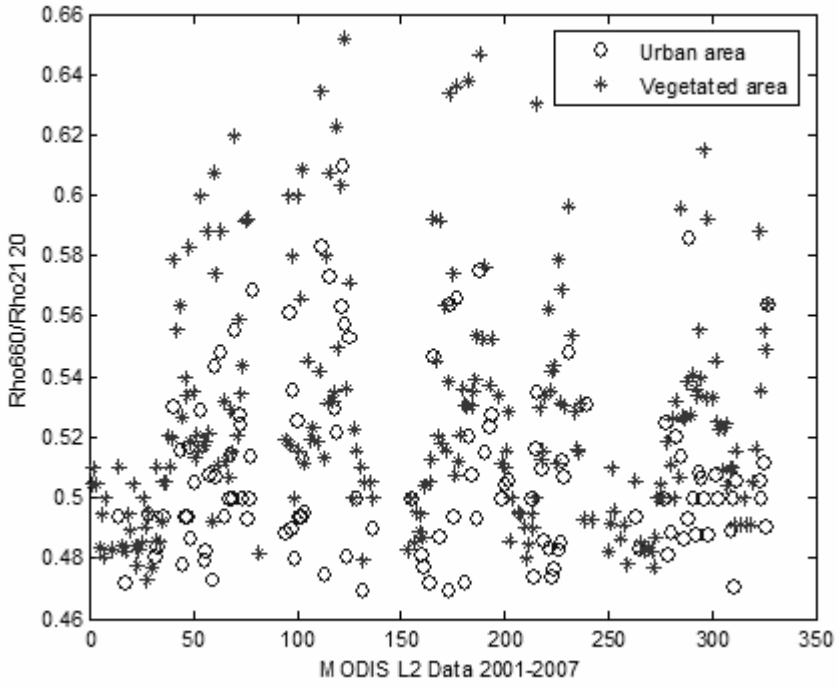

Figure 2.4. MODIS L2 Collection (5) VIS/SWIR surface albedo ratio

References

[1] Level-2 MODIS atmosphere product,: http://modis-atmos.gsfc.nasa.gov

[2] Holben, B.N., D. Tanre, A. Smirnov, et al., An emerging ground-based aerosol climatology: Aerosol optical depth from AERONET. *J. Geophys. Res*., 106, 12,067- 12,097, 2001

[3] AERONET, Aerosol Robotic Network: http://aeronet.gsfc.nasa.gov/

[4] Kaufman, Y.,J., Tanre, D., "Algorithm for Remote Sensing of Tropospheric Aerosol from MODIS" Mod04 ATBD Document (1998)

[5] Levy, R. C., L. A. Remer, et al. (2004). "Effects of neglecting polarization on the MODIS aerosol retrieval over land." Ieee Transactions on Geoscience and Remote Sensing **42**(11): 2576-2583.

[6] Levy, R. C., L. A. Remer, et al. (2005). "Evaluation of the MODIS aerosol retrievals over ocean and land during CLAMS." Journal of the Atmospheric Sciences **62**(4): 974-992.

[7] Levy, R.C., L.A. Remer and O. Dubovik et al. (2006), Aerosol optical properties and lookup tables for the new MODIS aerosol retrieval over land,

[8] Levy, R.C., L.A. Remer, S. Mattoo, E. Vermote, Y.J. Kaufman, (2006), A new algorithm for retrieving aerosol properties over land from MODIS spectral reflectance, JGR.

[9] Remer, L., A., R., Tanré, D., Kaufman, Y.,J., Levy, R., and Mattoo, S., "ALGORITHM FOR REMOTE SENSING OF TROPOSPHERIC AEROSOL FROM MODIS: Collection 005" ATBD document

[9] Levy, Robert C., Remer, Lorraine A., and Dubovik, Oleg " Global aerosol optical properties and application to Moderate Resolution Imaging Spectroradiometer aerosol retrieval over land", . *J. Geophys. Res*., 112, D13,210, 2007

[10] D'Almeida, G., P. Koepke, and E. P. Shettle, 1991: Atmospheric aerosols-global climatology and radiative characteristics. A Deepak ISBN 0-937194-22-0

[11] Gross, B., Ogunwuyi, O., Moshary, F., Ahmed, S.; Cairns, B. "Aerosol retrieval over urban areas using spatial regression between VIS/NIR and MIR Hyperion channels" Remote Sensing of Atmospheric Aerosols, IEEE Workshop, 43- 50 (2005)

CHAPTER 3

Surface Albedo Retrieval and Procedure

In this chapter, the high spatial resolution imagery data from Hyperion Imagery is examined. This dataset is optimal for investigating albedo variations with surface type due to the high spatial resolution. In addition, the image was obtained when atmospheric aerosols were low (and fine mode). By a suitable atmospheric correction using AERONET AOD, pixel level retrieval of VIS/SWIR reflection correlations are possible. The purpose of VIS/SWIR surface reflectance ratio in aerosol retrieval procedure is critical and discussed in the later part of this chapter. Basically, two methods can be considered to obtain surface reflectance. The first method is a statistical path reflectance method. This method has the advantage of not needing an atmosphere measurement but requires homogenous surface properties (although they can be illuminated with different intensities). The second approach uses a-priori optical depth (and phase function) which can be used for atmospheric correction and then obtain the surface albedo.

3.1 Path reflectance method

The TOA reflectance is a function of successive order of radiation interaction within the coupled surface–atmosphere system The TOA reflectance ρ^{TOA} can be described by Equation (3.1) when Lambertian surface reflectance is assumed , Kaufman [1-2],Levy [3].

$$\rho^{TOA}(\mu_0,\mu,\Delta\phi)=\rho^{Path}(\mu_0,\mu,\Delta\phi)+\frac{T_d(\mu_0)\rho^s T_u(\mu)}{1-\overline{S}\rho^s}$$

(3.1)

Where μ the satellite viewing direction, μ_o is the solar zenith angle, ρ^{Path} is the atmospheric reflectance, ρ^s is the ground reflectance and T_d T_u are the downward and upward total (direct + diffuse) atmospheric transmission. $\overline{S}$ is the atmospheric albedo. The path reflectance method is quite simple when applied to low atmospheric optical depth conditions. That condition allows the spherical atmospheric albedo $\overline{S}$ to be approximated as zero in Eq 3.1. Using that assumption, the Eq 3.1 is a simple combination of two parts, the atmospheric path reflectance part and the ground reflectance part, see Eq 3.2.

$$\rho^{TOA}(\mu_0,\mu)\approx\rho^{Path}+T_{atm}(\mu_0,\mu)\rho^s \qquad (3.2)$$

In the SWIR wavelength, the atmospheric path reflectance is approximately equal to zero and the upward transmittance and downward transmittance approximately equal to one for low atmospheric optical thickness and/or fine mode aerosol dominates in the atmosphere. Therefore in this condition, the TOA reflectance signal is directly coming from surface reflectance in SWIR wavelength while the atmosphere is almost transparent.

$$\rho_{SWIR}{}^{TOA}(\mu_0,\mu)=\rho_{SWIR}{}^{Path}(\mu_0,\mu)+\frac{T_d(\mu_0)\rho^s_{SWIR}T_u(\mu)}{1-\overline{S}\rho^s_{SWIR}}\ \approx\ =\rho^s_{SWIR}$$

(3.3)

Eq 3.3 shows that TOA reflectance in SWIR is approximately equal to the surface reflectance. In addition, assuming a linear correlation exits between the VIS and SWIR channels surface reflectance, according to Kaufman [4]., Eq 3.3 can be written as

$$\rho_{vis}^{s} = k\rho_{SWIR}^{s} = k\rho_{SWIR}^{TOA} \tag{3.4}$$

Hence under low optical thickness atmospheric condition, the TOA reflectance in the VIS wavelength is simply $\rho_{vis}^{TOA} \approx k\rho_{SWIR}^{TOA} + \rho_{vis}^{Path}$ (3.5)

When SWIR reflectance closes to the limit of zero, the TOA reflectance in the VIS wavelength is only the signal coming from atmospheric path reflectance.

$$\rho_{SWIR}^{TOA} \to 0 \Rightarrow \rho_{vis}^{TOA} = \rho_{vis}^{Path} \tag{3.6}$$

so that the regression plot between the TOA reflectance in the VIS and SWIR will be linear.. In particular, the slope of the regression line will include the correlation coefficient of VIS-SWIR surface reflectance through $k=cT_d(\mu_o)T_u(\mu)$. On the other hand, the correlations can have non-zero off-sets which make this approach less accurate. However, using this technique is simple to employ as a first estimate to observe the differences in correlation coefficients of VIS/SWIR surface reflectance of different surface type (urban and vegetation area).

This approach is applied in [5]. Hyperion data that was taken over NYC (Sept 12, 2001) with spectral coverage from 400nm to 2800nm with 10nm resolution and 30meter spatial resolution footprint is used. The image does not

include the WTC and the winds were blowing the smoke and ash in a southerly direction away from the image resulting in a very low aerosol loading, Fig 3.1. This image is particularly useful for surface modeling due to the very low AOD observed for this day. ($\tau_{500} \leq .05$) In Fig 3.1, several regions of the Hyperion Image representing water, vegetation (central park), low urban and high urban scenery can be seen .

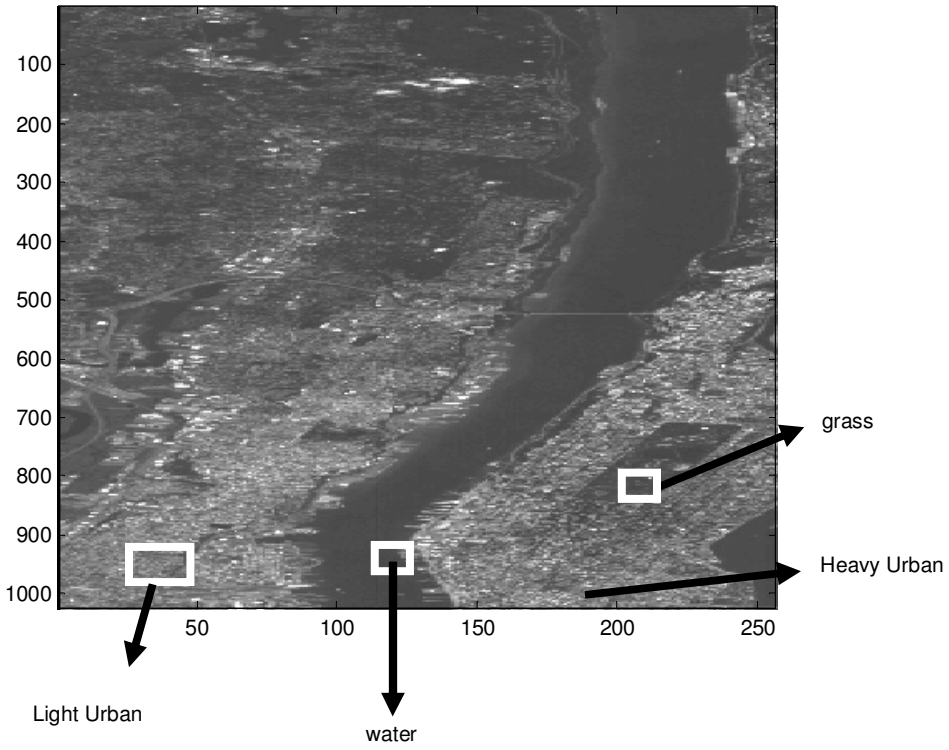

Figure 3.1 Hyperion image of New York City (600nm) Regions of interest include vegetation, Light urban areas, Heavy Urban Area and water

To illustrate the retrieved correlation coefficients of this method over different scenes, we plot histograms of the correlation coefficients for the three

different surface types which are vegetation, rural and urban can be identified. Note that in central park (proxy for vegetation) and in light urban areas, the correlation for the 660-2160nm bands is unbiased around the vegetation value of 0.55 although a surprisingly high variability is seen in the results. However, when considering light or heavy urban scenes, the value for the correlation coefficient is significantly higher with values peaking to 0.72 for heavy urban scenes in good agreement with the MILARGO results [6]

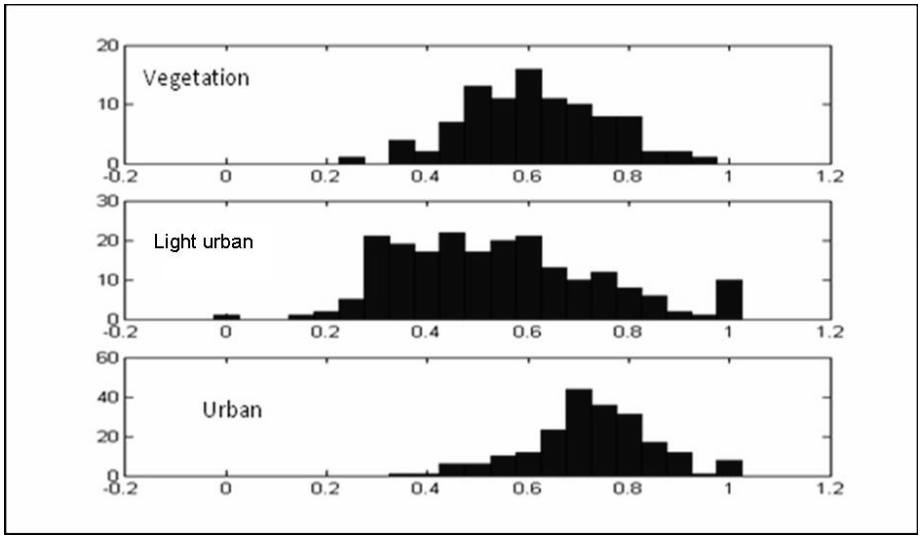

Figure 3.2 Statistical correlations for (i) vegetation, (ii) rural and (iii) urban pixels.

As discussed above, the results are based on an assumption that the correlation is constant except for intensity fluctuations. Another approach is to probe the surface reflectance directly using atmospheric correction schemes. As an example of this approach, the image can be segmented using supervised classification which allows us to better separate vegetation and urban scenes. The segmentation based on supervised classification on the Hyperion Image was performed using the standard ENVI segmenting tool is illustrated in Fig 3.3. . Once the

segmentation is complete, the atmospheric correction on each pixel for different atmospheric models and visibilities can be performed by using standard Hyper-spectral correction tools from the ENVI FLAASH software. This atmospheric correction was based on AERONET measurements which clearly identified the aerosols to be fine mode dominated and high visibility

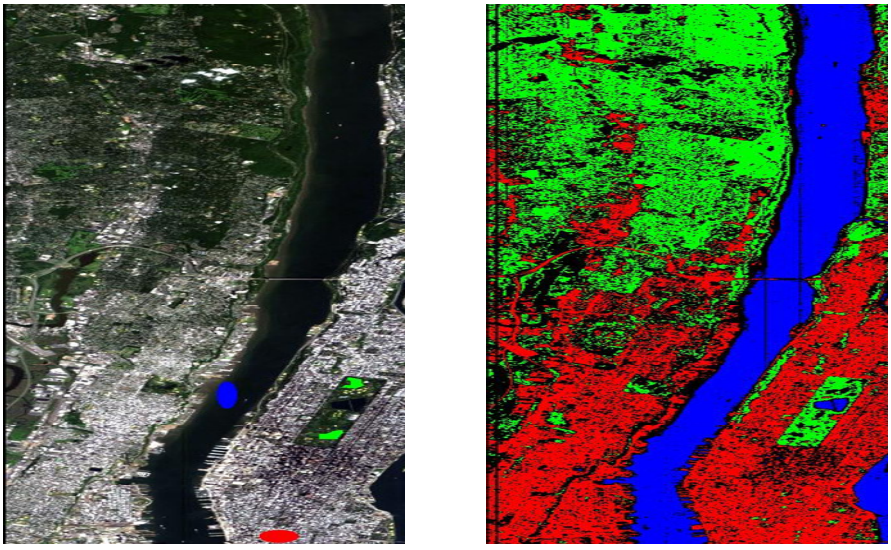

Figure 3.3 Original RGB image from Hyperion shown the three selected training regions of interest Blue: water, Green: vegetation and Red: buildings (Left). Segmented image obtained by training the image using the selected regions of interest. The green rectangle at the lower right corresponds to Central Park with its lake inside (Right)

The results of the correlation coefficients as function of visibility are seen in Fig 3.4. The visibility is inversely proportional to the aerosol optical thickness. The important result is that above a certain visibility, which is about 80 Km and above in this plot, the correlation coefficient for the VIS-SWIR ratio is quite stable. The TOA reflectance ratio of VIS-SWIR is approximately equal to the surface reflectance ratio of VIS-SWIR in this condition so the VIS/SWIR correlation coefficients can be calculated directly. In particular, we note that while the vegetation pixels are quite well described by the MODIS values in both C004 [1]

and C005 [2] algorithm, the urban pixels result in a significantly higher ratio which is consistent with the prior statistical based approach used above.

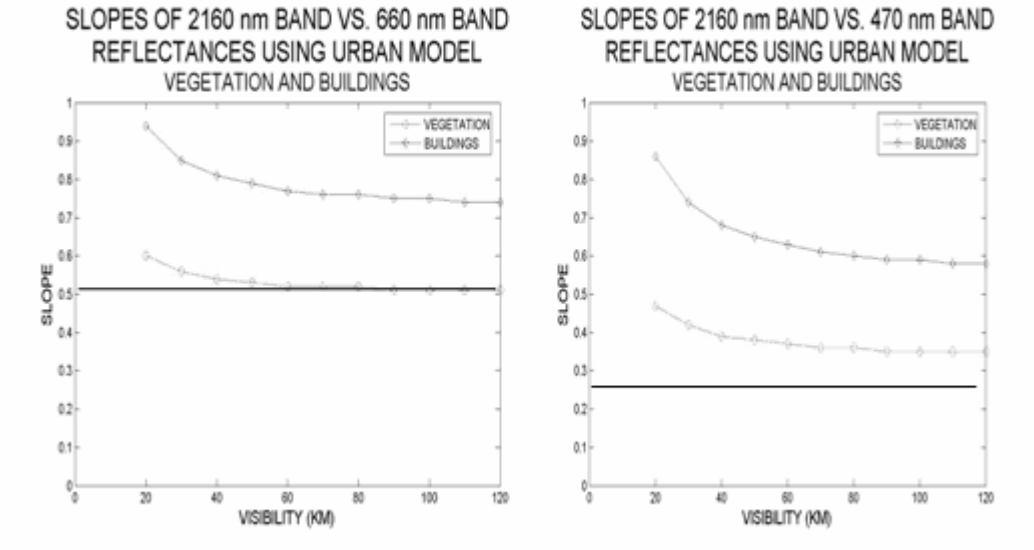

Figure 3.4 Mean slopes of the 2160 nm and 660 nm bands (left) and the 2160 nm and 470 nm bands (right) for the vegetation and buildings regions at each visibility. The lower bars correspond to the values of the MODIS C004 ATBD VIS-SWIR correlation coefficients of 0.5 for the 660 nm and 0.25 for the 470 nm band.

3.2 Path reflectance method with MODIS

Statistical approaches are difficult with MODIS data due to the low resolution available. Current MODIS L2 data such as aerosol optical thickness and surface reflectance provide only 10x 10 km^2 spatial resolution (MODIS L2 data can be downloaded from http://modis.gsfc.nasa.gov/data). In this case, statistical methods are not reasonable and a per-pixel evaluation of MODIS L1B data and atmospheric properties for aerosol as of MODIS LUT (Look Up Table) is needed. More details of the MODIS land operational LUT is discussed in section 3.2.2.

In adapting this approach as a way to monitor urban regions in detail, it is important that the spatial resolution of the AOD retrieval is improved. In the operational algorithm, cloud free pixels are identified and TOA reflectance is acquired but the cloud mask is operationally implemented at 10km resolution. However, there is no fundamental limit on applying the same ideas but with different thresholds and implement the cloud mask at 1.5 km. In particular, the thresholds we apply to the TOA reflectance variability is significantly lower for filtering the pixel in our high resolution cloud mask. This is necessary so we do not throw out higher surface albedo pixels with more variability over urban scenes. Since it is possible to retrieve at higher resolution, the cloud clearing in 3 resolutions (10 x 10 km^2, 3 x 3 km^2 and 1.5 x 1.5km^2) are analyzed.

3.2.1 Cloud masking procedure

In particular, the MODIS cloud mask algorithm identifies several conceptual domains according to surface type and solar illumination including land, water,

snow/ice, desert, and coast for both day and night [7]. Once a pixel is assigned to a particular domain, a series of threshold test attempts to detect the presence of clouds in the instrument field-of view. The assessment of cloud detection capability of the MODIS cloud mask algorithm can be found in [8] i.e. the comparison of the MODIS results with observations from active sensors and demonstrates the sensitivity of the cloud-masking approach to various thresholds and conditions.

The cloud masking procedure used in this thesis is very similar to the MODIS operational procedure [2]. MODIS L1B (500m) resolution data in band 3, band 7 and band 26 (1km) resolution data are applied to eliminate the cloud cover pixel. First compute the standard deviation of spatial variability of band3 (0.47μm) and band 26 (1.38μm) for each group of 3x3 pixel and discarded the group if any pixel in the group of 3x3 has the standard deviation in band3 (0.47μm) >0.01 or the standard deviation in band 26 (1.38μm) >0.003. In addition to that reflectance threshold test to reject the pixel if band 26 (1.38μm) >0.025 or band3 (0.47μm) > 0.4 to avoid cloud contamination to the aerosol retrieval is performed. Then only the pixels which are greater than 0.01 and less than 0.25 in the band 7 (2.12 μm) reflectance are selected. The procedure is the same as the MODIS defined procedure up to this stage except that MODIS defined procedure eliminates 50% of brightest and 20% of darkest to avoid partial cloud and water contamination. The final TOA reflectance pixels are completed with solar zenith angle correction and gas correction of L1 B data reflectance which is also explained in the MODIS C005 ATBD. In the MODIS Collection (5) procedure, the spatial variability

limitation for 0.47μm channel is 0.0025 which is a higher level than the operational mask. and is needed to account for the increased variability of the urban scene. Due to the less conservative assumptions in this research, it may be possible that cloud contamination may be more frequent. However, since cloud optical properties (i.e. angstrom coefficient) is quite different than the fine mode aerosol dominated events, an analysis of the fine /coarse mode mixing ratio should be sufficient to identify eliminate cloud contamination effects. Example of the step by step MODIS operational cloud masking procedure for one particular day (4^{th} of July, 2002) near NYC area is shown in figures (Fig 3.5 to Fig 3.10).

The area of each figure is 10x10 km box, since MODIS land band 1-7 are in (250 and/or) 500m resolution, 20x20 pixels are presented in each plot. This is the case for all bands except band 26 which has 1km resolution and therefore Fig 3.6 (a) is shown as 10x10 pixels.

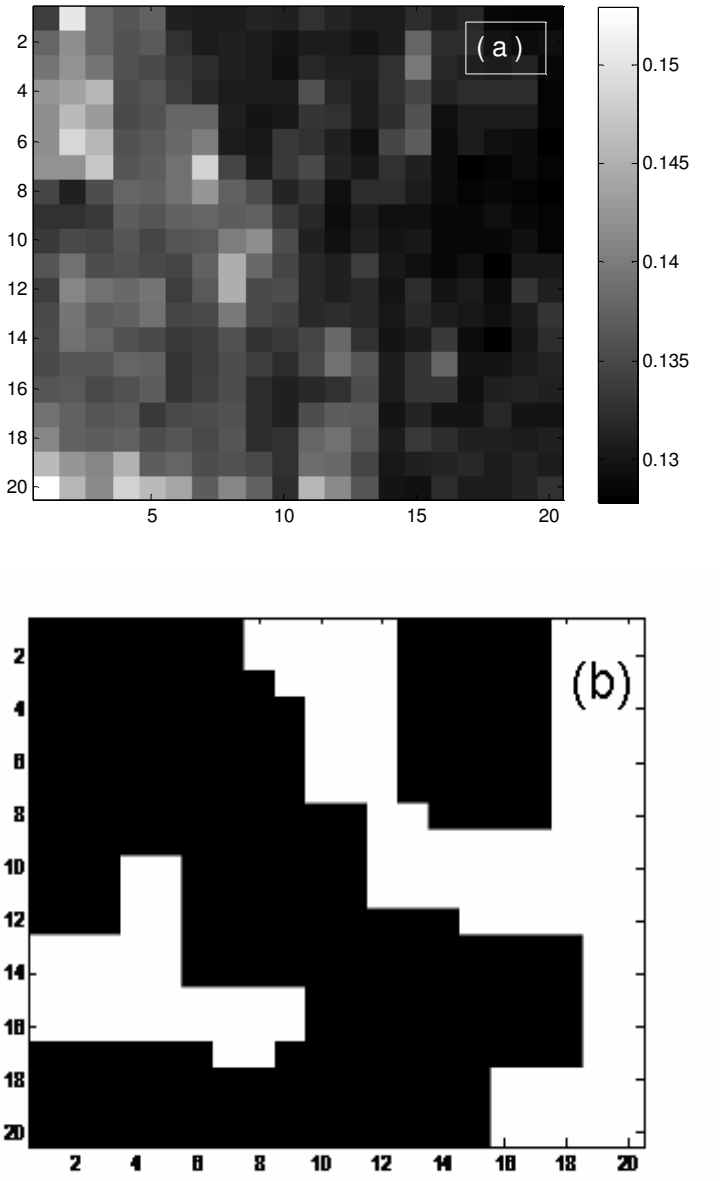

Figure 3.5 (a) Band 3 (0.47 µm TOA Reflectance) (b) Discard if pixels fail to the test (3x3 std < 0.0025& Ref <0.4) all failed pixels are masked with black

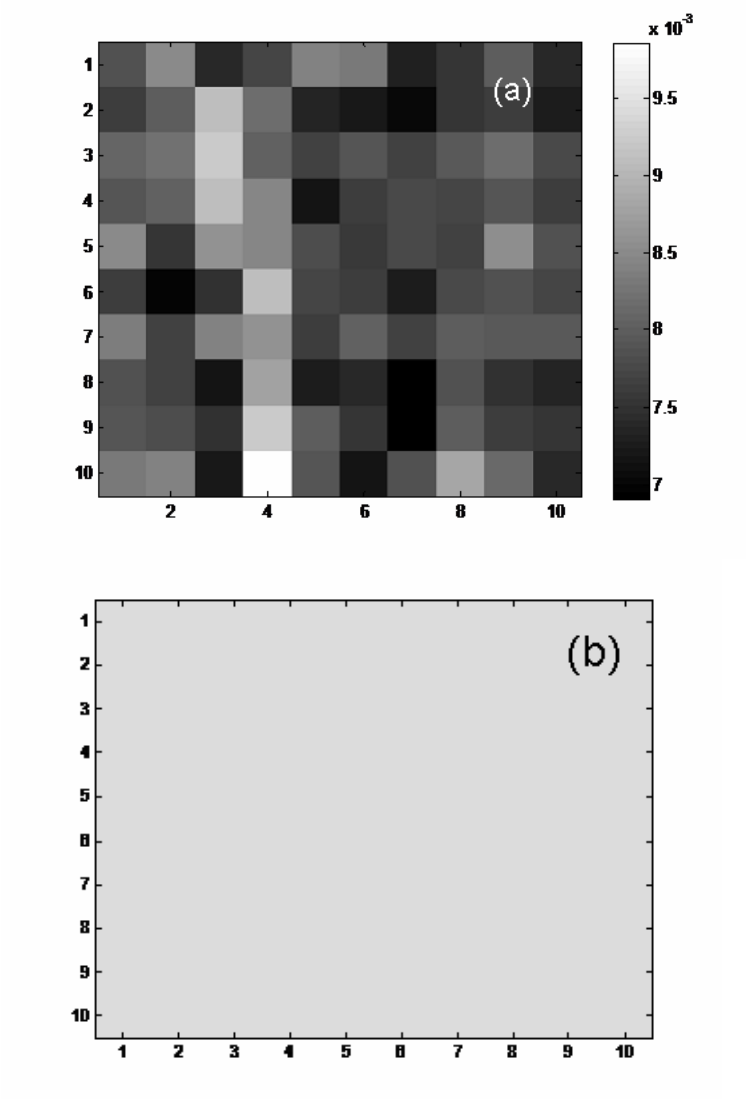

Figure 3.6 (a) Band26 (1.38μm TOA Reflectance) (b) Discard if pixels fail to the test (3x3 Std < 0.003 & Ref < 0.01) all failed pixels are masked with black

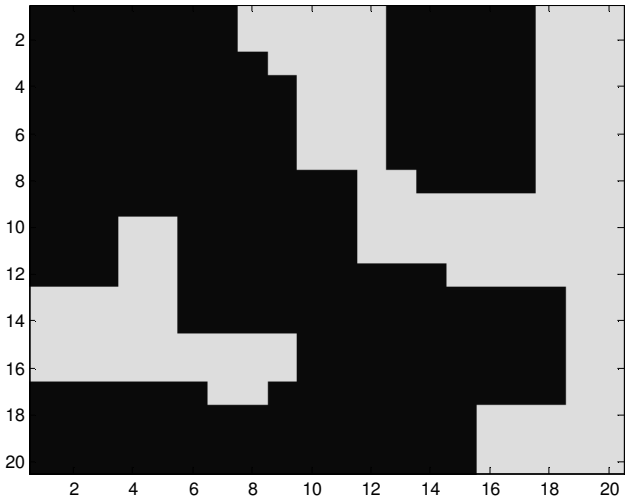

Figure 3.7 Resultant cloud free pixels of the combination of two cloud test

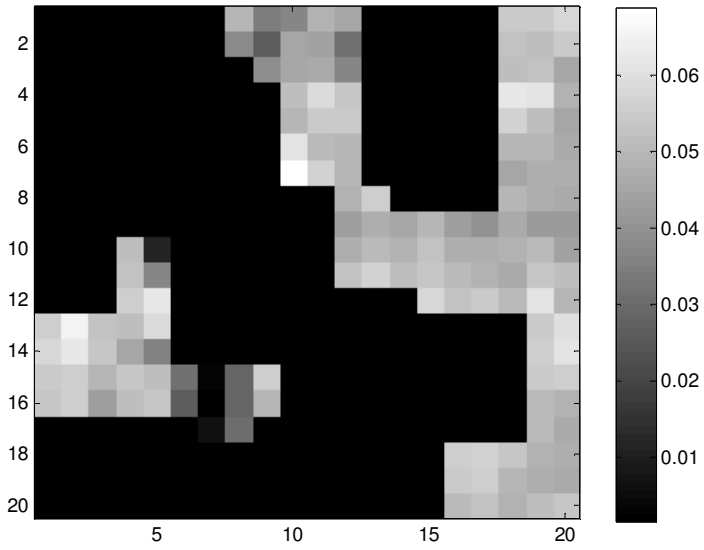

Figure 3.8 Cloud free Band 7 (2.12µm TOA reflectance) after discarding the reflectance pixels less than 0.01 and greater than 0.25 to ensure inland water and broken cloud pixels contamination

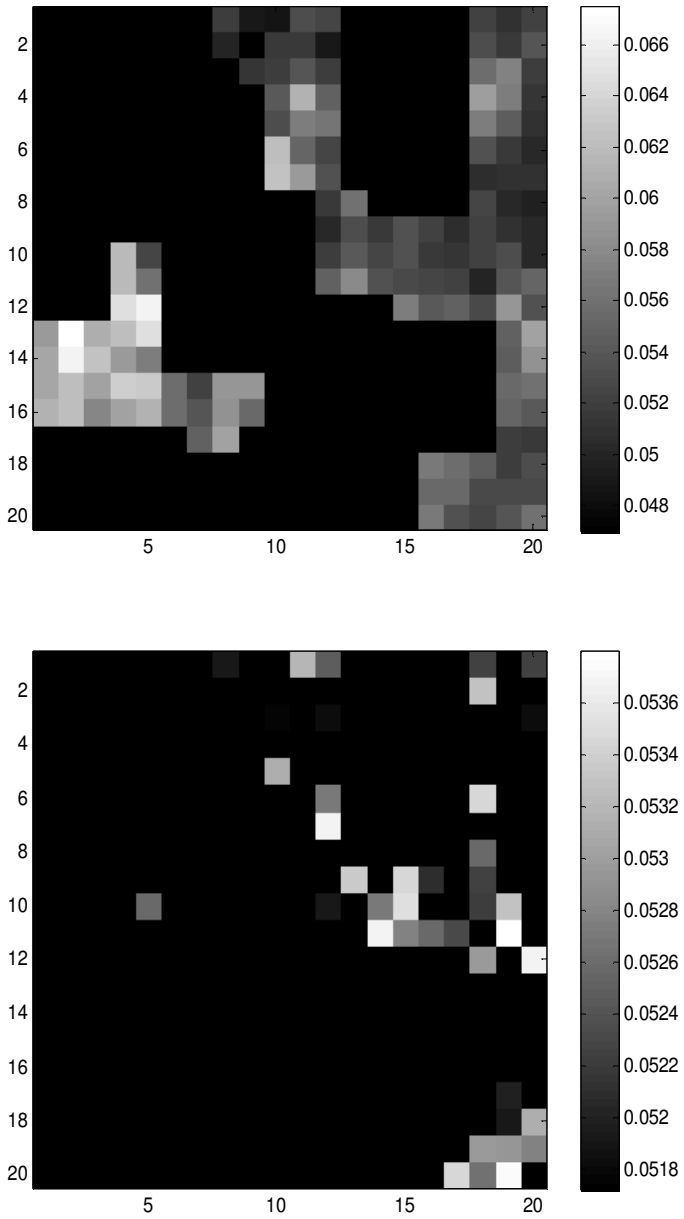

Figure 3.9 Cloud free Band 1(0.66µm TOA reflectance) before discarding 50% of the brightest and 20% of the darkest pixels (top) and after discarding (bottom)

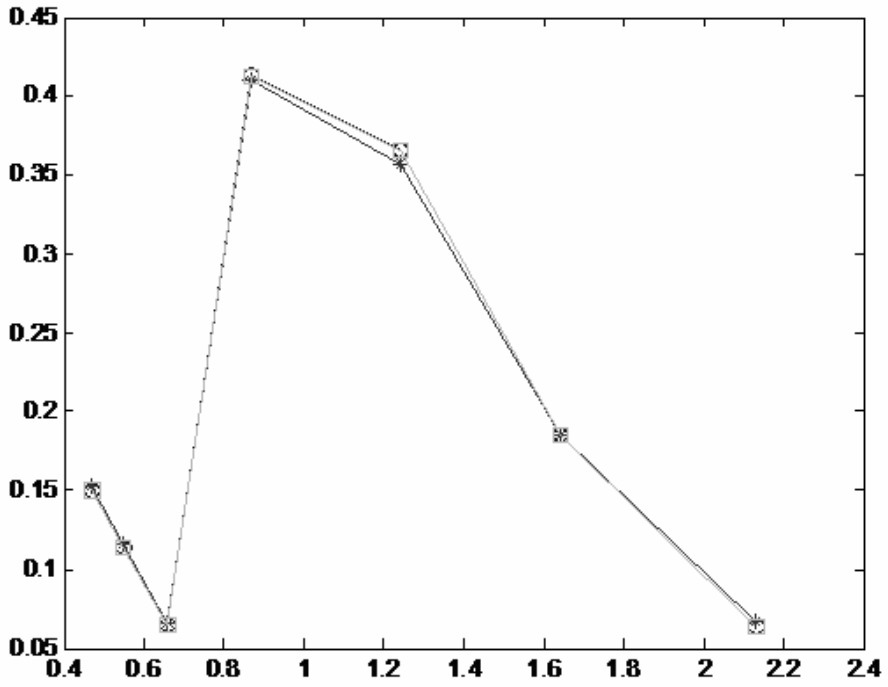

Figure 3.10 Comparison of MODIS L2 TOA 10x10km reflectance with derived TOA reflectance in 10x10km resolution is shown. '*' is the downloaded MODIS L2 data, 'o' is the derived data by CCNY, '□' is the derived data from Robert Levy (GSFC).

In using our own cloud mask, we wished to make sure that all issues regarding geolocation were done correctly. Therefore, we made sure that our TOA reflectances after cloud clearing were the same at 10km resolution as those from the Operational datasets on the NASA DAAC. Fig 3.10 shows that derived final cloud free TOA reflectance is in good agreement with MODIS L2 TOA reflectance. This examination shows that calculation of cloud clear procedure described in the ATBD is attainable and retrieving the higher resolution (3x3 km and 1.5x1.5 km) cloud free TOA reflectance is feasible.

3.2.2 MODIS Operational LUT (Look Up Table)

The MODIS land operational LUT contains pre-computed optical properties of aerosol at four discrete wavelengths (0.466, 0.553, 0.644 and 2.119 μm, representing MODIS channels 3, 4, 1 and 7, respectively) for several values of aerosol total loadings, and for a variety of geometry. For discrete optical depths (described by the AOD at 0.55 μm) each spherical aerosol model (Continental, Generic, Absorbing smoke and Non-absorbing urban) and non-spherical model (Dust), scattering/extinction properties of aerosol size distributions are calculated by either MIEV [9] or the Dubovik [10-12] T-matrix code. Assuming a Rayleigh atmosphere and realistic layering of the aerosol, the Legendre moments of the combined Rayleigh/aerosol are computed for each layer of a US Standard Atmosphere, more detail can be see at http://modelweb.gsfc.nasa.gov/ (U.S. Government, 1976). These moments are fed into RT3 [13] to simulate TOA reflectance and total fluxes. The atmospheric parameters of Equation (1) were calculated for seven aerosol loadings ($\tau_{0.55}$ = 0.0, 0.25, 0.5, 1.0, 2.0 3.0, and 5.0). TOA reflectance was calculated for 9 solar zenith angles (μ = 0.0, 6.0, 12.0, 24.0, 35.2, 48.0, 54.0, 60.0 and 66.0), 16 sensor zenith angles (μ' = 0.0 to 66.0, increments of 6.0), and 16 relative azimuth angles ($\Delta\phi$ = 0.0 to 180.0 increments of 12.0). All of these parameters are calculated assuming a surface reflectance of zero. When surface reflectance is present, the second term in Equation (1) is nonzero. In the MODIS LUT calculation, the flux is a function only of the atmosphere, however, the atmospheric albedo term, $\bar{s}$, and the transmission term, $T_u(\mu')$,are functions of both the atmosphere and the surface. RT3 was run two

additional times with distinct positive values of surface reflectance. The values of 0.1 and 0.25 for (ρ_1^s *and* ρ_2^s) surface reflectance were chosen.

$$\bar{s} = (1/\rho_1^s)(1-(T_d T_u \rho_1^s /(\rho^* - \rho^a))) \quad (3.7)$$

$$\bar{s} = (1/\rho_2^s)(1-(T_d T_u \rho_2^s /(\rho^* - \rho^a))) \quad (3.8)$$

These two equations (3.7) and (3.8) can be solved for the two unknown,($\bar{s}$ *and* T_u) and are saved into the LUT for each AOD index, wavelength and aerosol model. Other parameters contained in the LUT include the scattering and extinction coefficients Q and variables describing the physical properties (lognormal size parameters r_g and σ, real and complex refractive indices) of the aerosol models. Details of the optical properties and size distribution of aerosol models of MODIS land operational LUT is shown in Table 3.1. The optical properties and size distributions for the Continental model, the three spherical (neutral, absorbing smoke and non-absorbing urban) fine models and the one spheroid coarse aerosol (dust) models assumed for MODIS operational LUT is displayed. The fine aerosol models are assumed to be spherical particles. The combination of MIEV [9] and RT3 [13] are used in generating the MODIS LUT. For the spheroids of the coarse aerosol model, the MODIS LUT uses a version of the T-matrix code described in [12], to calculate the scattering properties of the model. Then a combination of the T-matrix and RT3 codes is used for the coarse (dust) model LUT. Assumed central wavelengths and Rayleigh optical depths are shown in Table 3.1.

Model	Mode	r_v (μm)	σ	V_0 ($\mu m^3/\mu m^2$)	Refractive Index: k	SSA/g (0.47/0.55/0.66/2.1μm) for $\tau_{0.55} = 0.5$
Continental						0.90/0.89/0.88/0.67 0.64/0.63/0.63/0.79
	Soluble	0.176	1.09	3.05	1.53-0.005i; 0.47 μm 1.53-0.006i; 0.55 μm 1.53-0.006i; 0.66 μm 1.42-0.01i; 2.12 μm	
	Dust	17.6	1.09	7.364	1.53-0.008i; 0.47 μm 1.53-0.008i; 0.55 μm 1.53-0.008i; 0.66 μm 1.22-0.009i; 2.12 μm	
	Soot	0.050	0.693	0.105	1.75-0.45i; 0.47 μm 1.75-0.44i; 0.55 μm 1.75-0.43i; 0.66 μm 1.81-0.50i; 2.12 μm	
Neutral/ Generic						0.93/0.92/0.91/0.87 0.68/0.65/0.61/0.68
	Accum	$0.0203\tau + 0.145$	$0.1365\tau + 0.3738$	$0.1642\,\tau^{0.7747}$	$1.43 - (-0.002\tau+0.008)i$	
	Coarse	$0.3364\tau + 3.101$	$0.098\tau + 0.7292$	$0.1482\,\tau^{0.6846}$	$1.43 - (-0.002\tau+0.008)i$	
Non-absorb/ Urban-Ind						0.95/0.95/0.94/0.90 0.71/0.68/0.65/0.64
	Accum	$0.0434\tau + 0.1604$	$0.1529\tau + 0.3642$	$0.1718\,\tau^{0.8213}$	$1.42 - (-0.0015\tau+0.007)i$	
	Coarse	$0.1411\tau + 3.3252$	$0.1638\tau + 0.7595$	$0.0934\,\tau^{0.6394}$	$1.42 - (-0.0015\tau+0.007)i$	
Absorbing/ Heavy Smoke						0.88/0.87/0.85/0.70 0.64/0.60/0.56/0.64
	Accum	$0.0096\tau + 0.1335$	$0.0794\tau + 0.3834$	$0.1748\,\tau^{0.8914}$	$1.51 - 0.02i$	
	Coarse	$0.9489\tau + 3.4479$	$0.0409\tau + 0.7433$	$0.1043\,\tau^{0.6824}$	$1.51 - 0.02i$	
Spheroid/ Dust						0.94/0.95/0.96/0.98 0.71/0.70/0.69/0.71
	Accum	$0.1416\,\tau^{-0.0519}$	$0.7561\,\tau^{0.148}$	$0.0871\,\tau^{1.026}$	$1.48\tau^{-0.021} - (0.0025\,\tau^{0.132})i$; 0.47 μm $1.48\tau^{-0.021} - 0.002i$; 0.55 μm $1.48\tau^{-0.021} - (0.0018\,\tau^{-0.08})i$; 0.66 μm $1.46\tau^{-0.040} - (0.0018\,\tau^{-0.36})i$; 2.12 μm	
	Coarse	2.2	$0.554\,\tau^{-0.0519}$	$0.6786\,\tau^{1.0569}$	$1.48\tau^{-0.021} - (0.0025\,\tau^{0.132})i$; 0.47 μm $1.48\tau^{-0.021} - 0.002i$; 0.55 μm $1.48\tau^{-0.021} - (0.0018\,\tau^{-0.08})i$; 0.66 μm $1.46\tau^{-0.040} - (0.0018\,\tau^{-0.36})i$; 2.12 μm	

Listed for each model are the individual lognormal modes, and the final SSA at different wavelengths. Listed for each mode are the mean radius r_v, standard deviation σ of the volume distribution, and total volume of the mode, V_0. The complex refractive index is assumed for all wavelengths (0.47, 0.55. 0.66 and 2.1 μm), unless otherwise noted. The Absorbing and Neutral model parameters (r_v, σ and k) are defined for $\tau \leq 2.0$; for $\tau > 2.0$, we assume $\tau = 2.0$. Likewise, the Non-absorbing and Spheroid model parameters are defined for $\tau \leq 1.0$. V_0 (for all models) is defined for all τ.

Table 3.1 Optical properties of the aerosol model used for the MODIS over land LUT

3.2.3 Aerosol Model Selection for New York City (CCNY)

Once the cloud clearing at a particular resolution is completed and MODIS LUT is available, an inversion to obtain surface properties can be performed. Although the MODIS defined Lookup Table (LUT) has 4 fine aerosol models (Continental, Generic, Smoke, Urban) and a Dust aerosol, the MODIS C005 ATBD document

shows that for the North East, nearly all aerosol events are modeled using the urban aerosol model. Since it is not always possible to get modified phase functions due to the need for very high degree of cloudless conditions, urban aerosols are assumed in obtaining the surface model.

During this comparison, only atmospheres which can be verified a-priori as fine mode are used. This is necessary so the surface reflectance at 2120 nm can be approximated as the TOA reflectance since the SWIR channel is transparent to the fine mode aerosol model. To ensure only fine mode aerosol dominant conditions occur, we perform matchups only days when the Ångstrom coefficient $\alpha > 1$ are selected. This restriction helps to reduce errors due to misclassification of aerosols. In addition, to further reduce surface retrieval error , the AOD is chosen less than 0.2 ($\tau_{550}<0.2$).

$$\alpha = \frac{\log(\tau_{675nm} / \tau_{1020nm})}{\log(1020/675)} \tag{3.9}$$

Moreover, to ensure homogeneity in the aerosol during the surface retrieval, at least 10 cloud cleared points exist in the 4 hour interval surrounding the MODIS observations and the full daily fractional error in the AOD are less than 20% is required. These filters provided us with the optimal matchup cases needed to retrieve surface parameters.

References

[1] Kaufman, Y.,J., Tanre, D., "Algorithm for Remote Sensing of Tropospheric Aerosol from MODIS" Mod04 ATBD Document (1998)

[2] Remer, L., A., R., Tanré, D., Kaufman, Y.,J., Levy, R., and Mattoo, S., "ALGORITHM FOR REMOTE SENSING OF TROPOSPHERIC AEROSOL FROM MODIS: Collection 005" ATBD document

[3] R. C. Levy, L. A. Remer, and Y. J. Kaufman "Effects of Neglecting Polarization on the MODIS Aerosol Retrieval Over Land" *IEEE Trans. Geos. Rem. Sens.,* vol 42 Pp 2576-2583, 2004

[4] Kaufman, Y., J., Wald, A., E., Remer, L., A., Gao, B-C., Li, R-R., Flynn, L., "The MODIS 2.1- mu m channel-correlation with visible reflectance for use in remote sensing of aerosol"; IEEE Transactions on Geoscience and Remote Sensing 35 1286-98, (1997)

[5] Gross, B., Ogunwuyi, O., Moshary, F., Ahmed, S.; Cairns, B. "Aerosol retrieval over urban areas using spatial regression between VIS/NIR and MIR Hyperion channels" Remote Sensing of Atmospheric Aerosols, IEEE Workshop, 43- 50 (2005)

[6] Castanho, A., A.D. de, Prinn, R., Martins, V., Herold, M., Ichoku, C. and Mollna, L. T., "Urban Visible/SWIR surface reflectance ratios from satellite and sun photometer measurements in Mexico City", Atmos. Chem. Phys, Discuss., 7, 8113-8139, (2007)

[7] S. Platnick, M.D. King, S.A. Ackerman, W.P. Menzel, B.A Baum, J.C Riedi, R.A Frey, R.A. ,"The MODIS cloud products: algorithms and examples from Terra", *IEEE Trans Geos. Rem. Sens.*, Vol 41, pp 459- 473, (2003)

[8] S. A. Ackerman, R. E. Holz, R. Frey, E. W. Eloranta, B. C. Maddux, and M. McGill "Cloud Detection with MODIS. Part II: Validation", Journal of Atmospheric and Oceanic Technology, Volume 25, Issue 7 (July 2008)

[9] Wiscombe, W. J. (1981). "Improved Mie scattering algorithms." Appl. Opt. **19**: 1505-1509.

[10] Dubovik, O., B. Holben, et al. (2002). "Variability of absorption and optical properties of key aerosol types observed in worldwide locations." Journal of the Atmospheric Sciences **59**(3): 590-608.

[11] Dubovik, O., B. N. Holben, et al. (2002). "Non-spherical aerosol retrieval method employing light scattering by spheroids." Geophysical Research Letters **29**(10): art. no.-1415.

[12] Dubovik, O. and M. D. King (2000). "A flexible inversion algorithm for retrieval of aerosol optical properties from Sun and sky radiance measurements." Journal of Geophysical Research-Atmospheres **105**(D16): 20673-20696.

[13] Evans, K.F. and G. L. Stephens, 1991, A New Polarized Atmospheric Radiative Transfer Model, *J. Quant. Spectrosc. Radiat. Transfer,* **46**(5):413-423

CHAPTER 4

Derivation of VIS/SWIR surface reflectance ratios procedure

In this chapter, details of the VIS/SWIR surface reflectance ratio calculation are discussed. Following the procedure in Chapter 3, the surface reflectances in the VIS channel (0.47 and 0.66 μm) can be calculated.

4.1 Derivation of surface reflectance from radiative transfer model

To use the AERONET AOD directly, AOD and aerosol model information must be able to ingest directly into the Radiative transfer code. In the Lambertian approximation, the surface reflectance can be written as

$$\rho_\lambda^{surf}(\theta_0,\theta,\Delta\phi,\tau)=\frac{\rho_\lambda^{TOA}(\theta_0,\theta,\Delta\phi,\tau)-\rho_\lambda^{path}(\theta_0,\theta,\Delta\phi,\tau)}{\bar{s}(\theta_0,\tau)(\rho_\lambda^{TOA}(\theta_0,\theta,\Delta\phi,\tau)-\rho_\lambda^{path}(\theta_0,\theta,\Delta\phi,\tau))+T_\lambda^{up}(\theta_0,\theta,\tau)F_\lambda^{dn}(\theta_0,\tau)} \quad (4.1)$$

In Equation (4.1), ρ_λ^{TOA} is the measured top of atmosphere reflectance form MODIS L1 B cloud free data, ρ_λ^{path} is the atmospheric path reflectance, $\bar{S}$ is the atmospheric albedo, F_λ^{dn} is the downward transmission, and T_λ^{up} is the upward

transmission.θ_0 , θ, and $\Delta\phi$ are the solar zenith angle, senor (satellite) zenith angle and relative solar sensor azimuth angle respectively. Clearly, ingesting the aerosol AOD and urban phase function from MODIS operational LUT with particular geometric angles (the solar zenith angle, senor (satellite) zenith angle and relative solar sensor azimuth angle) provides all the atmospheric parameters from the above Equation (4.1) and it is sufficient to obtain the surface reflections for both visible channels (0.47 and 0.66 μm) independently. Since the aerosols are fine mode dominated, the atmosphere is approximately transparent at 2.12 μm (except under cloudy or unusually dusty conditions). Therefore the clear sky TOA reflectance at that wavelength can be assumed as the reflectance from the ground (surface). Therefore, the ground reflectance at 2.12 μm is simply the TOA reflectance allowing for calculation of the VIS-SWIR correlation coefficients in this stage.

4.2 Urban area surface reflectance ratios

New York City urban area surface reflectance ratios can be calculated from above procedure using AERONET station at the City College of New York (Manhattan, NY) as a function of the scattering angle. The results are shown in Fig 4. 1 for 3 spatial resolutions (10x10km, 3x3km and 1.5x1.5km boxes) surrounding the CCNY (AERONET site in Manhattan, NY). We first note that the calculated VIS/SWIR reflectance ratios are higher than those implemented from MODIS operational algorithm defined VIS/SWIR reflectance ratios and these ratios are in good agreement with Hyperion results, which is approximately ~0.58 for 470nm/2160nm surface reflectance ratio and ~0.74 for 660nm/2160nm surface

reflectance ratio. Furthermore, we do not detect any meaningful trend behavior as a function of angle. Any trend observed is significantly smaller than the fluctuations around the trend line. However, we also note a serious anomaly in which the correlation coefficient increases significantly as the spatial resolution is increased from 10x10km to 1.5x1.5 km, see Fig 4.1 (e) and (f). This is not expected for normal homogenous surface types.

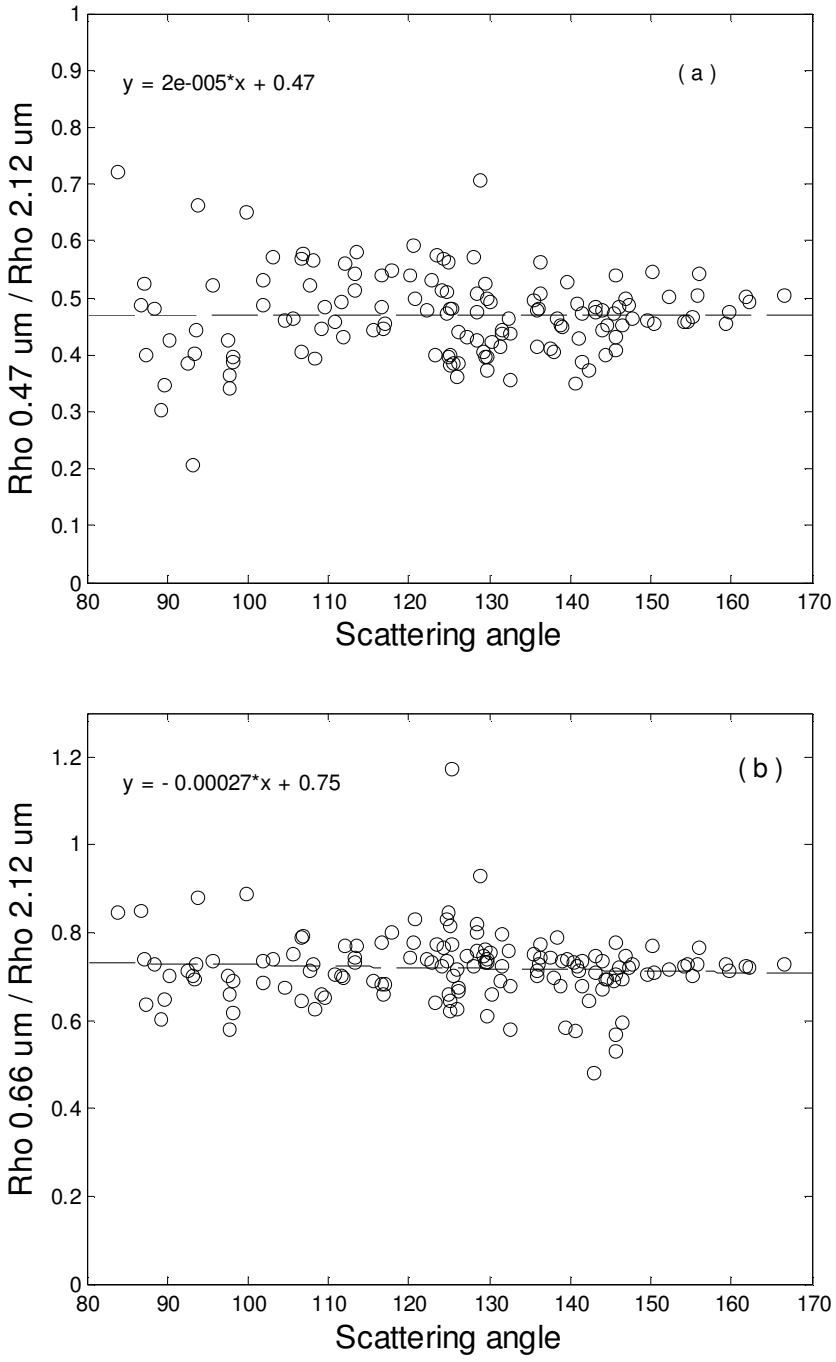

Figure 4.1 (a-b) Surface reflectance ratio of (a) 0.47 / 2.12 μm and (b) 0.66 /2.12 μm with respect to (x axis) scattering angle. Mean reflectance ratio for different spatial resolution: 10x10-km surrounded to the nearest pixel to AERONET site at CCNY from 2001 to 2006 with fine mode aerosol dominant atmosphere (not masked for inland water bodies)

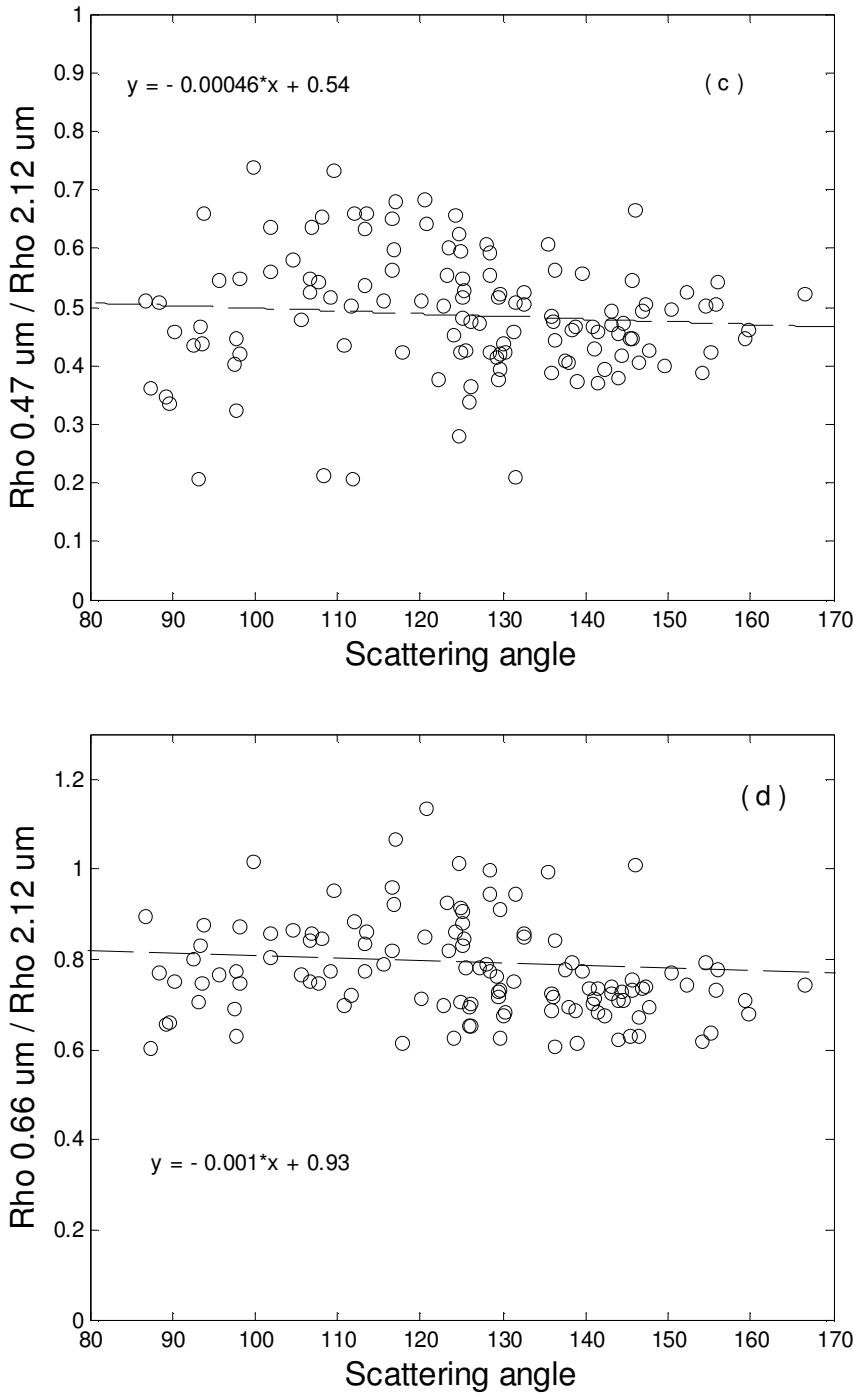

Figure 4.1(c-d) Surface reflectance ratio of (c) 0.47 / 2.12 μm and (d) 0.66 /2.12 μm with respect to (x axis) scattering angle. Mean reflectance ratio for different spatial resolution: 3x3km surrounded to the nearest pixel to AERONET site at CCNY from 2001 to 2006 with fine mode aerosol dominant atmosphere (not masked for inland water bodies)

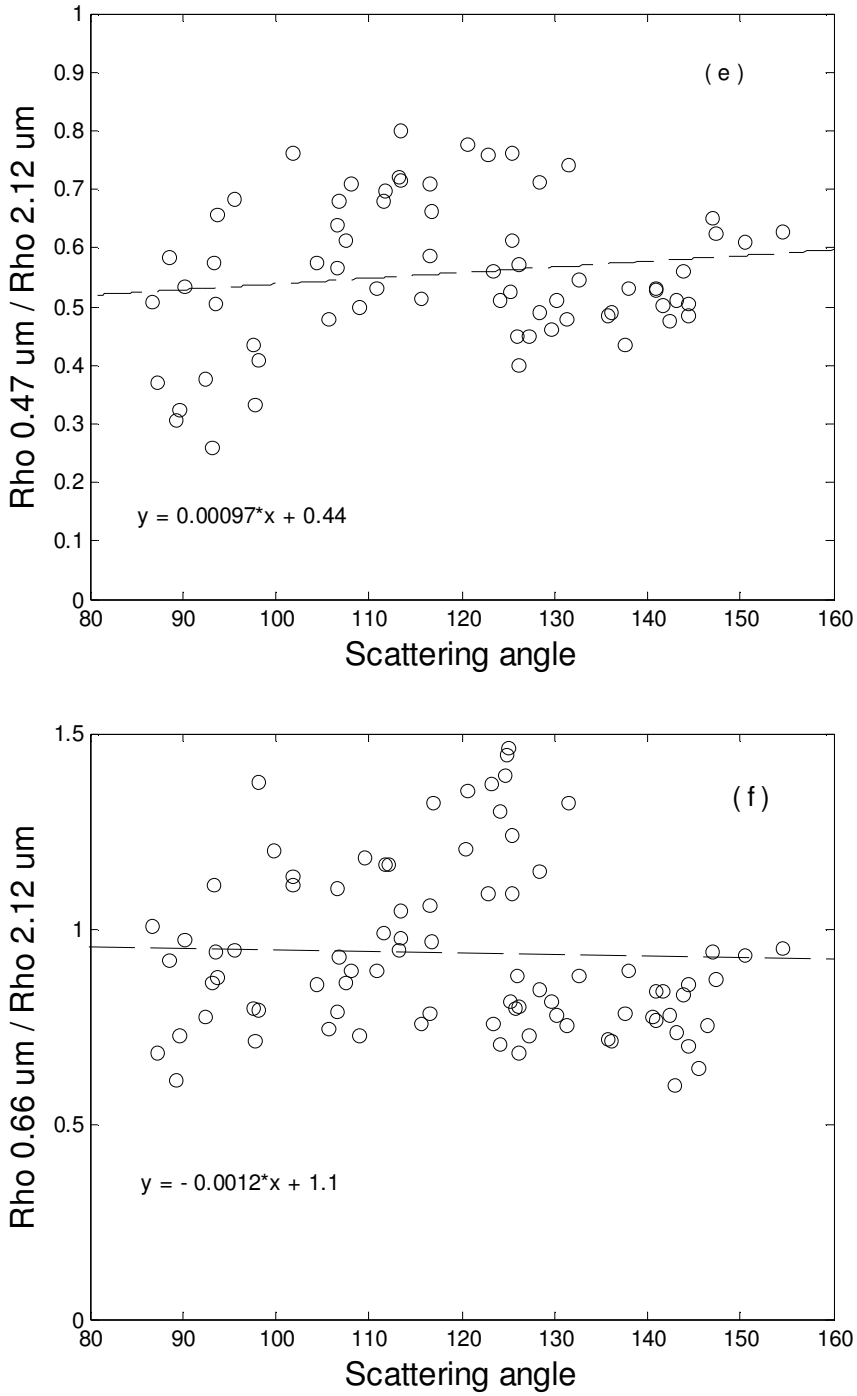

Figure 4.1(e-f) Surface reflectance ratio of (e) 0.47 / 2.12 μm and (f) 0.66 /2.12 μm with respect to (x axis) scattering angle. Mean reflectance ratio for different spatial resolution 1.5x1.5km surrounded to the nearest pixel to AERONET site at CCNY from 2001 to 2006 with fine mode aerosol dominant atmosphere (not masked for inland water bodies)

However, this anomaly can be explained when we consider the water contamination due to the nearby Hudson river. In fact, when the spatial resolution is low (10x10km box), only a small portion of the region is contaminated by water. The effect of water in the pixel is to force the value of the correlation coefficient of the VIS/SWIR up since for any clean water body, no reflection at 2120nm occurs but due to highly turbid water condition in the metro city river a small but non zero value is present. In effect, this leads to an anomalously high VIS/SWIR reflectance ratio which distorts the correlation values for the surface pixels.

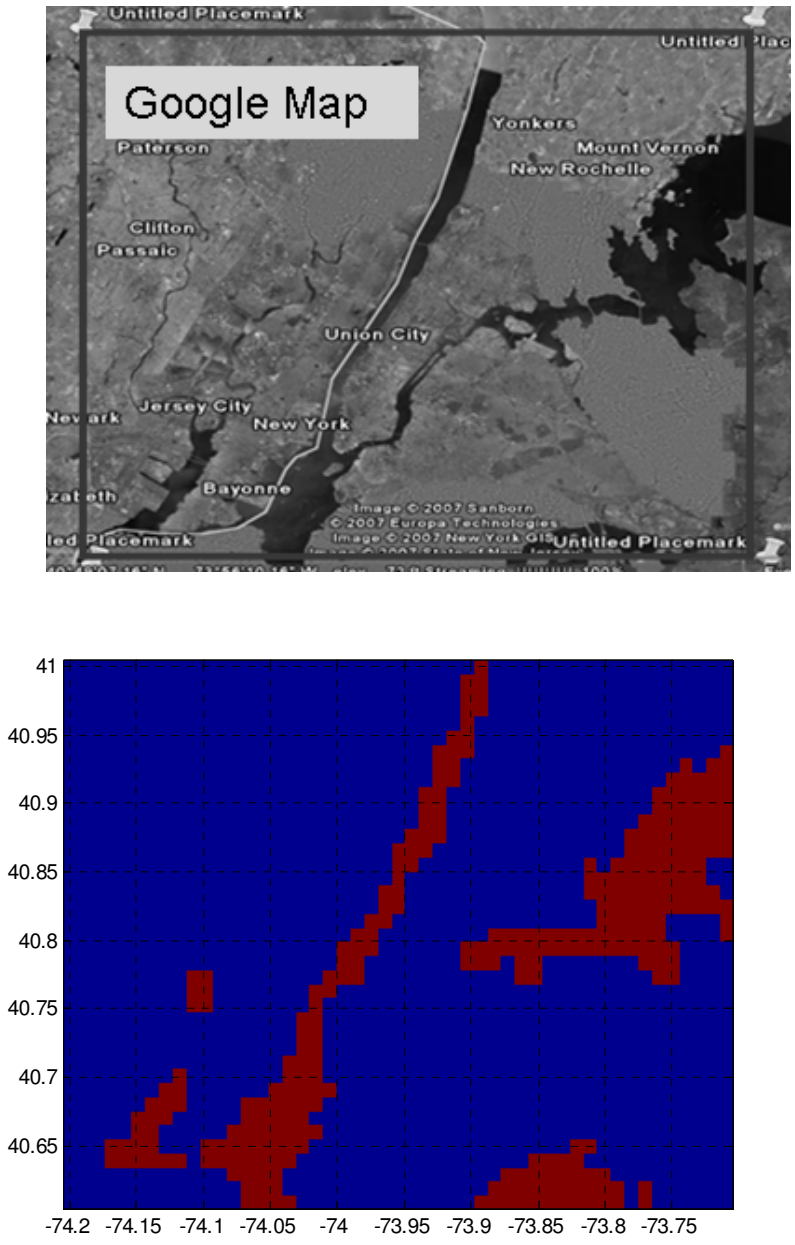

Figure 4.2 NYC area local maps (top) and result from masked inland water body in MODIS data (bottom)

This explanation can be tested if in the calculation the VIS/SWIR surface reflectance ratios, we mask all water contamination pixels using a 2120nm filter directly (i.e. $\rho_{TOA} > 0.05$). The results are shown in Fig 4.3 and illustrate the fact

that the correlation values are much more independent of the scene resolution as expected.

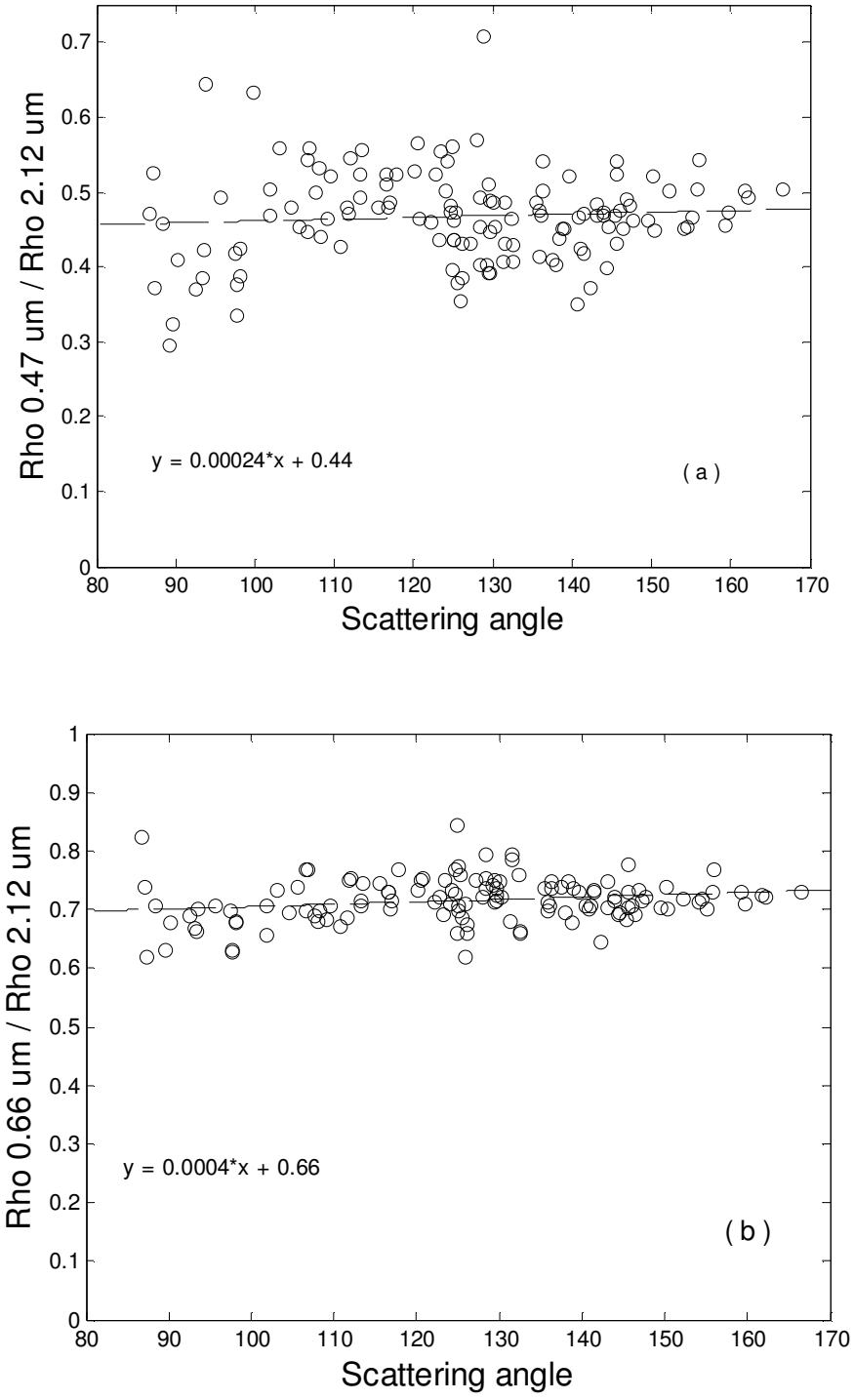

Figure 4.3(a-b) Surface reflectance ratio of (a) 0.47 / 2.12 μm and (b) 0.66 /2.12 μm with respect to (x axis) scattering angle. Mean reflectance ratio for different spatial resolution: 10x10 km surrounded to the nearest pixel to AERONET site at CCNY from 2001 to 2006 with fine mode aerosol dominant atmosphere (masked for inland water bodies)

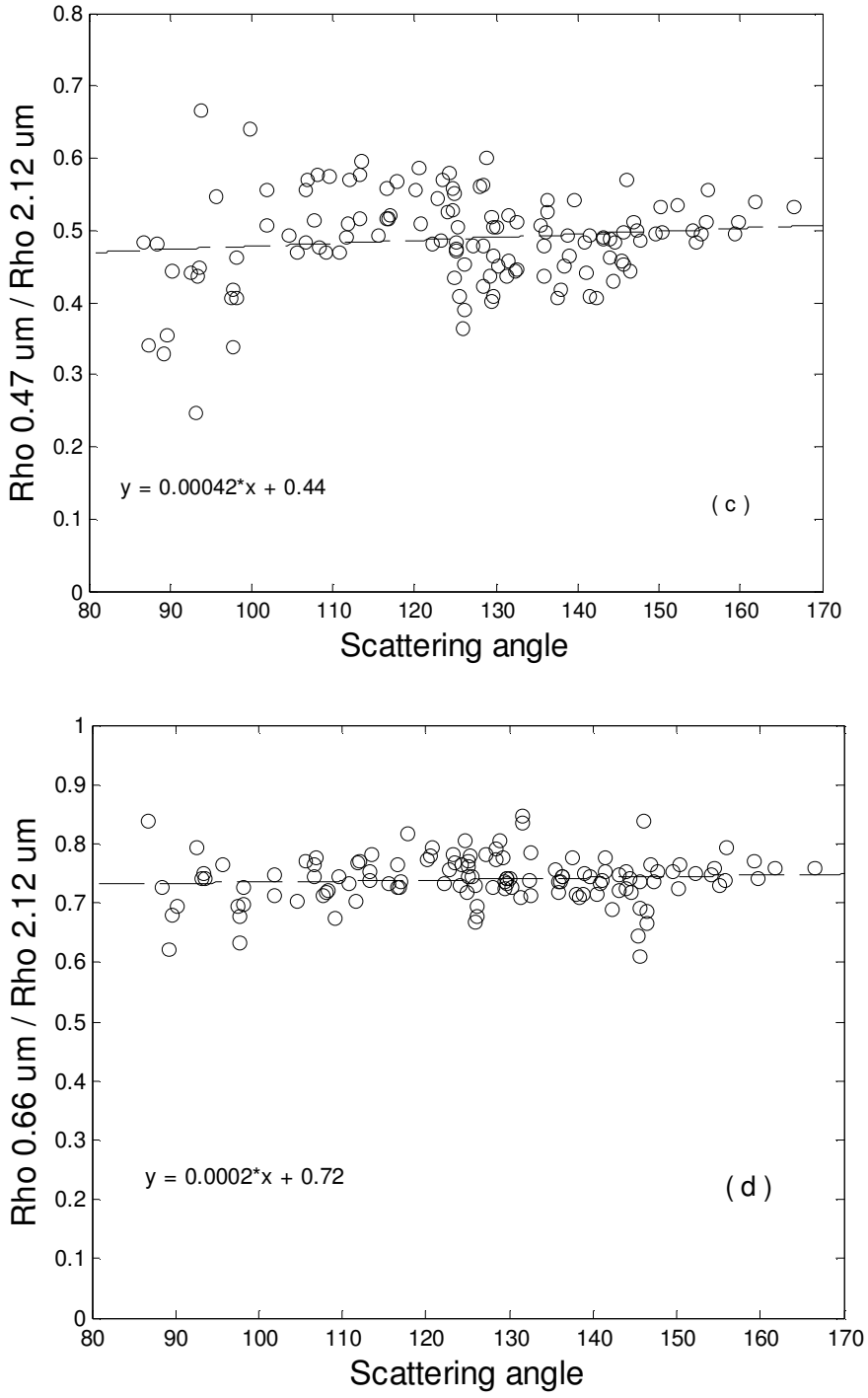

Figure 4.3(c-d) Surface reflectance ratio of (c) 0.47 / 2.12 μm and (d) 0.66 /2.12 μm with respect to (x axis) scattering angle. Mean reflectance ratio for different spatial resolution: 3x3 km surrounded to the nearest pixel to AERONET site at CCNY from 2001 to 2006 with fine mode aerosol dominant atmosphere (masked for inland water bodies)

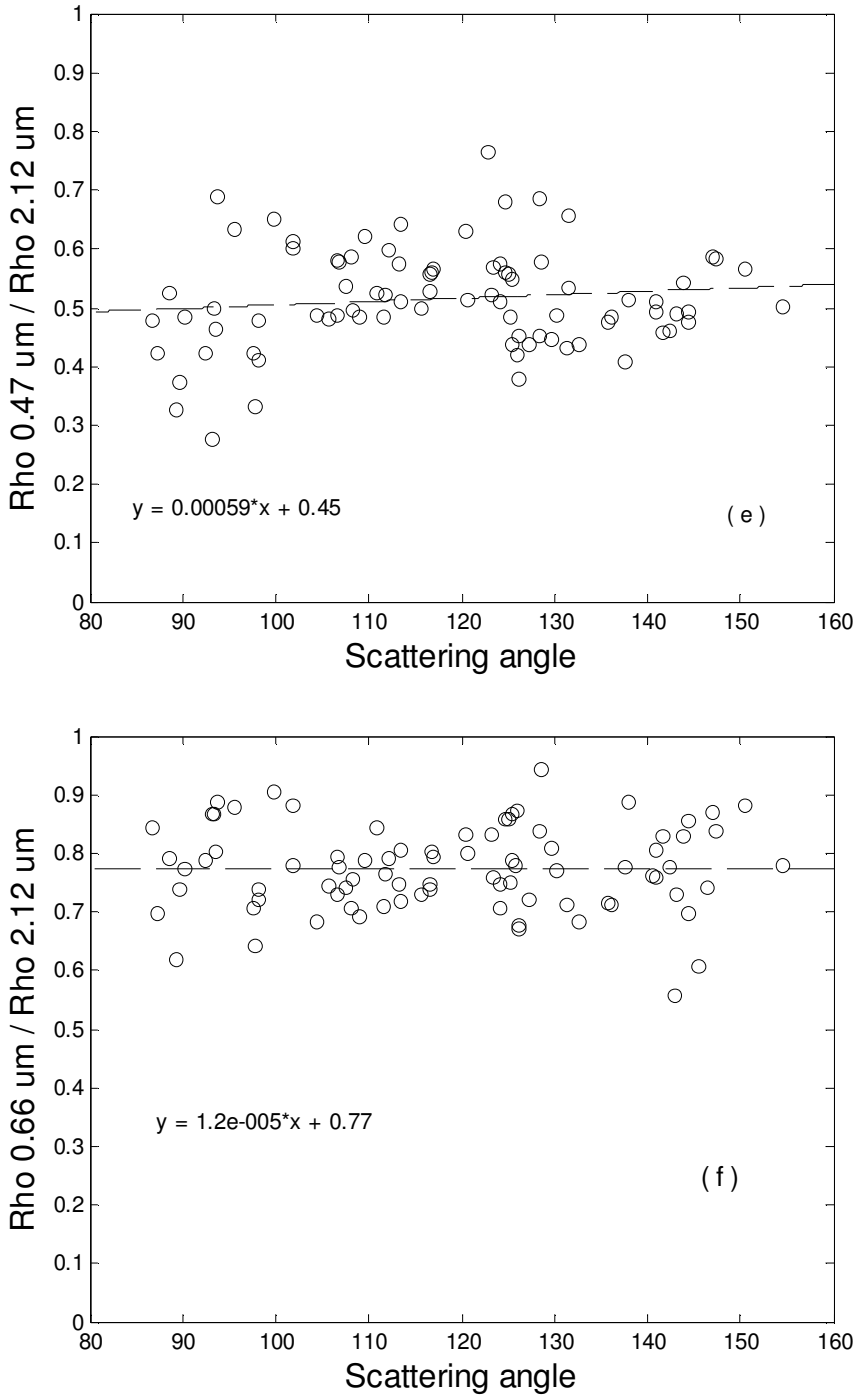

Figure 4.3 Surface reflectance ratio of (e) 0.47 / 2.12 μm and (f) 0.66 /2.12 μm with respect to (x axis) scattering angle. Mean reflectance ratio for different spatial resolution: 1.5x1.5km surrounded to the nearest pixel to AERONET site at CCNY from 2001 to 2006 with fine mode aerosol dominant atmosphere (masked for inland water bodies)

4.3 Vegetated area surface reflectance ratios

It is expected that the VIS/SWIR surface reflectance ratios in vegetation area and urban area (tar, concrete, glasses and miscellaneous materials) are not the same. To see the VIS/SWIR surface reflectance ratios in the urban pixel compares with a vegetation pixel, we choose an area which is about 40 km to the north of New York City which is dominated by vegetation. That area is selected from the combination of the satellite observation and Google Map to ensure all geographic information such as latitude and longitude are accurate. Once the vegetation pixels dominated area is selected, the surface reflectance retrieval can be done by using the same procedure as before. The results of surface reflectance ratios in vegetation dominated area are shown in Fig 4.4(a-b), showing good agreement with the values used in MODIS Collection (4) surface VIS/SWIR correlation coefficients [1] but slightly lower than MODIS Collection (5) assumption. According to MODIS C005 latest version, V5.2, small magnitude negative AOD retrievals are valid. About 10-11% of the total AOD retrievals are now retrieved as below zero, of which only about 3% are below -0.05. This result indicates that V5.2 has reasonable ability to detect very clean condition within the expected error of +/- 0.05 as said by the MODIS ATBD [2]. However, the negative value (or underestimated AOD) AOD can be the result of slightly over estimation in MODIS VIS/SWIR surface ratios assumption over vegetation area. More discussion is shown in Chapter 5 of this thesis with comparison MODIS/ AERONET AOD data from the AERONET station at Billerica, Massachusetts.

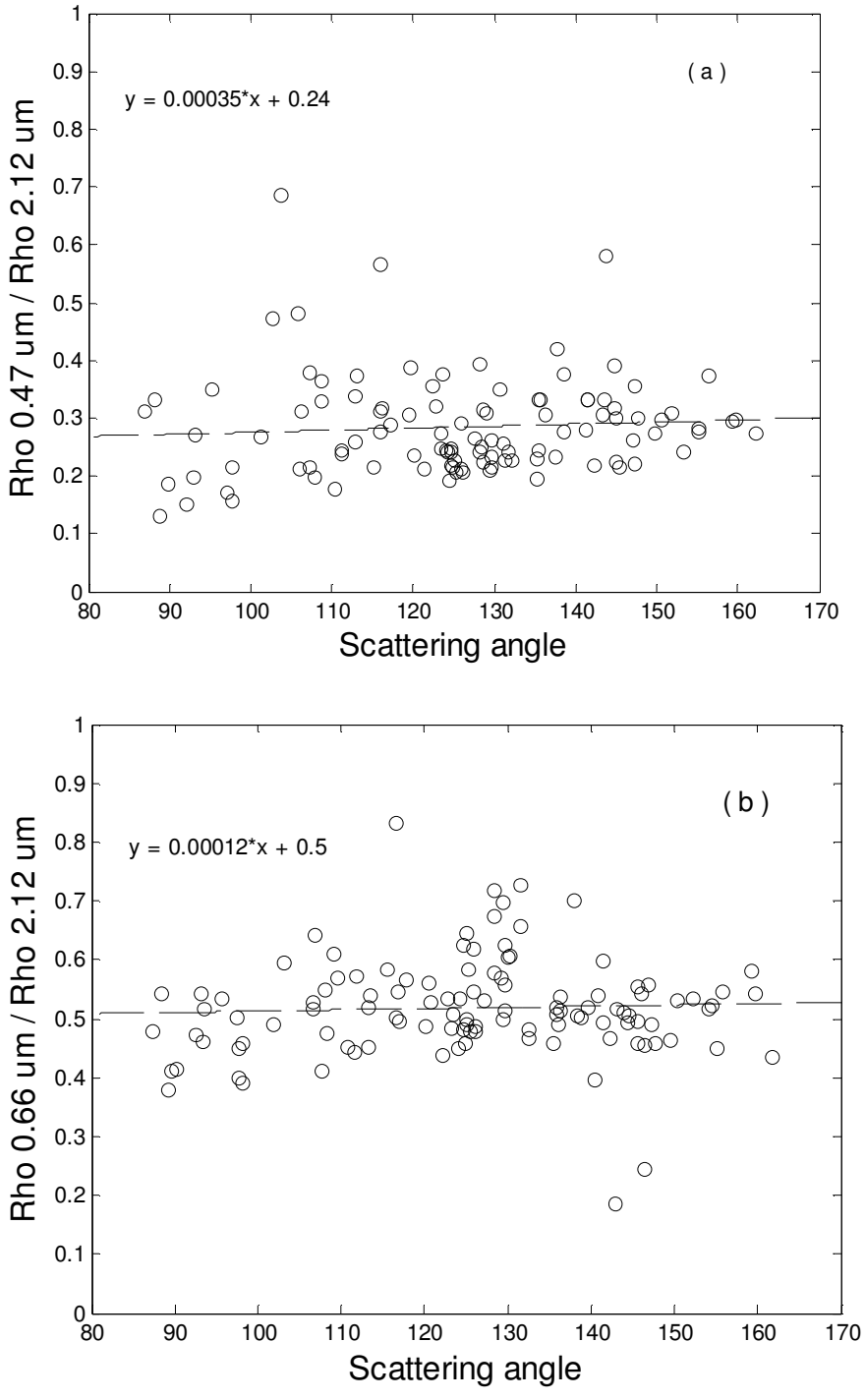

Figure 4.4 Surface reflectance ratio of: (a) 0.47 / 2.12μm and (b) 0.66 /2.12μm with respect to (x axis) scattering angle, mean reflectance ratio of 1.5x1.5km box in vegetated area 40 Km to the North of New York City

Note also that, in Fig 4.4, the fractional error in the retrieval is a little higher than in urban pixels. This is due to the fact that not only is the ground reflection ratio smaller than for urban scenes but the total reflection is lower over vegetation. Therefore, the retrieval of the surface properties is expected to have a larger fractional error.

The results in Fig 4.2 and Fig 4.3 were for a single point around the CCNY site and north of New York City. In both cases, the angular dependence of the surface reflectance ratios of VIS/SWIR was not significant even though the individual VIS and SWIR reflectance varies with the scattering angle in urban area as seen in Fig 4.5. We also note that angular dependence of VIS and SWIR reflectances is less in the vegetation area; see more details in [2].

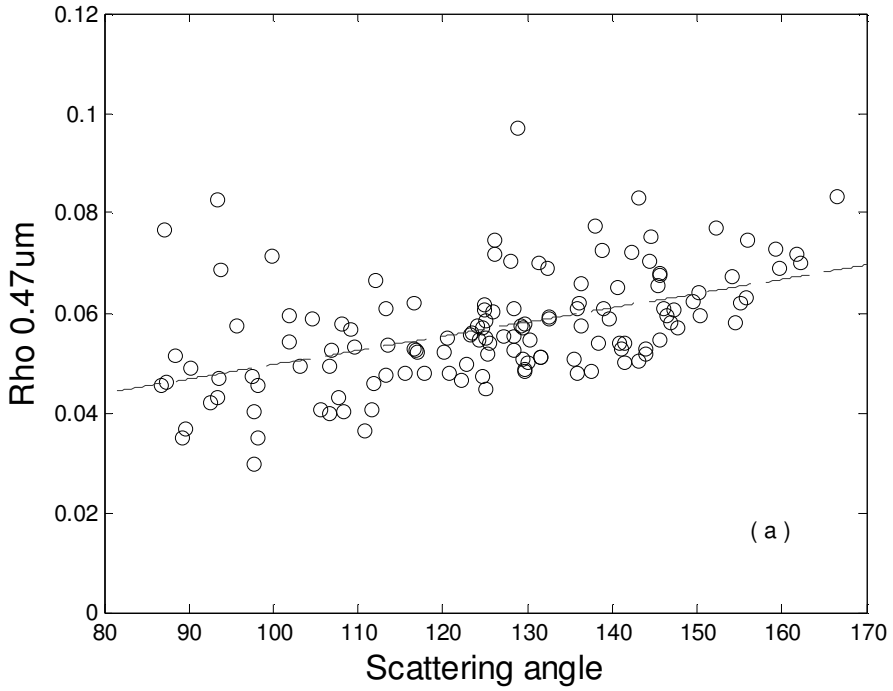

Figure 4.5 (a) Retrieved surface reflectance of the 10km box surrounding CCNY at 0.47μm

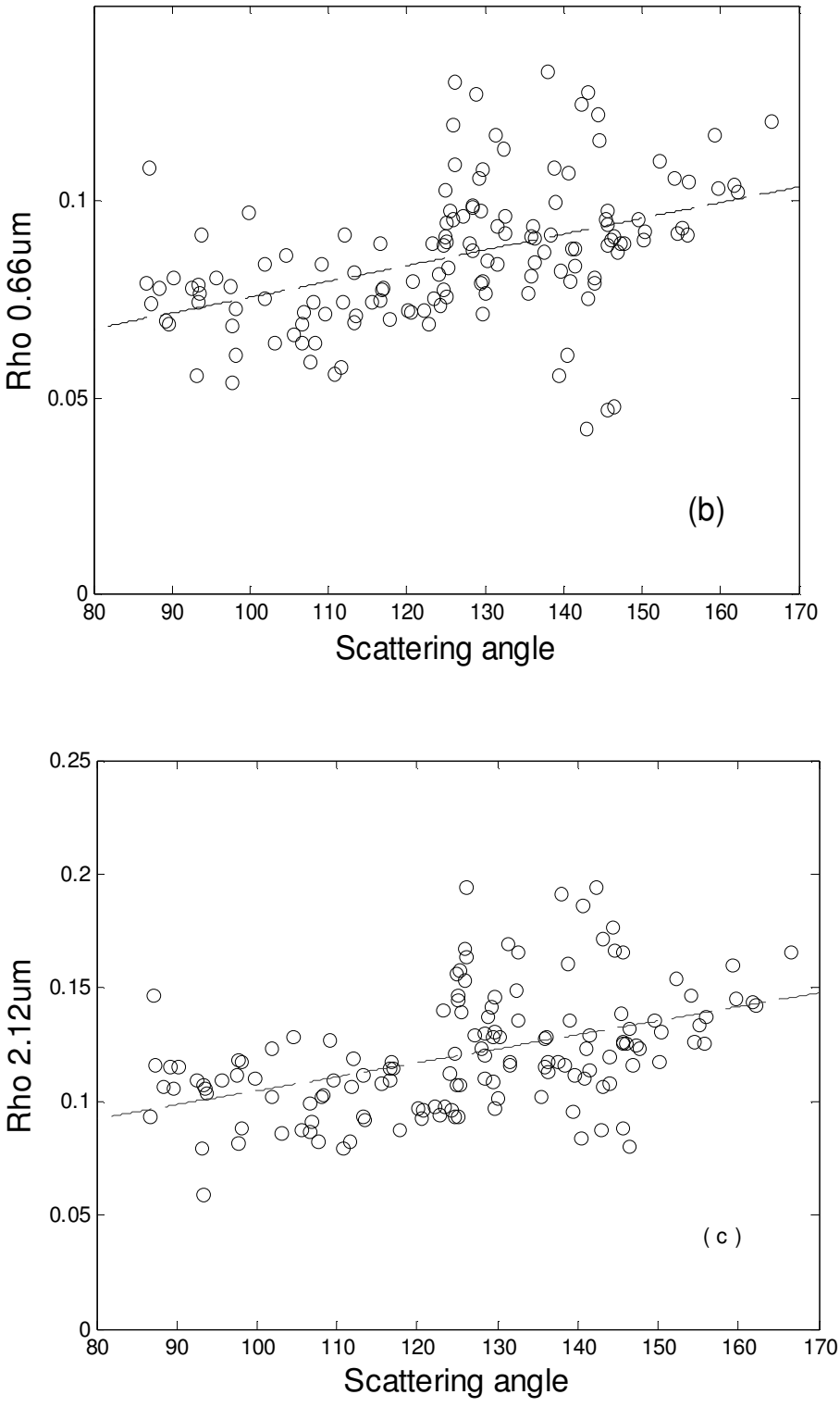

Figure 4.5(b-c) Retrieved surface reflectance of the 10km box surrounding CCNY (b) 0.66μm (c) 2.12μm

4.4 Surface reflectance ratios map over New York City areas

Determination of VIS/SWIR surface reflectance ratio as the mean correlation coefficient of each pixel (averaged over all angles) within a reasonable distance from the CCNY site is reasonable due to the results from the previous section (i.e. Fig 4.3, 4.4). Therefore, it is possible to obtain correlation maps for the entire region. The results of VIS/SWIR surface reflectance ratios at 1.5 km resolution are shown in Fig 4.6 and clearly illustrate the need for a regional surface correlation model.

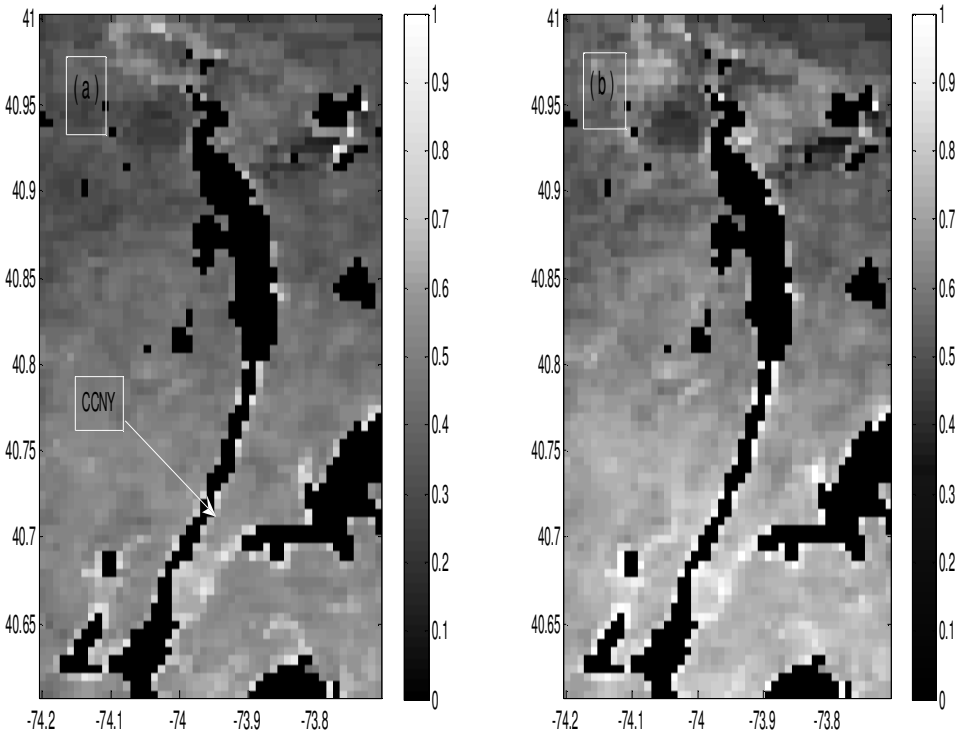

Figure 4.6 VIS/SWIR correlation coefficient ratios of 0.47/2.12 μm ((a) left panel) and 0.66/2.12 μm ((b) right panel) in nearby New York City area

The regional map extends from 40.61N latitude to 41.4N Latitude, 74.2 W longitudes to 73.71 W longitudes. Basically the VIS/SWIR ratios are significantly higher in the urban area compared to the vegetated areas, as shown in Fig 4.6. In the northern vegetated areas, the VIS/SWIR 0.47/2.12 µm ratio is ~ 0.25 and the 0.66/2.120 µm ratio is ~0.5 to 0.6 which agrees well with the MODIS Collection (5) documentation but the VIS/SWIR ratio in the urban area is much higher. This is particularly clear in urban scenes on both sides of the Hudson River (i.e., New Jersey and Manhattan). The modification in the surface properties with surface type can be illustrated by plotting the MVI map.

The mean MVI of the New York City area (NYC) is as shown in Fig 4.7.

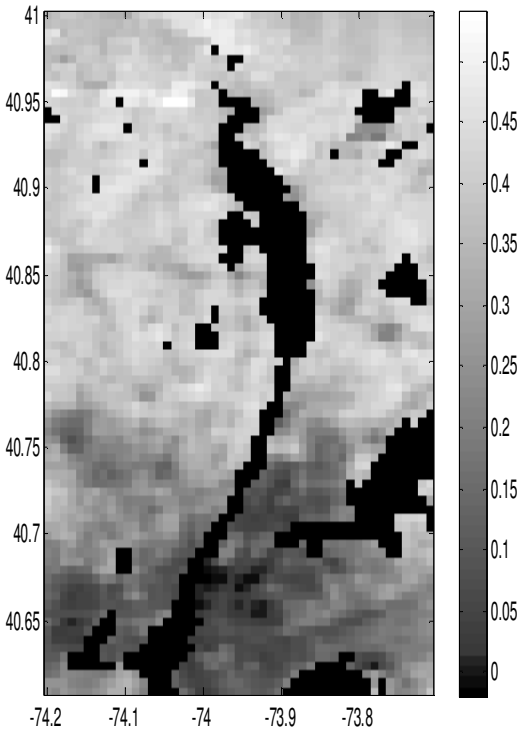

Figure 4.7 Modified Vegetation Index of NYC areas

In the area north of the NYC, the MVI is higher and also associates with lower VIS/SWIR surface reflectance ratios, Fig 4.7. In fact, this observation does not agree with the Collection (5) surface algorithm assumption [2].

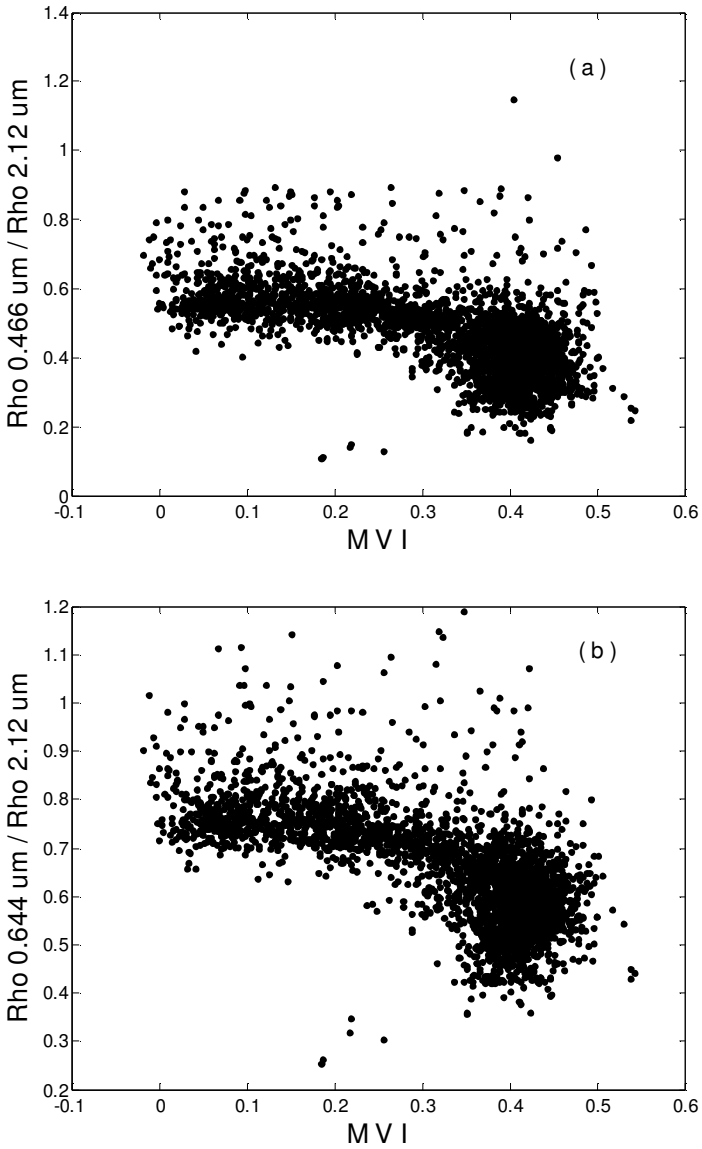

Figure 4.8 MVI versus VIS/SWIR surface reflectance ratios (a) 0.47/2.12 µm (b) 0.66/2.12 µm which is opposite to the Fig 4.8 results. as seen in the C005 correlation coefficient model as function of MVI plotted in Fig 4.9

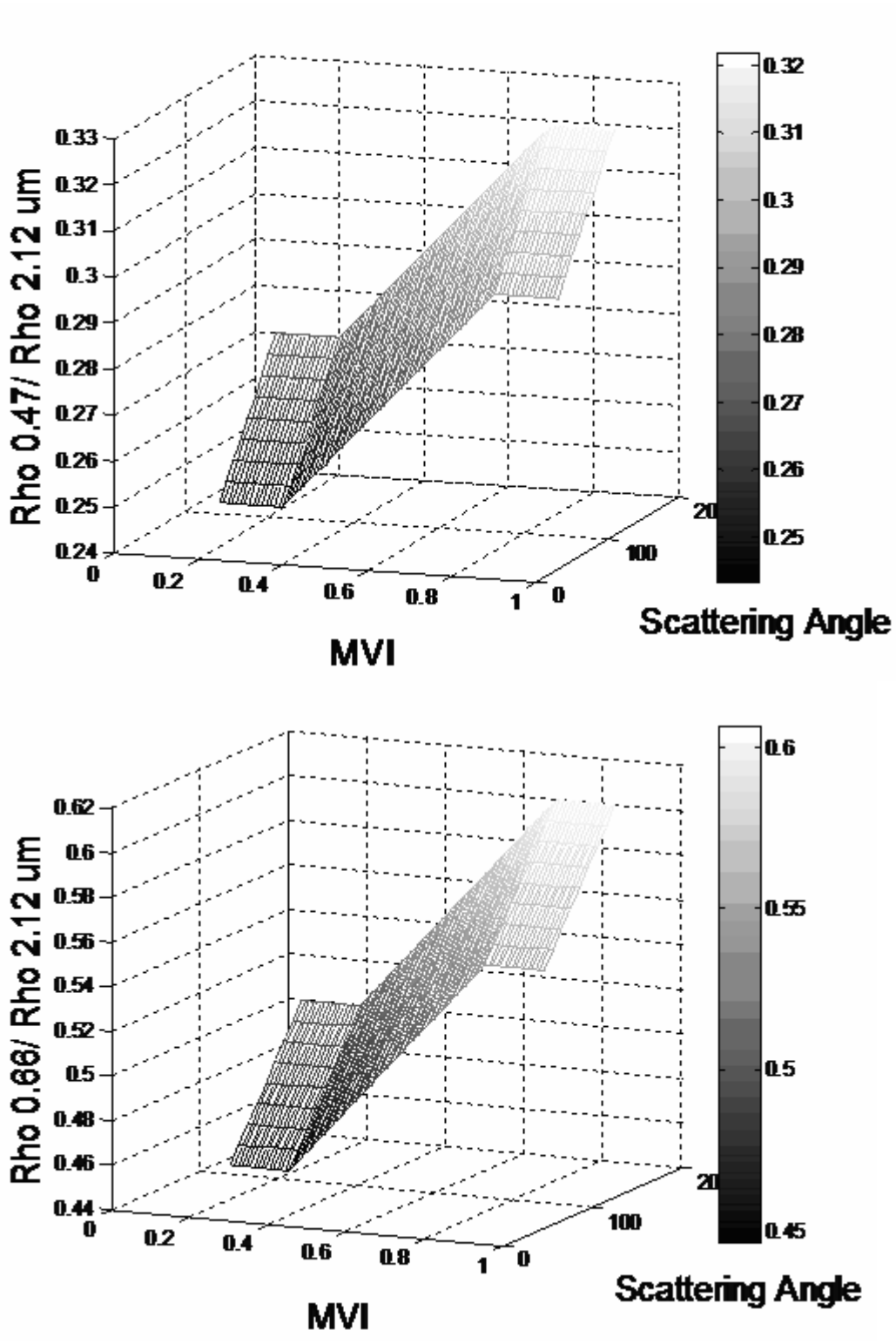

Figure 4.9 MVI Vs VIS/SWIR surface reflection ratios of MODIS land algorithm, solid line is the Collection (4) assumption

The fact that the surface reflectance ratios of VIS/SWIR in the regional retrieval opposes the operational algorithm model is a major reason why MODIS AOD retrieval overestimated in urban area and slightly underestimated in vegetated area. More discussion of this issue is provided in Chapter 5.

References

[1] Kaufman, Y.J.; Tanre, D. “Algorithm for Remote Sensing of Tropospheric Aerosol from MODIS” Mod04 ATBD Document (1998)

[2] L. A. Remer, D. Tanré, Y. J. Kaufman, R. Levy, and S. Mattoo, “ALGORITHM FOR REMOTE SENSING OF TROPOSPHERIC AEROSOL FROM MODIS: Collection 005” ATBD document

[4] Levy, R. C., L. A. Remer, et al. (2005). "Evaluation of the MODIS aerosol retrievals over ocean and land during CLAMS." Journal of the Atmospheric Sciences **62**(4): 974-992.

[4] R. C. Levy, L. A. Remer, and Y. J. Kaufman “Effects of Neglecting Polarization on the MODIS Aerosol Retrieval Over Land” *IEEE Trans. Geos. Rem. Sens.,* vol 42 Pp 2576-2583, 2004

CHAPTER 5

AOD retrieval procedure and results

In this chapter, MODIS land AOD retrieval procedure is discussed in more details. MODIS operational land algorithms use radiance measured in two visible (0.47 and 0.66μm) and one short wave infrared channel (2.12μm) to retrieve AOD in visible channel. Based on MODIS land algorithm, a new AOD retrieval can be done with refined VIS/SWIR surface ratios model derived from previous chapter insert directly into the operational procedure. The results are shown that using regional refined surface model AOD retrieval over land is significantly improved in New York City urban area. Moreover, the AOD retrieval procedure with refined surface model is validated with another heavily populated urban area, Mexico City. Similar improvement and results are found. In addition to that, MODIS AOD retrieval over vegetated area is evaluated with AERONET station at Billerica, Massachusetts and some interesting result are found. Finally, effect of AOD retrieval in Lambertian surface and BRDF surface reflectance assumption is analyzed and shown that the error due to Lambertian assumption is within the order of error due to standard deviation in VIS/SWIR ratio.

Introduction

MODIS retrieves clear sky (after masking cloud) AOD over ocean and land, using two separate algorithms. In fact, both algorithms make use of LUT, wherein TOA spectral reflectance is simulated by radiative transfer model calculations [1]. The ocean algorithm retrieves AOD in seven wavelength bands, centered near 0.47, 0.55, 0.66, 0.87, 1.24, 1.64, and 2.12 μm, by inverting reflectance in six of the seven bands (because 0.47 μm is contaminated by variable ocean surface reflectance and is not used in the retrieval). The isolation of the signals from atmosphere and surface is relatively easy in the ocean algorithm due to negligible signal from the ocean surface. Unlike the ocean algorithm, the land algorithm has a challenge to separate atmospheric signal from TOA radiance since the reflectance from the ground is very significant. This explains our efforts in the last chapter in developing regional correlation maps. Once these correlation models are developed, the AOD is retrieved by simultaneous TOA matchup in the three bands (0.47, 0.66, and 2.12 μm).

5.1 MODIS operational land aerosol retrieval algorithm

The MODIS aerosol retrieval operational algorithm over land surface is based on a LUT approach, i.e., radiative transfer calculations of TOA reflectance are pre-computed for a set of aerosol models (4 fine modes and 1 coarse mode). Because the MODIS over-land retrieval employs only three channels, it is not able to retrieve the fine aerosol model [2]. Therefore, the aerosol retrieval algorithm must assign the fine aerosol model a priori of the retrieval by using cluster analysis. In

particular, the aerosol model is assigned as a function of season and location from a global aerosol models obtained from AERONET. For example, non absorbing urban aerosol model is assigned to the U.S. East Coast such as New York City for all seasons.

The details of the aerosol retrieval assuming knowledge of the correlation coefficient models are outlined as follows:

1. TOA reflectance signal (cloud cleared Level-2 product in 10 x10 km resolution) at band 7 (2.12μm) measured by MODIS sensor (Terra satellite in this thesis) can be converted to surface reflectance at the SWIR by subtracting the path reflectance and compute with others atmospheric parameters (such as atmospheric *s* parameter, upward and down ward transmission) from pre-calculated LUT. Note LUT parameters at 2.12 μm can be interpolated to exact satellite-solar geo-location to mimic the atmospheric parts of the TOA reflectance. The AOD is unknown at this stage; therefore surface reflectance at SWIR varies as a function of AOD (τ), (i.e.; AOD = 0, 0.25, 0.5, 1.0, 2.0, 3.0, and 5.0) for two size parameters (one fine mode and one coarse mode aerosol model). SWIR surface reflectance can be calculated as Eq 5.1

$$\rho_{2.12}^{s,f,c}(\tau) = \frac{\rho_{2.12}^{atm,f,c}(\tau) - \rho_{2.12}^{measured}}{\overline{s^{f,c}(\tau)}(\rho_{2.12}^{atm,f,c}(\tau) - \rho_{2.12}^{measured})T_d{}^{f,c}(\tau)T_u{}^{f,c}(\tau)} \qquad (5.1)$$

2. Then, visible surface reflectance can be calculated from the SWIR 2.12 μm surface reflectance. This is done by correlate the SWIR surface reflectance into visible surface reflectance directly. Details of this step in MODIS Collection (5) are as follow:

(a) calculate MVI from band 5 (1.24μm) and band 7 (2.12μm) measured TOA reflectance

$$MVI = \frac{\rho_{1240}^{TOA} - \rho_{2120}^{TOA}}{\rho_{1240}^{TOA} + \rho_{2120}^{TOA}} \qquad \text{(4.2 of Chapter 4)}$$

(b) Since MVI is available, VIS surface reflectance can be calculated from correlation coefficient of VIS/SWIR as follow:

$$\rho_{0.66}^{s,f,c}(\tau) = f(\rho_{2.12}^{s,f,c}(\tau)) = \rho_{2.12}^{s,f,c}(\tau) * slope_{0.66/2.12} + y\text{int}_{0.66/2.12} \qquad (5.2)$$

$$\rho_{0.47}^{s,f,c}(\tau) = f(\rho_{0.66}^{s,f,c}(\tau)) = \rho_{0.66}^{s,f,c}(\tau) * slope_{0.46/0.66} + y\text{int}_{0.47/0.66} \qquad (5.3)$$

where

$$slope_{0.66/2.12} = slope_{0.66/2.12}^{MVI} + 0.002\Theta - 0.27 \qquad (5.4)$$

$$y\text{int}_{0.66/2.12} = -0.00025\Theta + 0.033684$$

$$slope_{0.47/0.66} = 0.49 \qquad (5.5)$$

$$y\text{int}_{0.47/0.66} = 0.005 \qquad (5.6)$$

where in turn

$$slope_{0.66/2.12}^{MVI} = 0.48; MVI < 0.25 \qquad (5.7)$$

$$slope_{0.66/2.12}^{MVI} = 0.58; MVI > 0.75 \qquad (5.8)$$

$$slope_{0.66/2.12}^{MVI} = 0.48 + 0.2(MVI - 0.25);\ 0.25 \le MVI \le 0.75 \qquad (5.9)$$

(c) Once 0.47μm and 0.66μm surface reflectances are accessible, TOA reflectance for all 3 bands (0.47μm, 0.66μm and 2.12μm) can be recomputed with atmospheric parameters from LUT. At this stage, simulated (or computed) TOA reflectance in all bands vary as a function of AOD for two sizes (fine mode and coarse mode aerosol model)

$$\rho_\lambda^f(\tau) = \rho_\lambda^{af} + T_d{}^f T_u{}^f \rho_\lambda^s / (1 - s_\lambda^f \rho_\lambda^s) \qquad (5.10)$$

$$\rho_\lambda^c(\tau) = \rho_\lambda^{ac} + T_d{}^c T_u{}^c \rho_\lambda^s / (1 - s_\lambda^c \rho_\lambda^s) \qquad (5.11)$$

where ρ_λ^{af} and ρ_λ^{ac} are the fine and coarse model atmospheric path reflectance, $T_{d\lambda}^{f}$ and $T_{d\lambda}^{c}$ are normalized downward fluxes for zero surface reflectance, T_λ^f and T_λ^c represent upward total transmission into the satellite field of view, and s_λ^f and s_λ^c are atmospheric albedo.

Note, $\rho^{a,f,c} = \rho^{a,f,c}(\tau,\theta_0,\theta,\phi), T_d{}^{f,c} = T_d{}^{f,c}(\tau,\theta_0), T_u{}^{f,c} = T_u{}^{f,c}(\tau,\theta), s^{f,c} = s^{f,c}(\tau)$, $\rho^{s,f,c} = \rho^{s,f,c}(\tau)$ therefore those terms are the angular and AOD dependence and are contained within LUT.

3. Using calculated TOA reflectance at 0.47, 0.66, and 21.2μm, apparent spectral reflectance of the combined fine mode and coarse mode can be recalculated by combination of fine and coarse mode aerosol models reflectance varies with weighted sum (η) of fine and coarse mode aerosol.

$$\rho_\lambda^* = \eta\rho_\lambda^f + (1-\eta)\rho_\lambda^c \qquad (5.12)$$

where ρ_λ^f and ρ_λ^c are the each composite of the surface reflectance ρ_λ^s and atmospheric path reflectance of the separate aerosol model.

Note that this superposition is possible since we are combining only components with the same optical depth so the normalized weighted superposition has the same optical depth as the pure components.

4. Then the algorithm attempts to find the AOD at 0.55 μm and the surface reflectance at 2.12 μm that exactly matches the MODIS measured reflectance at 0.47 μm. Note that this is done within loop of fine mode weight (η) in Eq. 5.12.

5. In each loop of fine mode weight (η), the apparent TOA reflectance of all land bands (0.47, 0.66 and 2.12μm) can be recomputed with AOD derived at 0.55μm. Therefore TOA reflectances are available for each fine mode weight (η) for all 3 land bands.

6. Final step of this procedure is to find the right fine mode weight (η) from the best solution of the Equations (5.13 a,b,c).There will be some error, ε, at 0.66 μm. The best solution is the one where the error at 0.66 μm is minimized.

$$\rho^{m}_{0.47} - \rho^{*}_{0.47} = 0 \qquad (5.13a)$$
$$\rho^{m}_{0.66} - \rho^{*}_{0.66} = \varepsilon \qquad (5.13b)$$
$$\rho^{m}_{2.12} - \rho^{*}_{2.12} = 0 \qquad (5.13c)$$

Primary products are AOD at 0.55μm, fine mode weight (η) and the surface reflectance at 2.12μm.The error ε is also noted.

The flow chart of the MODIS over land algorithm is shown in Fig 5.1.

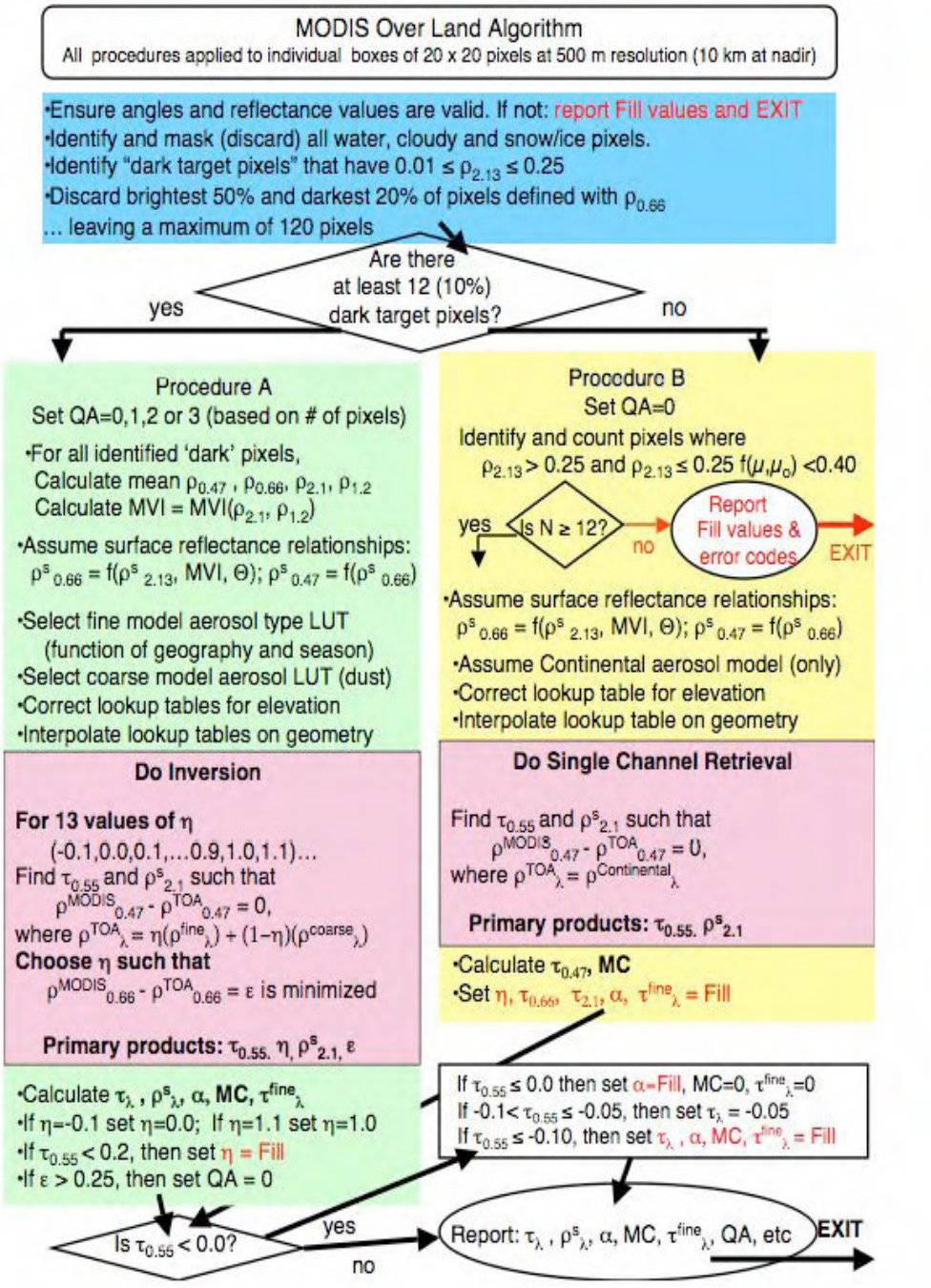

Figure 5.1 Flowchart illustrating the derivation of aerosol over land for MODIS Collection (5)

5.2 Improvement in AOD retrieval using regional VIS/SWIR surface model

As discussed earlier, the correlation coefficient ratios results from the previous chapter are significantly higher than the MODIS Collection (5) version. When this surface reflection in VIS wavelengths are approximated as a linear relationship with SWIR surface reflectance and substitute back into the AOD retrieval processing stream, a significant improvement as seen in Fig 5.2 is obtained. Note however that the fluctuations increase dramatically with higher resolution which is clearly due to the large uncertainties in the correlation coefficient due to water contamination. When the water body is masked and the procedure is repeated, the uncertainty even at higher resolution is quite small as seen in Fig 5.3. The standard deviation both before and after masking inland water body is shown in Table 5.1 to help in the comparison. In particular, removing the water contamination greatly improves the STD error in the correlation coefficients and the results also become more independent of the spatial resolution scale can be found. This is reasonable since the water contamination is due to a narrow river which is most prominent when considering observations on the 1.5km scale. The increase in these correlation coefficients in the absence of a suitable mask are due to the fact that the SWIR signal is negligible while the VIS signals are not resulting in an anomalously high coefficient. To see how good the retrieval is, we can benchmark it against the MODIS expected error in AOD retrieval over land of $\pm(0.05+0.15\tau)$ where τ is AOD. Fig 5.4 shows that AOD retrieved by using refined surface ratios in 3 resolutions (10x10km, 3x3km, 1.5x1.5km) are well

within the expected error limits while MODIS L2 derived AOD is significantly overestimated.

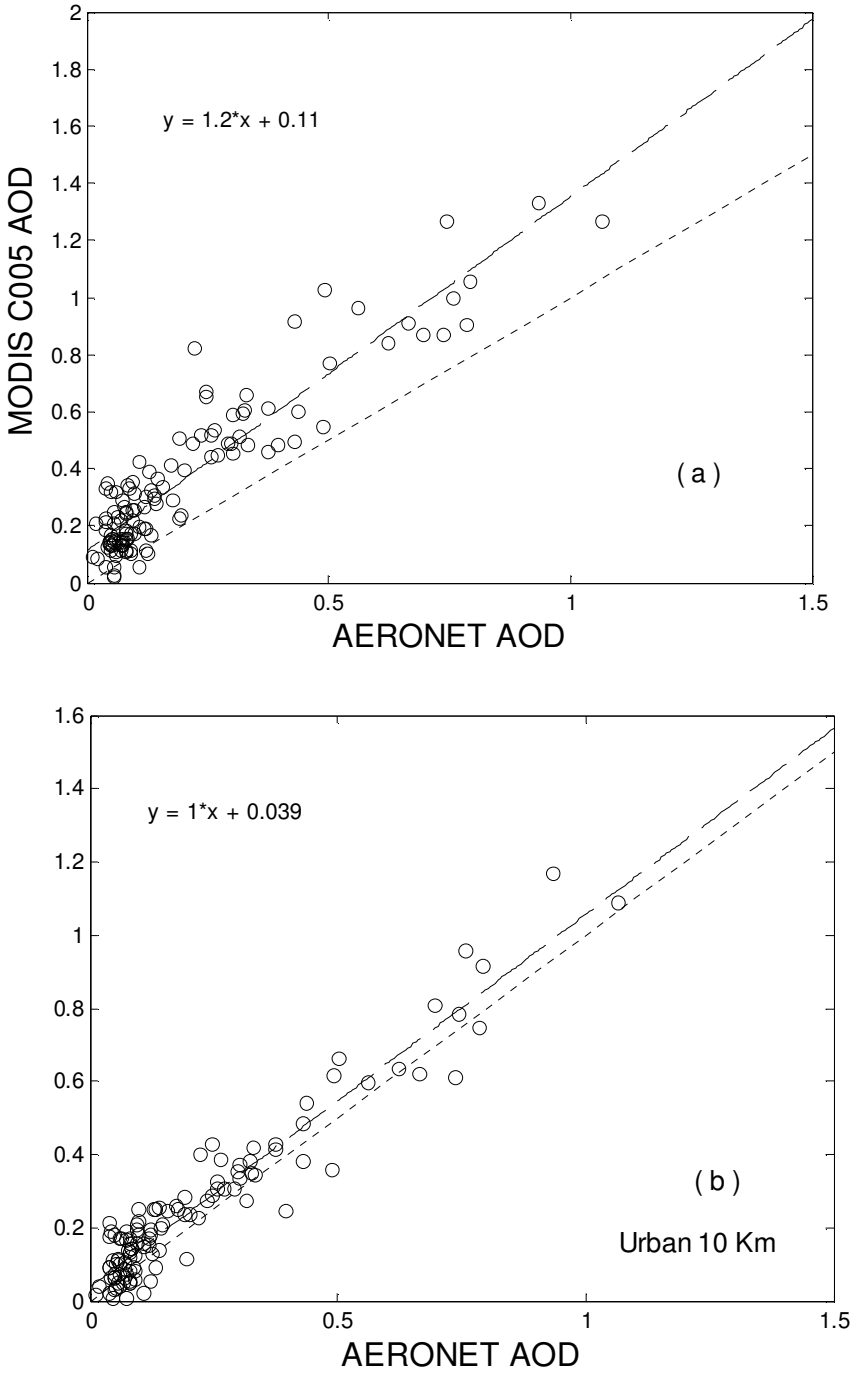

Figure 5.2 (a) MODIS L2 Aerosol Optical Depth at 0.55μ*m* compared with 4 hour (~ 2hr before and 2hr after MODIS (Terra) satellite overpass time) average of AERONET aerosol optical thickness. (b) Retrieved AOD with new surface reflectance VIS/SWIR ratio (10x10km resolution) plot with average of AERONET aerosol optical thickness. The dot line is the one to one line and the dash line is the linear fit line. (CIMEL sun-photometer data acquired in New York City (the City College of New York) from 2001 to 2007 (without inland water areas and rivers masked)

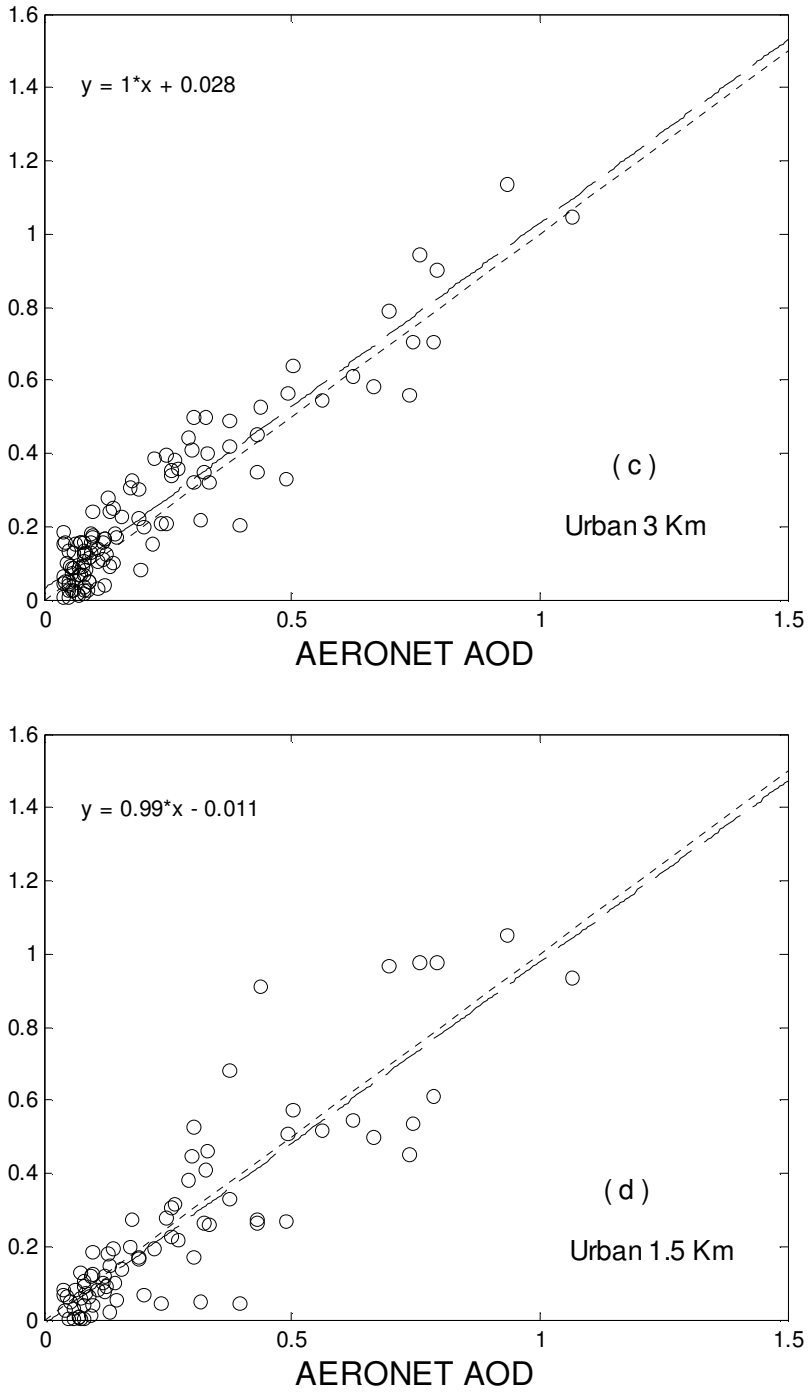

Figure 5.2 (c) and (d) are retrieved AOD with new surface reflectance VIS/SWIR ratio (3x3 km and 1.5x1.5km resolution respectively) plot with average of AERONET aerosol optical thickness. The dot line is the one to one line and the dash line is the linear fit line. (CIMEL sun-photometer data acquired in New York City (the City College of New York) from 2001 to 2007 (without inland water areas and rivers masked)

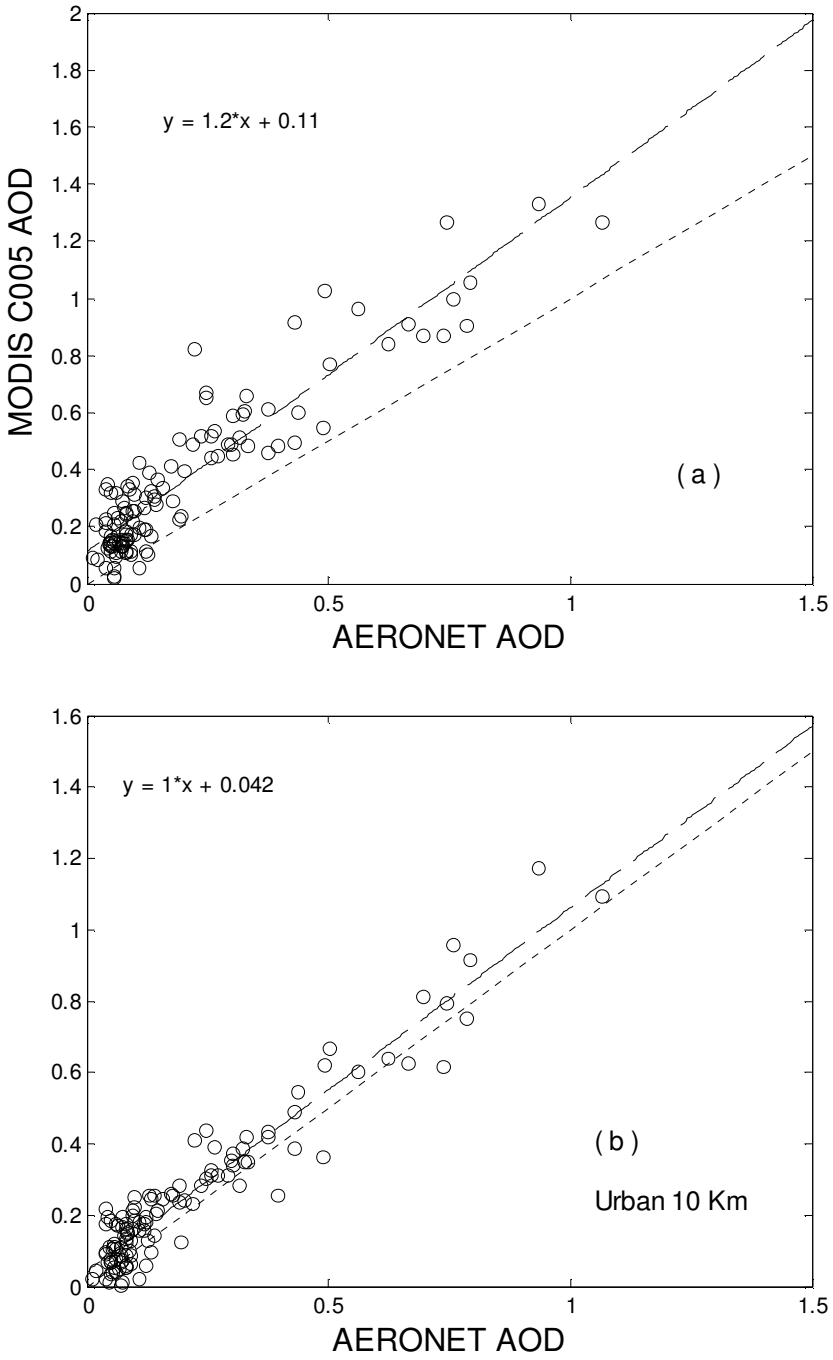

Figure 5.3 (a) MODIS L2 Aerosol Optical Depth at 0.55μm compared with 4 hour (~ 2hr before and 2hr after MODIS (Terra) satellite overpass time) average of AERONET aerosol optical thickness. (b) Retrieved AOD with new surface reflectance VIS/SWIR ratio (10x10km resolution) plot with average of AERONET AOD. The dot line is one to one line and the dash line is linear fit line. (CIMEL sun-photometer data acquired in New York City (the City College of New York) from 2001 to 2007 (with inland water areas and rivers masked

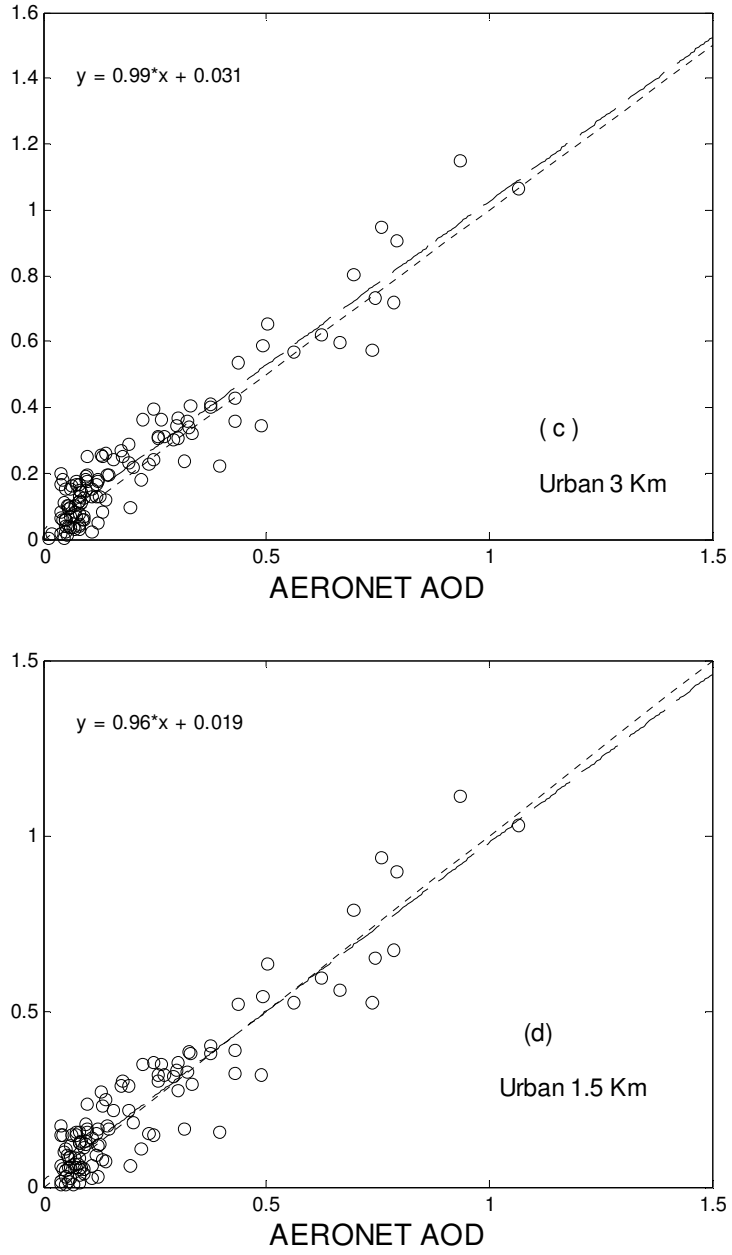

Figure 5.3 (c) and (d) are retrieved AOD with new surface reflectance VIS/SWIR ratio (3x3 km and 1.5x 1.5km resolution respectively) plot with average of AERONET AOD. The dot line is one to one line and the dash line is linear fit line. (CIMEL sun-photometer data acquired in New York City (the City College of New York) from 2001 to 2007 (with inland water areas and rivers masked)

Table 5.1 VIS/SWIR surface reflectance ratios mean and standard deviation of no mask inland water body and river and mask inland water body and river

	No Mask				Mask			
	470/2120 nm		660/2120 nm		470/2120 nm		660/2120 nm	
	Mean	std	Mean	std	mean	std	mean	std
10x10	0.4683	0.0746	0.7256	0.0565	0.4671	0.0619	0.7155	0.0378
3x3	0.4863	0.1052	0.7741	0.1075	0.4882	0.0636	0.7402	0.0404
1.5x1.5	0.5564	0.2153	0.9326	0.2761	0.5153	0.0858	0.7734	0.0729

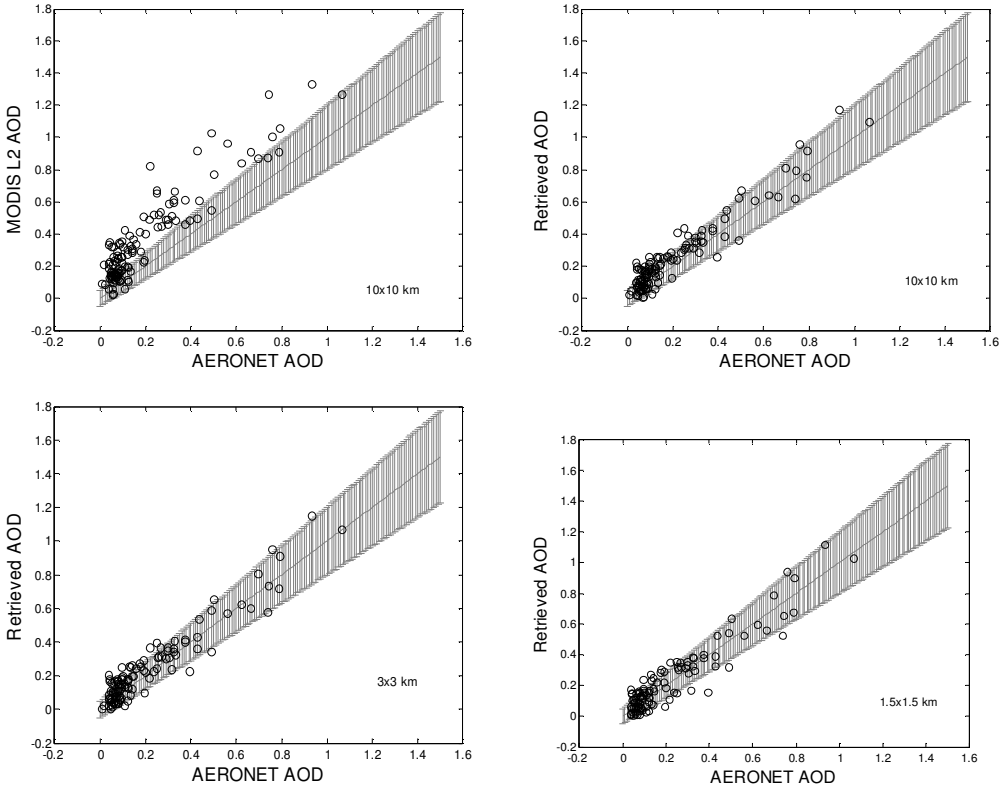

Figure 5.4 AERONET retrieved AOD versus (top left) MODIS derived L2 AOD. Retrieved AOD with modified 10x10 km surface model (top right) Retrieved AOD with modified 3x3 km surface model (bottom right) Retrieved AOD with modified 1.5x1.5 km surface model (bottom left). Error bar is the expected error of MODIS land algorithm $\pm(0.05+0.15\tau)$

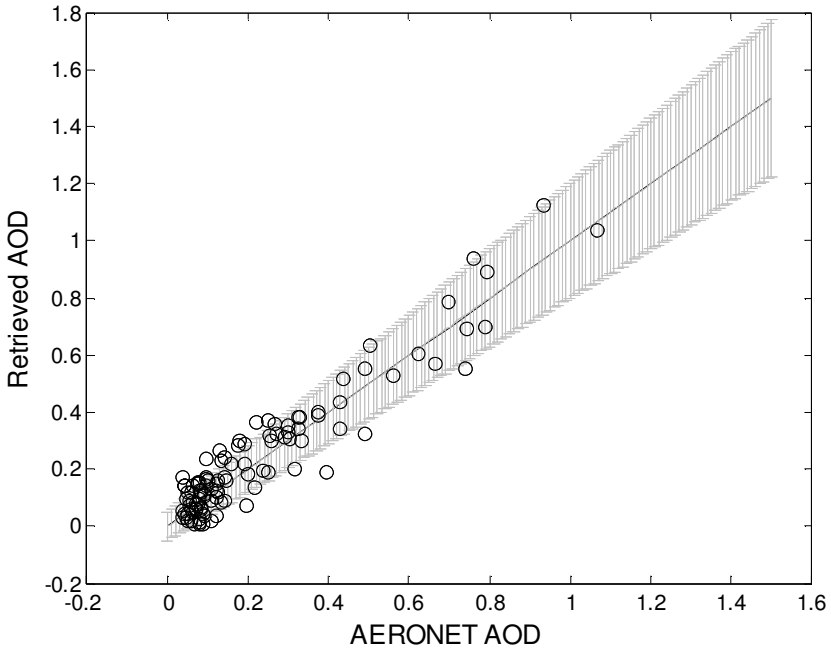

Figure 5.5 Retrieved AOD using mean surface reflectance VIS/SWIR ratio in 1.5x1.5 km resolution plot against AERONET AOD. Error bar is the expected error of MODIS land algorithm $\pm(0.05+0.15\tau)$

Clearly, the accuracy in this approximation is limited to the STD error seen in these correlation coefficients (shown in table 5.1). Therefore, in assessing AOD retrieval accuracy, the uncertainty in the correlation coefficients must be included. We analyze the 1.5 km resolution case since the 1.5km resolution has the highest STD error of the 3 resolutions. The results of this sensitivity exercise are shown in Fig 5.6 where the uncertainty in aerosol retrieval is determined by reprocessing the MODIS data using the full variability of the correlation coefficients.

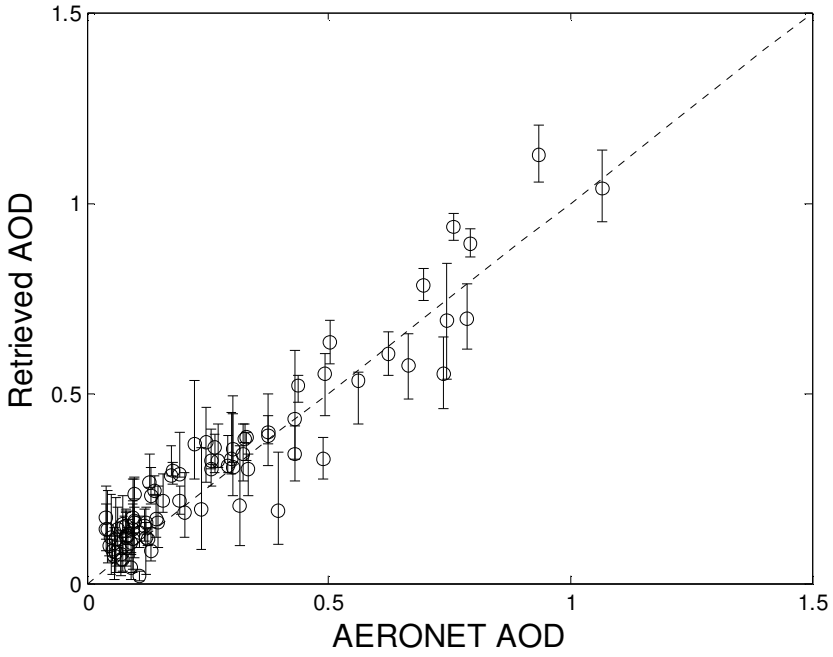

Figure.5.6. Retrieved AOD with mean (and standard deviation) of surface reflectance VIS/SWIR ratio in 1.5x1.5 km resolution plot against with average of AERONET AOD

In particular, defining $C_j = R_g(\lambda_j)/R_g(2120)$, the retrievals using $\overline{C}_j \pm \sigma(C_j)$ are processed. This is sufficient due to the high correlation between the two correlation coefficients, so that both regressions coefficients can be considered as co varying. We see in fact that the retrieved AOD is retrieved within reasonable limits. However, it should be noted that a constant correlation coefficient does not imply a Lambertian surface albedo in general. Comparison of STD variation error with the errors when using a full BRDF [3] treatment is discussed in section 5.5 of this chapter.

At this stage, since the surface correlation map is generated in Fig 4.5 of chapter 4, we can finally retrieve an AOD map for the entire New York City area within the operational algorithm at higher resolution where the only change is in

the correlation surface models. As an example, a relatively cloud free day is taken (seen by (AERONET) CIMEL radiometer data, Fig 5.7.) and used to explore the retrieved AOD using both the operational and regional surface models.

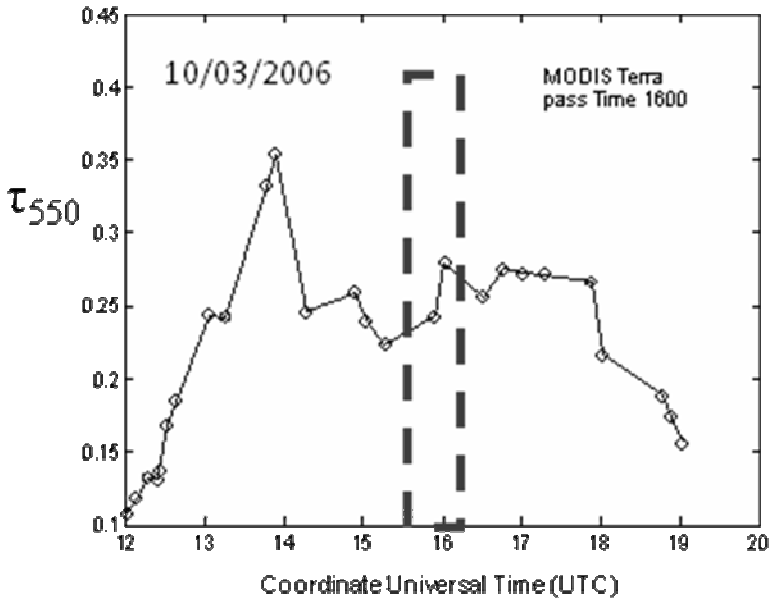

Figure 5.7 Time versus AERONET derived AOD

The results are shown in Fig 5.8. The right panel (Fig 5.8 b) is processed with the Collection (5) algorithm while the left panel (Fig 5.8 a) uses the modified regional model. Clearly, a significant improvement can be observed as artificial hot spots in the AOD map are reduced. Although the spatial distribution cannot be directly validated, by examining the histogram of data over the region we can assess the statistics of aerosol AOD and compare to the statistics based on the AERONET time series which we use as an imperfect proxy in place of distributed AOD data. In Fig.5.9, the statistics of the regional AOD map results are in much better agreement to the statistics seen in the AERONET time series retrieval of Fig 5.7.

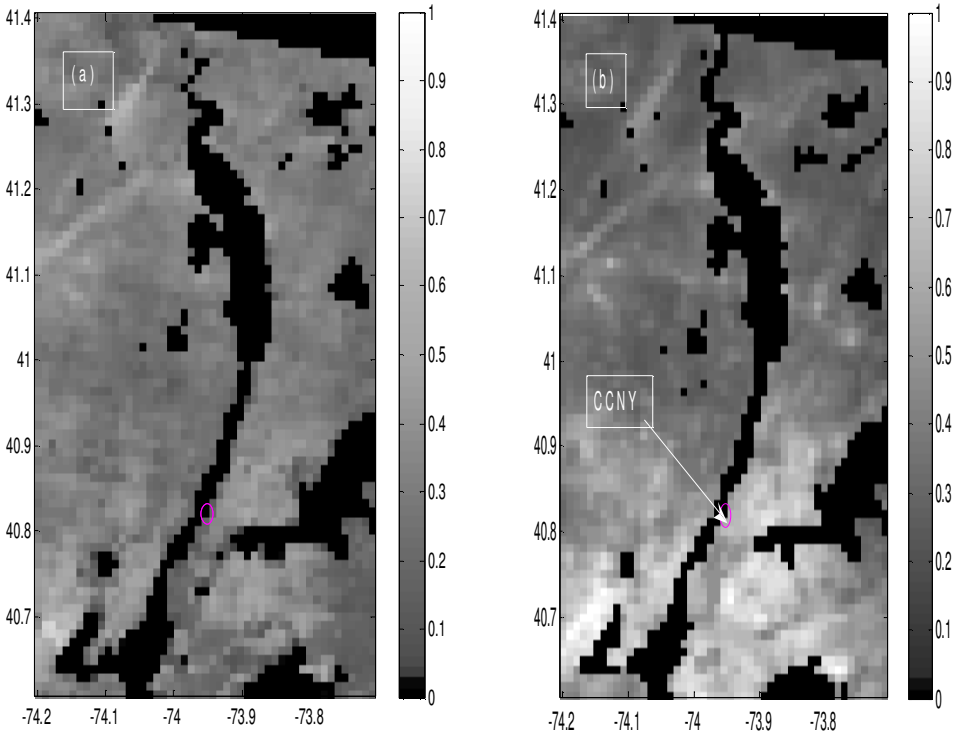

Figure 5.8 (a) Regional map of AOD (550nm) retrieval with modified VIS/SWIR ratio and (b) retrieval with Collection (5) algorithm Date: 10-03-2006. Map goes from 40.61N latitude to 41.4N Latitude, 74.2 W longitudes to 73.71 W longitudes with 0.01 latitude/ longitude resolution.

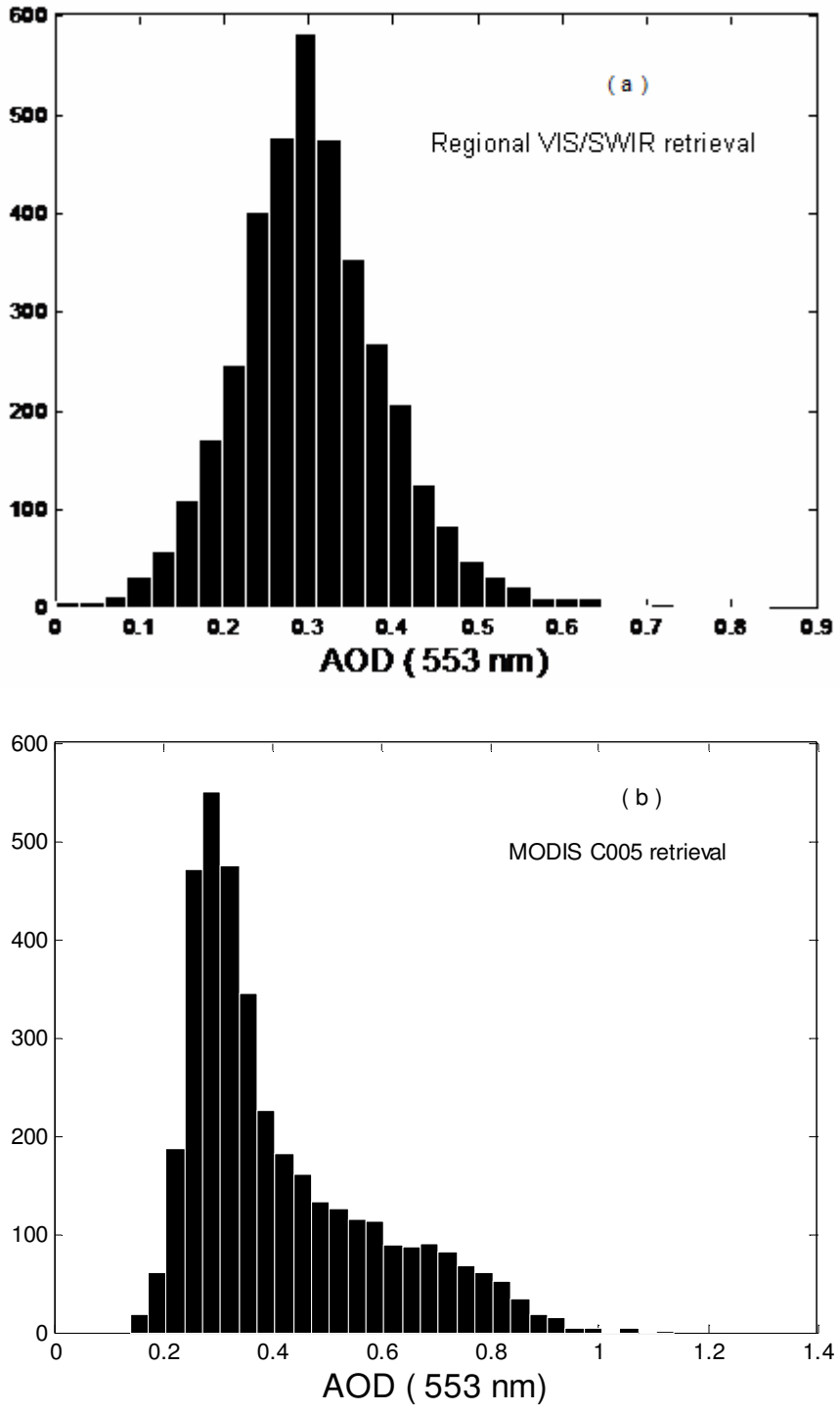

Figure 5.9 Histogram of retrieved AOD. a) Regional surface map b) MODIS Collection (5) approaches

Moreover, we can perform a spatial verification at Medger Evers College, where Multi-Filter Rotating Shadowband Radiometer (MFRSR) has been set up. In particular, even for locations with significant separation from CCNY (16km), the use of the surface results obtained from CCNY can be used. In Fig.5.10, the result at 1.5km resolution for the matchups over Medger Evers College (and their locations) is shown. This data set is not extensive with only 2 months available in Sept and Oct 2007 but large improvement is seen. The reason for residual over bias is difficult to determine at present but can possibly be due to errors in MFRSR processing (not as accurate as AERONET).

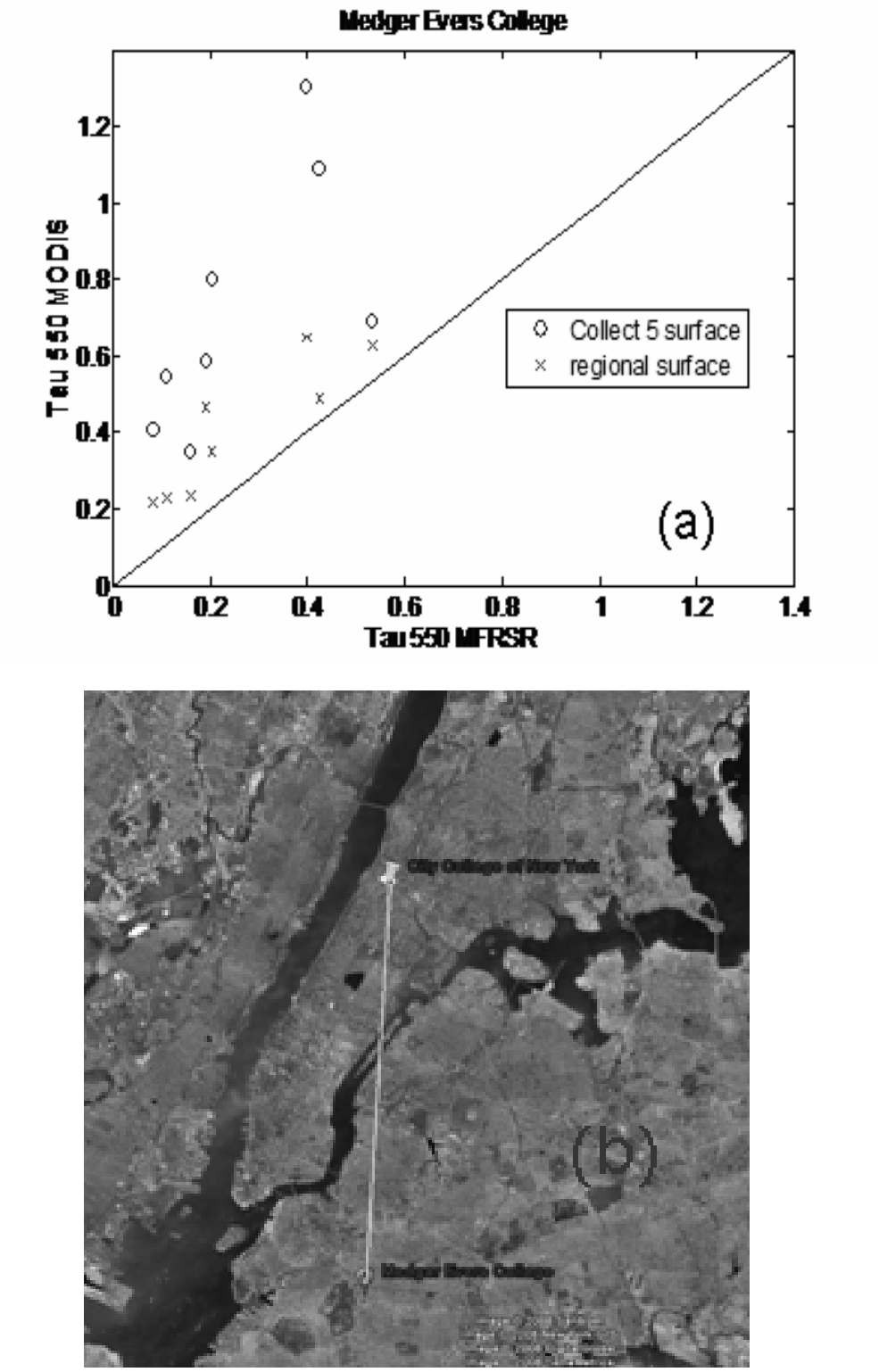

Figure 5.10 a) Comparison of MODIS derived AOD with MFRSR AOD results b) Geo-location of Medger Evers College Sites

5.3 Result from Validation with Mexico City

We have also examined another heavily urban region in a different location to confirm that the processing method is robust and the results of NYC are more justified. For this purpose, the Mexico City region is selected. Unlike New York City area, Mexico City is located approximately more than 2 Km above the sea level (in tropical zone) and most of the fine mode aerosols are within Smoke Aerosol model category (in MODIS LUT). The data acquired from the Mexico City AERONET station during 2000-2007 is used. In fact, the MODIS derived AOD over the Mexico City area is also overestimated in comparison to AERONET retrieved AOD as seen in Fig 5.11. The procedures of the surface reflectance retrieval are the same as described for the NYC region. In addition, due to the height of Mexico City, a pressure correction was implemented, [2]. The resultant VIS/SWIR surface ratios are very similar to New York City urban results. The averages of the 0.47/2.12 μm and 0.66/2.120 μm surface reflectance ratios are approximately 0.43 and 0.70 at 10x10km resolution and 0.44 and 0.71 at 3x3km resolution. Using the new refined regional VIS/SWIR surface reflectance ratios, the significant improvement in AOD retrieval can be observed in Fig 5.12. It should be pointed out however that Mexico City aerosol climatology has a smaller percentage of fine-mode aerosol cases. Therefore, the number of training measurements when compared to New York is much smaller. At 1.5km resolution, too few cases of fine mode clear sky cases were available so analysis was limited to 3x3km.

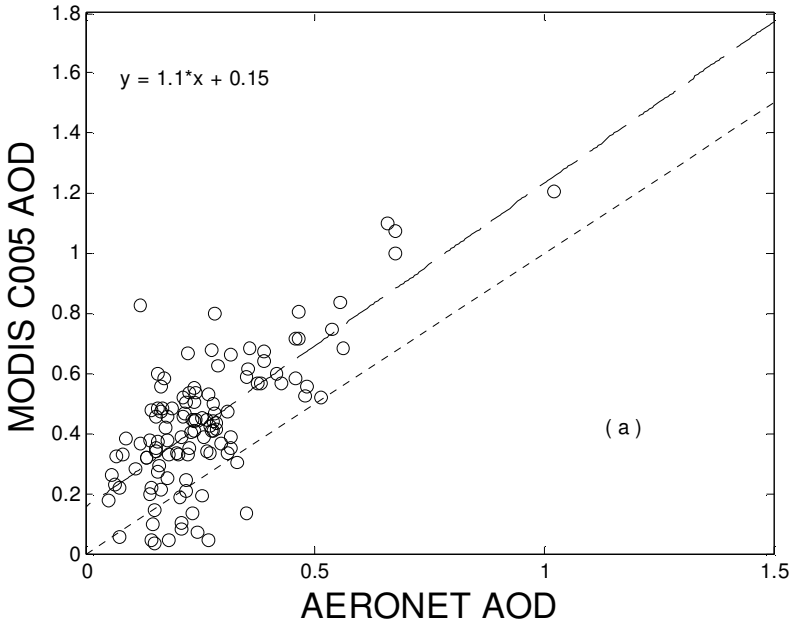

Figure 5.11 MODIS L2 Aerosol Optical Depth at 0.55μm compare with 4 hour (~ 2hr before and 2hr after MODIS (Terra) satellite overpass time) average of AERONET aerosol optical thickness. The dot line is the one to one line and the dash line is linear fit line

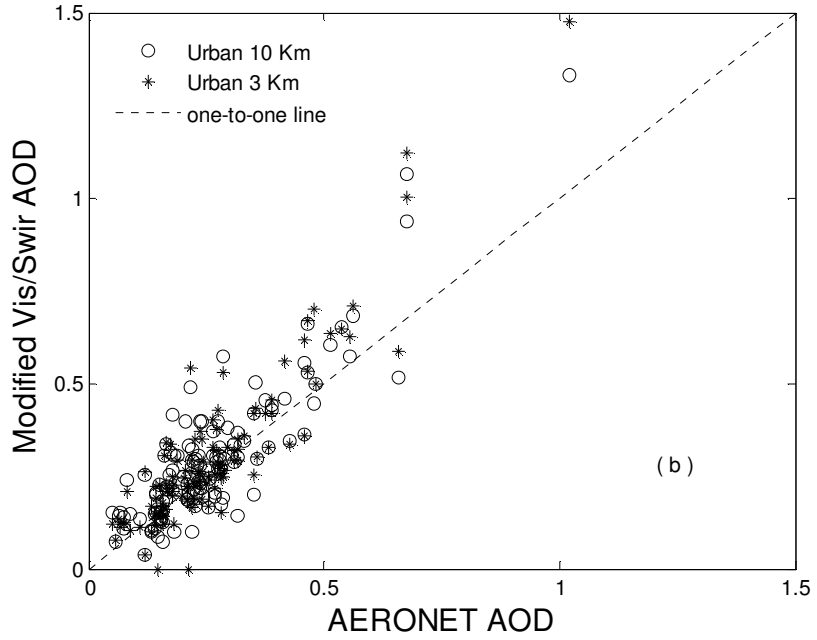

Figure 5.12 Retrieved AOD with new surface reflectance VIS/SWIR ratio versus AERONET AOD; the 'o' is 10x10km resolution and the '*' is 3x3km resolution

5.4 Result from Validation with Billerica, Massachusetts AERONET station

Billerica's AERONET station, Massachusetts, is located at latitude 42.528 and longitude -71.269. Note that AERONET station is surrounded by vegetated area as shown in Fig 5.13 (a) and is a very good analysis point for aerosol retrieval over vegetated area. The MVI of the nearest 10x10 km pixel is calculated form MODIS L2 TOA reflectance and is shown in Fig 5.13 (b). In particular, we note high and low seasonal variation of the MVI can be seen significantly in this figure which is expected for vegetation scenes.

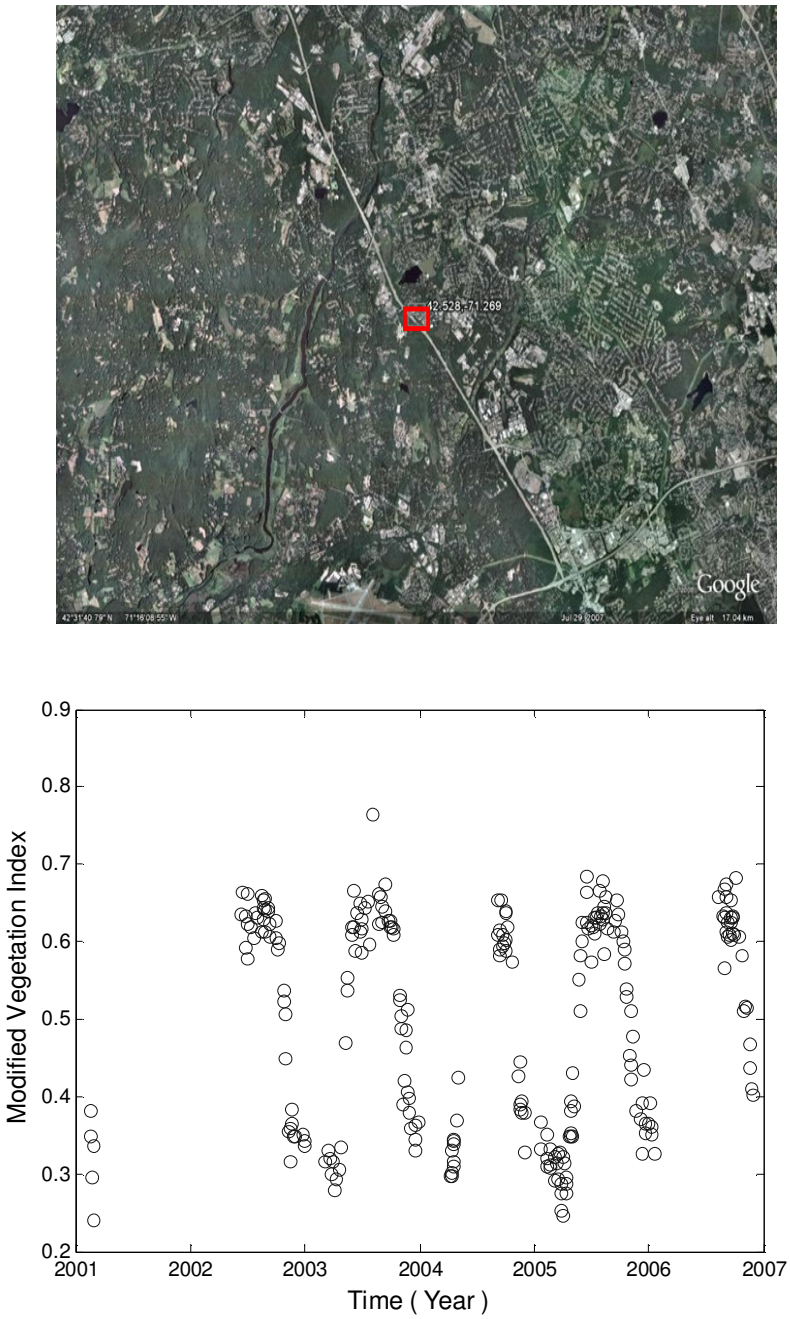

Figure 5.13 a) Geo-location of Billerica, Massachusetts Sites (top) (b) MVI of the site (bottom)

In Fig 5.14, MODIS derived AOD is plotted against AERONET retrieved AOD. In general, as seen in figure, the MODIS derived AOD is in good agreement in comparison with AERONET retrieved AOD but there are some small errors in the

derived AOD especially in low AOD. The error is well within the uncertainty bounds $\pm(0.05+0.15\tau)$ as seen in Fig 5.15.

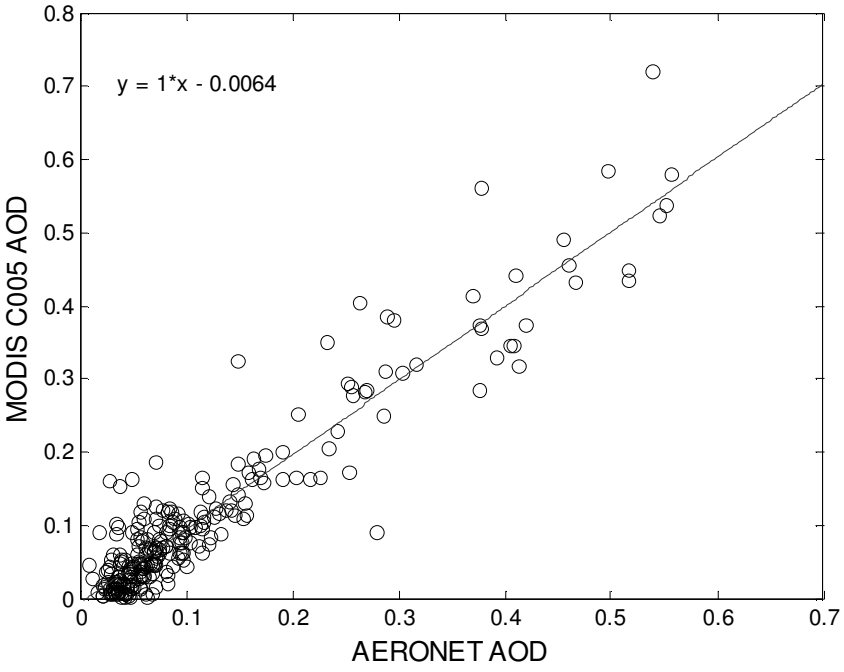

Figure 5.14 AERONET retrieved AOD versus MODIS derived AOD over vegetated area, data collected from 2002-2007 at AERONET station at Billerica, Massachusetts

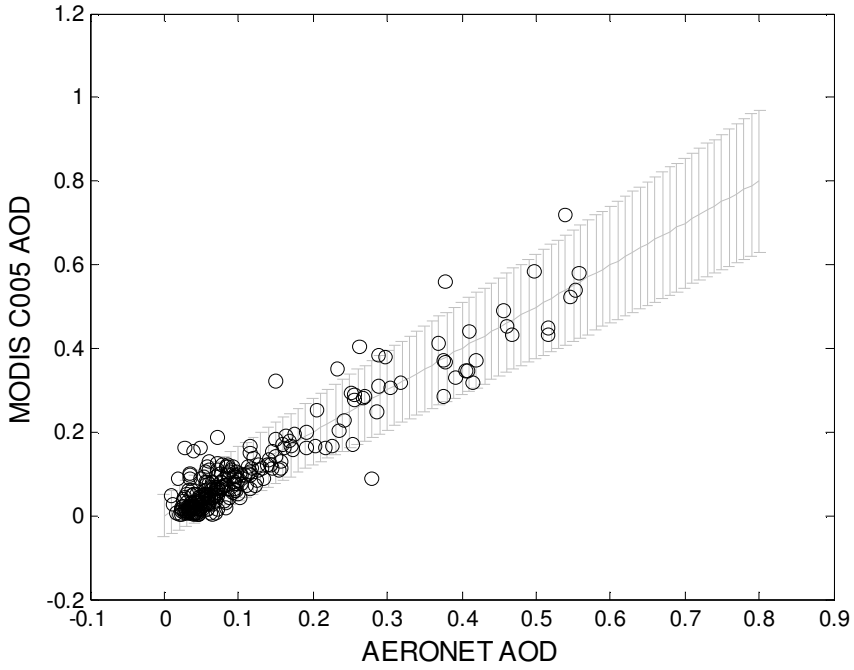

Figure 5.15 AERONET retrieved AOD versus MODIS derived AOD and expected error of MODIS land algorithm $\pm 0.05 \pm 0.15\tau$ in vegetated area, data collected from 2002-2007 at AERONET station at Billerica, Massachusetts

5.5 Construction of common surface model for both urban and vegetated area

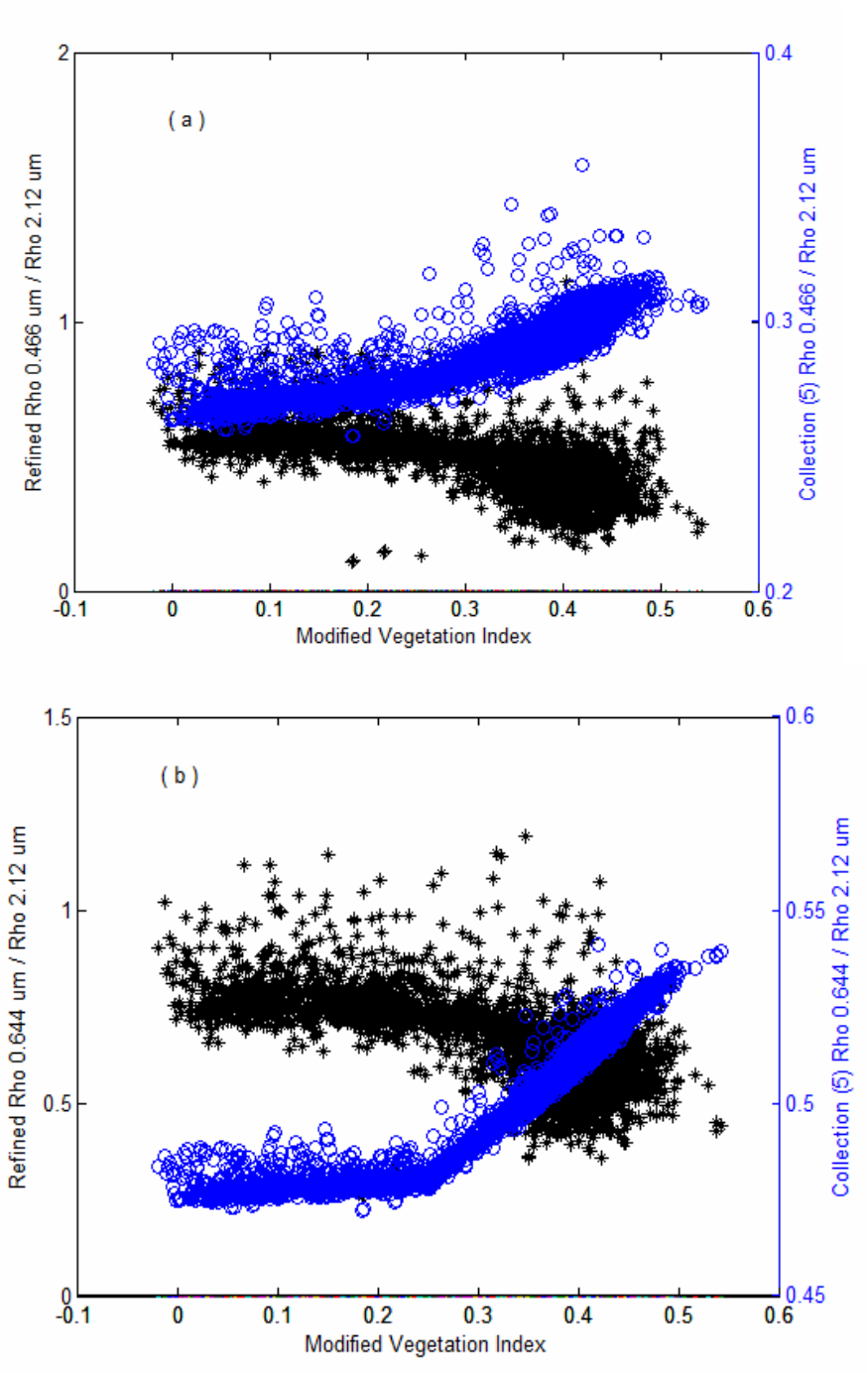

Figure 5.16 Modified Vegetation Index versus VIS/SWIR surface reflectance ratios, the '*' is the refined surface model and the 'o' is the MODIS Collection (5) surface model, (a) 0.466μm/ 2.12μm (b) 0.644μm/ 2.12μm.

In Fig 5.16, the variation of MODIS VIS/SWIR correlation coefficient with MVI and regional derived surface correlation coefficient with MVI are overlapped with that calculated according to the MODIS land operational algorithm [2] (see Equation. 5.2 to 5.9). Obviously the surface reflectance ratios of 0.66/2.12μm can be as high as ~0.63 if MVI is greater than 0.75 and scattering angle is high but the ratios can also be as low as ~0.41 if MVI is lower than 0.25 and scattering angle is low, according to equations 5.7 and 5.8. Clearly, as seen in Fig 5.16, MODIS VIS/SWIR surface ratios vary directly proportional to MVI, but regional surface model shows the opposite direction of the MODIS assumption.

To see if we can see differences in AOD bias as a function of the ground correlation coefficients, we analyze the 256 points of data form AERONET station at Billerica, Massachusetts during 2001-2007. The AOD comparisons are plotted for two different correlation ratio cases in Fig 5.17. Clearly, overestimation occurs when the correlation coefficient is lower than 0.52, in the other word when MVI is lower in MODIS algorithm. The correlation ratios of VIS/SWIR of MODIS algorithm is plotted in Fig 5.18 to observe the range of VIS/SWIR ratios and are seen to oscillate as expected for vegetative scenes.

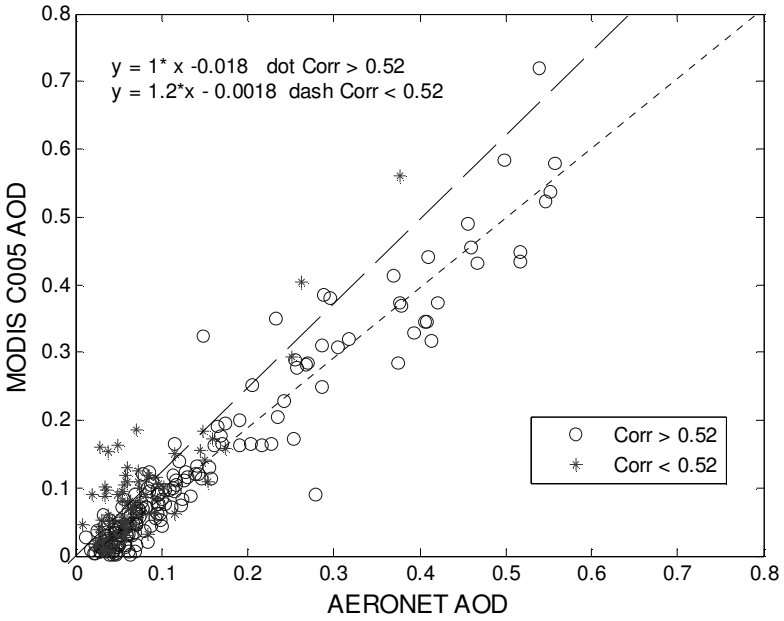

Figure 5.17 AERONET retrieved AOD versus MODIS derived AOD."o" and "*" are the 0.66/2.12 µm surface reflectance ratio greater than 0.52 and less than 0.52 respectively. (Data collected from 2002-2007 at AERONET station at Billerica, Massachusetts)

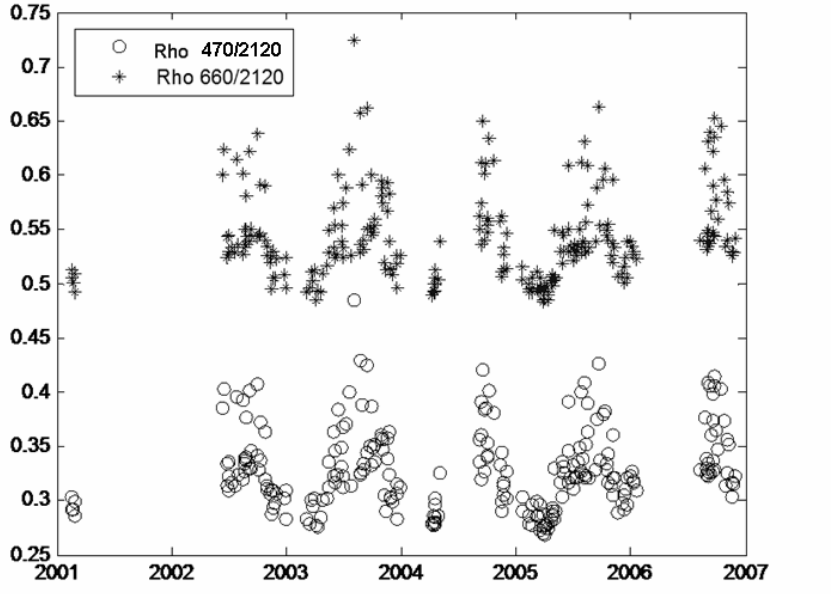

Figure 5.18 MODIS L2 surface albedo ratios of VIS/SWIR

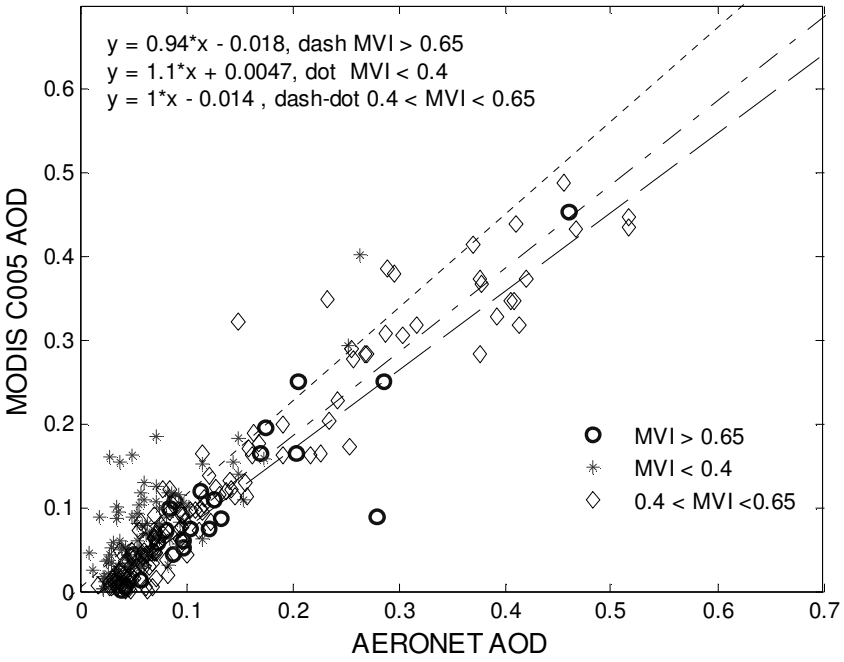

Figure 5.19 AERONET retrieved AOD versus MODIS derived AOD in vegetated area, including MVI parameter characteristic

To see more detail about the origin of this small error, MODIS L2 AOD is plotted against AERONET AOD with inclusion of MVI as additional information. As seen in Fig 5.13 (b), MVI can be separated into 3 groups, MVI higher than 0.65, lower than 0.4 and a group between these two. Clearly, slight AOD overestimation occurs when MVI is less than 0.4 and slight AOD underestimation occurs when MVI is greater than 0.65. This is clearly due to the reverse correlation of VIS/SWIR surface ratio with MVI in comparison to the MODIS operational algorithm. Therefore it is useful to see if using the MVI connection with the VIS-SWIR based on a reconstruction the retrieval of New York City's MVI and VIS-SWIR correlation will improve the retrievals.

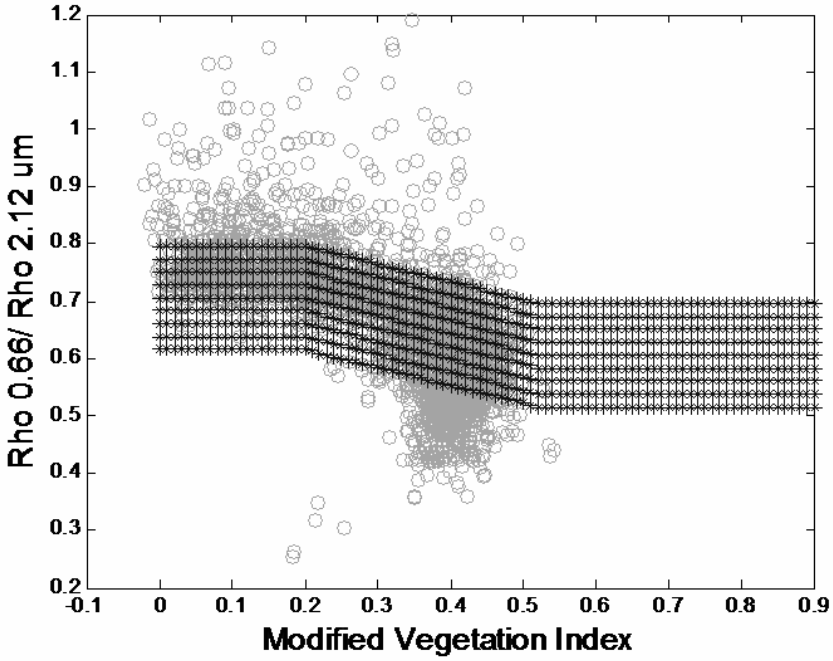

Figure 5.20 Reconstructed MVI- 660nm/SWIR ratios correlation model "*"and NYC's surface VIS/SWIR ratios "o"

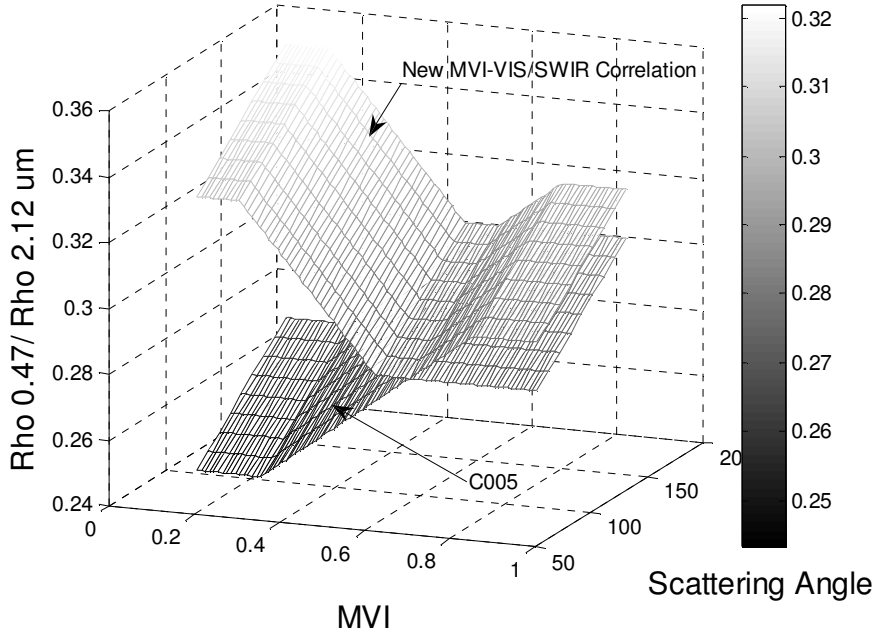

Figure 5.21 Reconstructed MVI- 0.47μm/SWIR ratios correlation model Vs MODIS Collection (5) MVI-VIS/SWIR ratios correlation model

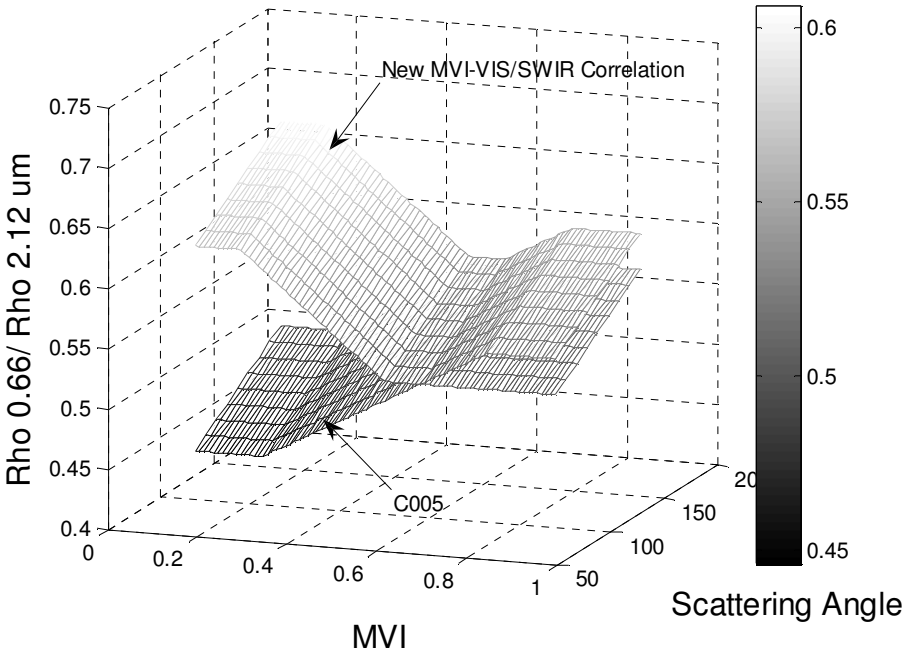

Figure 5.22 Reconstructed MVI- 0.66μm/SWIR ratios correlation model Vs MODIS Collection (5) MVI-VIS/SWIR ratios correlation model

The reconstructed MVI - 660/2120 nm correlation model and NYC's MVI - 660/2120 nm correlation model are shown in Fig 5.20. The new model assumptions are based on combination of NYC urban area result combined with MODIS Collection (5) assumptions. In particular, it does not rely solely on New York City reflectance ratios but combines with the vegetation results.

The new MVI-VIS/SWIR correlation equations are:

$$slope_{0.66/2.12}^{MVI} = 0.85; MVI \le 0.20 \qquad (5.7b)$$

$$slope_{0.66/2.12}^{MVI} = 0.55; MVI \ge 0.52 \qquad (5.8b)$$

$$slope_{0.66/2.12}^{MVI} = 0.65 + (10/32)(0.25 - MVI); 0.2 > MVI < 0.52 \qquad (5.9\ b)$$

Fig 5.21 and Fig 2.22 show comparison of the new VIS/SWIR assumptions, Eq 5.7b, 5.8b, and 5.9b , as function of MVI and overlayed on MODIS Collection

(5) algorithm. Clearly, in the new MVI-VIS/SWIR relation, VIS/SWIR ratios are significantly higher than C005 algorithm for low MVI and slightly lower than C005 for high MVI. With this new surface reflection model (Eq 5.7b, 5.8b and 5.9b substituted in Eq 5.7 to 5.9), surface reflectance in the VIS wavelengths is approximated as before (Eq 5.2 to 5.6) and the AOD is retrieved. There is no major improvement as seen in Fig 5.23 since the MODIS AOD retrieval over the vegetated area is quite good in general. Note however that the fluctuation for low AOD is decreased.

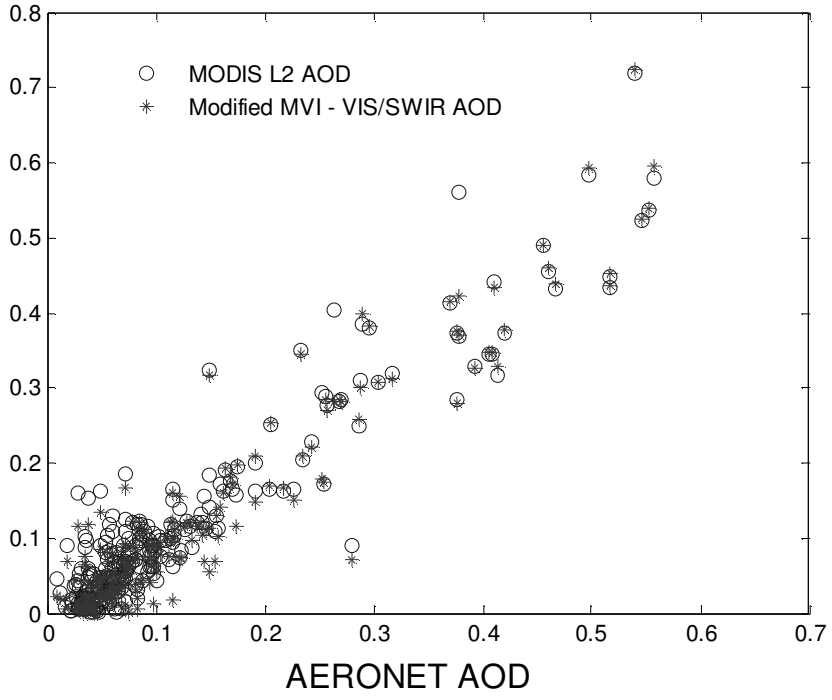

Figure 5.23 AERONET retrieved AOD versus MODIS derived AOD ”o” and derived AOD with new MVI-VIS/SWIR ratios correlation model “*” (data collected from 2002-2007 at AERONET station at Billerica, Massachusetts)

5.6 Revalidation with New York urban data

Since the new MVI-VIS/SWIR model is aimed for both urban and vegetated area, the NYC urban area AOD retrieval is recalculated with the new model to assess. The new MVI –VIS/SWIR model can be substituted directly into the AOD retrieval processing stream and the new derived AOD can be obtained. Note that the new result does not result in the significant improvement seen in section 5.2, but moderate improvement in AOD retrieval is obtained as seen in Fig 5.24. Therefore the new MVI-VIS/SWIR model might not be ideal choice for non-vegetated urban surface but still better than MODIS C005 land surface algorithm for all surface type.

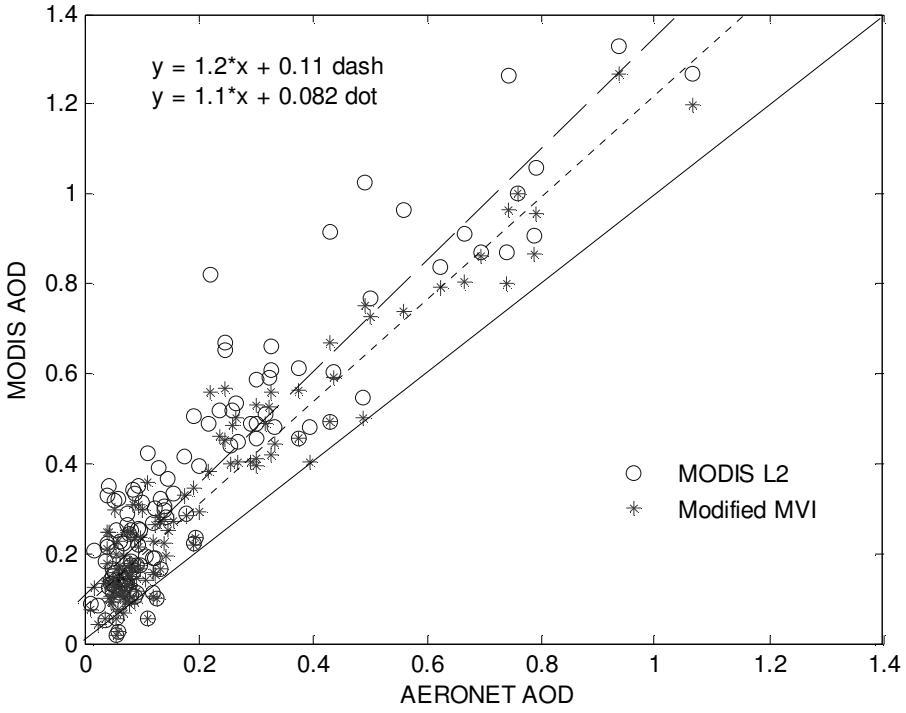

Figure 5.24 MODIS L2 Aerosol Optical Depth at 0.55μm compared with AERONET aerosol optical thickness 'o' and retrieved AOD with new MVI-VIS/SWIR ratios correlation model (the same dataset of CIMEL sun-photometer acquired in New York City (the City College of New York) from 2001 to 2007 is used

References

[1] R. C. Levy, L. A. Remer, and Y. J. Kaufman "Effects of Neglecting Polarization on the MODIS Aerosol Retrieval Over Land" *IEEE Trans. Geos. Rem. Sens.,* vol 42 Pp 2576-2583, 2004

[2] L. A. Remer, D. Tanré, Y. J. Kaufman, R. Levy, and S. Mattoo, "ALGORITHM FOR REMOTE SENSING OF TROPOSPHERIC AEROSOL FROM MODIS: Collection 005" ATBD document

[3] A. Lyapustin and Y. Wang, "MAIAC: multi-angle implementation of atmospheric correction for MODIS" NASA, GFSC, ATBD (Feb, 2007)

[4] Sensing of Vegetation: Reflectance spectra of ground vegetation, http://www.aai.ee/bgf/

[5] Levy, R. C., L. A. Remer, et al. (2005) "Evaluation of the MODIS aerosol retrievals over ocean and land during CLAMS." Journal of the Atmospheric Sciences **62**(4): 974-992.

Chapter 6

Effect of BRDF Model in AOD retrieval

Our surface modeling would not be complete unless the differences and the effect of Lambertian surface reflectance assumption and BRDF surface reflectance assumption in AOD retrieval is discussed. As seen earlier, there still seems to be significant deviations which are most significant for smaller optical depths. This behavior is consistent with the possibility that directional reflectance effects are relevant. In this section, the effects of the directional surface reflectance are explored. In this effort, the SHARM (Spherical Harmonics code) radiative transfer software is used to calculate the atmospheric component coupling with the BRDF surface reflectance. To simplify the analysis, we focus on the case where the urban fine mode dominates the atmospheric state and utilize MODIS derived BRDF model surface reflectance parameters. Therefore, it is necessary to explain the background and methodology inside the SHARM software and MODIS BRDF algorithm.

6.1 Radiative Transfer Modeling with BRDF surface reflectance

The radiance in the solar spectrum which reaches the MODIS instrument at the top of the atmosphere valid for non-Lambertian surface reflectance, can be described as [ref]

$$L_{TOA} = L_0(\mu_s, \mu_v, \phi) + \frac{F_o \mu_s (T(\mu_s) R T(\mu_v) - e^{\tau/\mu_s} |R| e^{\tau/\mu_v})}{\pi(1 - \overline{\overline{\rho_s}} \rho_a)} \quad (6.1)$$

$$\text{where R} = \begin{bmatrix} \rho_s(\mu_s, \mu_v, \phi) & \overline{\overline{\rho_b}}(\mu_s) \\ \overline{\rho_s}(\mu_s; \mu_v, \phi) & \overline{\overline{\rho_s}}(\mu_s) \end{bmatrix} \quad (6.2)$$

Here, L_{TOA} is the radiance received by the satellite at the top of the atmosphere, L_0 is the path radiance, $T(\mu_s)$ is the total transmittance from the top of the atmosphere to the ground along the path of the incoming solar beam, $T(\mu_v)$ is the total transmittance from the ground to the top of the atmosphere in the view direction of the satellite, F_o is the solar radiance at the top of the atmosphere, $\overline{\overline{\rho_s}}(\mu_s, \mu_v, \phi)$ is the diffuse to diffuse surface reflectance, ρ_a is the reflectance of the atmosphere for isotropic light entering the base of the atmosphere, μ_s is the cosine of the solar zenith angle, μ_v is the cosine of the view angle and ϕ is the azimuthally difference between the two zenith angles.

In equation (6.2), the R matrix accounts for both surface reflectance properties and the degree of diffuse illumination. The determinant |R| has the physical meaning of a correction term for using BRDF in multiple bouncing between surface and atmosphere. ρ_s is the directional surface reflectance (BRDF), ρ_b is the directional hemispherical integral ("black sky albedo") of the BRDF.

$$\rho_b(\mu_s) = \frac{1}{\pi} \int_0^{2\pi} \int_0^{\frac{\pi}{2}} \rho_s \cos(\vartheta_v) \sin(\vartheta_v) d\vartheta_v d\phi \quad (6.3)$$

$\overline{\rho_s}(\mu_s; \mu_v, \phi)$ is the diffuse irradiance that is directly scattered into the viewing direction (μ_v, ϕ) under illumination μ_s,

$$\overline{\rho_s}(\mu_s;\mu_v,\phi)=\frac{\int_0^{2\pi}\int_0^{\frac{\pi}{2}} L_{\downarrow}(\mu_s;\mu,\phi')\rho_s(\mu,\mu_v,\phi'-\phi)\cos(\vartheta)\sin(\vartheta)d\vartheta d\phi'}{\int_0^{2\pi}\int_0^{\frac{\pi}{2}} L_{\downarrow}(\mu_s;\mu,\phi')\cos(\vartheta)\sin(\vartheta)d\vartheta d\phi'} \tag{6.4}$$

where $L_{\downarrow}(\mu_s;\mu,\phi')$ is the downwelling diffuse irradiance distribution with the sun at μ_s, and $\overline{\overline{\rho_s}}(\mu_s)$ is the diffuse to diffuse reflectance ("white sky albedo") under illumination from μ_s

$$\overline{\overline{\rho_s}}(\mu_s)=\frac{1}{\pi}\int_0^{2\pi}\int_0^{\frac{\pi}{2}}\overline{\rho_s}(\mu_s;\mu,\phi)\cos(\vartheta_v)\sin(\vartheta_v)d\vartheta_v d\phi \tag{6.5}$$

The radiances are again can be normalized by the incident solar flux, $F_0\mu/\pi$ which results in the following equation:

$$\rho_{TOA}=\rho_{path}(\mu_s,\mu_v,\phi)+\frac{T_{total}(\mu_s)RT_{total}(\mu_v)-e^{\tau/\mu_s}|R|e^{\tau/\mu_v}}{1-\overline{\overline{\rho_s}}\rho_a} \tag{6.6}$$

where ρ_{TOA} is the reflectance at the top of the atmosphere and ρ_{path} is the path radiance of the atmosphere in reflectance units.

It is of specific interest to note that any correction to the MODIS retrieval will require information on the aerosol properties. This can either be done by self-consistently using the MODIS aerosol optical depth and assumed aerosol model to estimate the atmospheric parameters or to rely on ground measurements from a scanning radiometer to determine a better estimate of the downwelling radiances and the resultant diffuse transmittances. The goal is to utilize the MODIS BRDF products to get an estimate on the magnitude of the anisotropy and see how it may

affect the final aerosol product. The MODIS BRDF product is particularly well suited since the albedo is modeled as a linear combination of kernel functions multiplied by retrieved coefficients. Therefore, given a set of kernels, the corrections may be expressed directly from the non-isotropic terms.

6.2 Kernel driven parameters for BRDF reflectance

Kernel-driven models for the bidirectional reflectance distribution function of vegetated land surfaces attempt to describe the BRDF as a linear superposition of a set of kernels that describe basic BRDF shapes, with the coefficients or weights chosen to adapt the sum of the kernels to the given case. Typically, semi-empirical kernels are based either on one of several possible approximations to a radiative transfer scenario of light scattering in a horizontally homogeneous plant canopy (*e.g.*, a crop canopy), or on one of several approximations feasible in a geometric-optical model of light scattering from a surface covered with vertical projections that cast shadows (*e.g.*, a forest canopy). Deriving a kernel of this nature requires simplifying and manipulating a model for the BRDF until it reaches the form:

$$R = k\,C_1 + C_2 \qquad (6.7)$$

in which k is a function only of view and illumination geometry, $C1$and C2 are constants containing physical parameters, and R is the modeled value of the true BRDF.

Semi-empirical kernels can be of two types. First, they may contain only geometric terms, but no physical parameters. The complete model then is linear,

and may be scaled to arbitrary scales even for mixed scenes neglecting adjacency effects, the weights of the kernels will be linear functions of the areal proportions of the subpixel weights. The so-called Ross-kernels, which are approximations to the radiative transfer theory in plant canopies of Ross (1981) [1] described below, belong to this class, as does the so-called Roujean geometric-optical kernel (Roujean *et al.*, 1992) [2]. In the second case, kernels contain one or very few physical parameters and thus instead of having one kernel, provide a family of kernels depending on these parameters. The geometric-optical Li-kernels (Wanner *et al.*, 1995) [3] belong to this type. The following discussion presents each of the kernels used in the BRDF/Albedo algorithm.

The MODIS algorithm uses as a default, the combination of Ross thick and Li sparse kernals. The Ross kernels are derived from a formula presented by Ross (1981) [1] for the directional reflectance above a horizontally homogeneous plant canopy calculated from radiative transfer theory in a single scattering approximation. The Ross-thick kernel was derived and described by Roujean *et al.* (1992) [2]. It is based on an approximation for large LAI values:

$$k_{thick} = \frac{(\pi/2 - \xi)\cos\xi + \sin\xi}{\cos\theta_i + \cos\theta_v} - \frac{\pi}{4} \qquad (6.8)$$

In the kernel, θ_i and θ_v are zenith angles for illumination and view, respectively, ϕ is the relative azimuth of illumination and view directions; and ξ is the phase angle of scattering

$$\cos\xi = \cos\vartheta_i \cos\vartheta_v + \sin\vartheta_i \sin\vartheta_v \cos\phi \qquad (6.9)$$

The Li kernels are derived from the modeling approach of Li and Strahler [4]. In this approach, the surface is taken as covered by randomly-placed projections (*e.g.*, tree crowns) that are taken to be spheroidal in shape and centered randomly within a layer above the surface. The BRDF is modeled as a function of the relative areas of sunlit and

shaded, crown and background that are visible from the viewing position in the hemisphere. For the Li-sparse kernel, it is assumed that shaded crown and shaded background are black, and that sunlit crown and background are equally bright. Under these circumstances, and with some further approximations in the way that view and illumination shadows overlap, the Li-sparse kernel is:

$$k_{sparse} = O(\theta_i, \theta_v, \phi) - \sec\theta_i' - \sec\theta_v' + \tfrac{1}{2}(1+\cos\xi')\sec\theta_v' \tag{6.10}$$

where $O = \frac{1}{\pi}(t - \sin t\cos t)(\sec\theta_i' + \sec\theta_v')$ (6.11)

$$D = \sqrt{\tan^2\theta_i' + \tan^2\theta_v' - 2\tan\theta_i'\tan\theta_v'\cos\phi} \tag{6.12}$$

$$\cos t = \tfrac{h}{b}\frac{\sqrt{D^2 + (\tan\theta_i'\tan\theta_v'\sin\phi)^2}}{\sec\theta_i' + \sec\theta_v'} \tag{6.13}$$

$$\vartheta' = \tan^{-1}(\tfrac{b}{r}\tan\vartheta) \tag{6.14}$$

In these expressions, b is the vertical radius of the spheroid; r is the horizontal radius of the spheroid; and h is the height of the center of the spheroid. For the MODIS product, $\frac{h}{b} = 2, \frac{b}{r} = 1$. The combination of the Ross-Thick with the Li-Sparse kernel has been called the Ross-Thick Li-Sparse model, but will here be simply referred to as the Ross-Li BRDF model as it is the standard model to be used in MODIS BRDF processing.

Finally, the effective BRDF reflectance is considered as a combination of the reflectance of Isotropic, Ross-thick and Li-Sparse, Eq (6.15)

$$\rho_g(\mu_s', \mu_v') = \rho_{iso} + f_{sur} k_{sur}(\mu_s', \mu_v') + f_{vol} k_{vol}(\mu_s', \mu_v') \quad (6.15)$$

Fig 6.1 shows the shapes of these kernels for different solar zenith angles and Fig 6.2 shows the shape of the resulting BRDF when using realistic model parameters taken from BRDF datasets observed in the field over a variety of land cover types. Note that the behavior of the two kernels is different in nature over large angular ranges. While they are not perfectly orthogonal functions, as would be ideal for the inversion process, they are sufficiently independent to allow stable recovery of the parameters for many angular sampling distributions. The absence of excessive kernel-to-kernel correlation is a key to reliable inversions. Note in particular the geometric reflectance effects reduce the reflection due to the modeling of shadows which decreases the reflectance. Also note the backscatter hotspot.

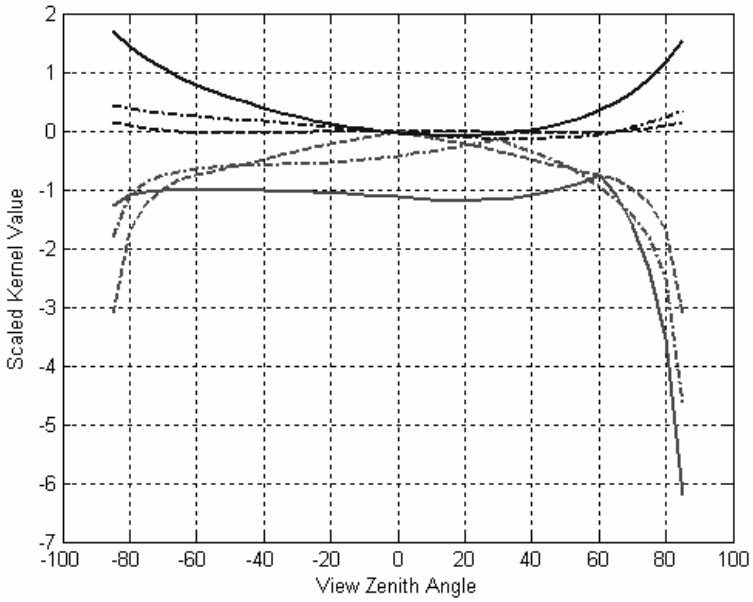

Figure 6.1 Principal plane plot of the Ross-Thick (upper curves) and Li-Sparse (lower curves) BRDF model kernel values (arbitrary units; the Li-Sparse kernel values were divided by 2 for better plotting). The sun is located at positive zenith angles of 0 (dotted lines), 30 (dashed lines), 60 (solid lines solar zenith angle. The parameter h/b of the Li-Sparse kernel was set to 2.0, the parameter b/r to 1.0.

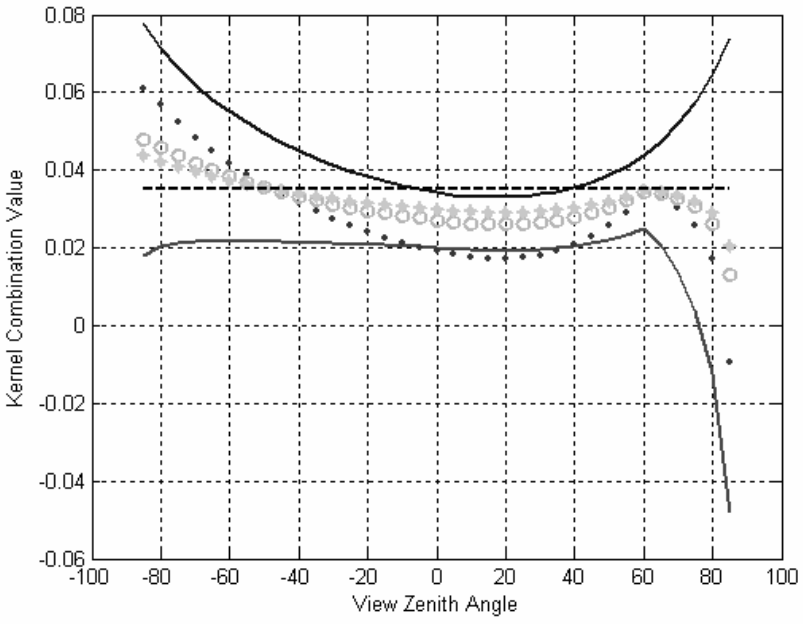

Figure 6.2 The BRDF shapes which the Ross-Li BRDF model acquires under particular/natural conditions (f _iso =0.0351,f_vol=0.0254, f_geo=0.0067) on the principal solar plane for a solar zenith angle of 60 degrees. The two solid lines represent the maximal volume scattering and geometric-optical scattering. The dot, o , * and dotted line are intermediate cases where the parameters f_vol and f_geo take on either their respective half of maximal value, one third of it, or are zero in all possible combinations.

6.3 Comparison of Lambertian Vs Effective BRDF Surface reflectance

When trying to assess the effect of the BRDF, it is important to ensure that the angular BRDF takes on the value of the reflection measuresd from the sensor at the specific set of angles. In particular, for a given solar and view geometry $\mu_{s,0}, \mu_{v,0}$

$$\rho_g(\mu_s', \mu_v') = \rho_{g,MODIS} \frac{[\rho_{iso} + f_{sur}k_{sur}(\mu_s', \mu_v') + f_{vol}k_{vol}(\mu_s', \mu_v')]}{[\rho_{iso} + f_{sur}k_{sur}(\mu_{s,0}, \mu_{v,0}) + f_{vol}k_{vol}(\mu_{s,0}, \mu_{v,0})]} \quad (6.16)$$

As a first example, the BRDF Model (f_iso= 0.0351, f_vol= 0.0254 , f_geo= 0.0067) is used for different solar illumination angles

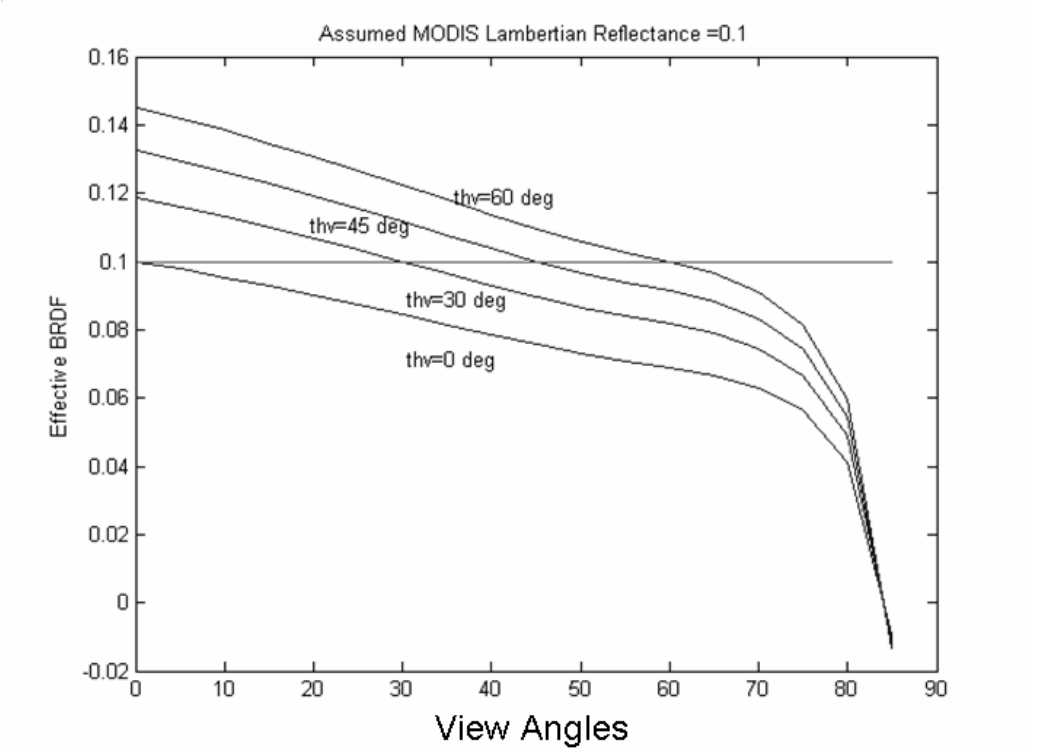

Figure 6.3 Effective BRDF value at hemispherical angles

Fig 6.3 illustrates the normalization to an assumed Lambertian of 0.1 for a nadir sun and different view angles. Note that the case of nadir observation is on the peak of the reflectance curve so the resultant Lambertian overestimates the ground albedo over the entire scattering hemisphere. However, for more oblique view angles, a significant underestimation of the overall reflectance can occur.

6.4 SHARM Radiative Transfer model

SHARM (Spherical Harmonics code) is a one dimension radiative transfer code, as accurate as the Discrete Ordinate Radiative Transfer (DISORT) code, yet faster [5]. The code is designed to compute monochromatic radiance/flux in the shortwave spectral region over a Lambertian or anisotropic surface. The atmospheric properties can change arbitrarily in the vertical dimension. The algorithm uses the method of spherical harmonics (MSH) [6, 7] with the boundary conditions in the form of Marshak [8]. The code is rigorous in a sense that its solution converges to the true value at increase of the order of MSH. It also performs simultaneous calculations for different solar zenith angles, view zenith angles, and view azimuths and allows the user to make multi-wavelength calculations in one run. The Δ-M method is implemented for calculations with highly anisotropic phase functions. Rayleigh scattering is automatically included as a function of wavelength, surface elevation, and the selected vertical profile of one of the standard atmospheric models. The SHARM code does not explicitly include atmospheric gaseous absorption, which should be provided by the user.

However, since our main purpose is sensitivity comparisons, we do not need to determine this directly from observations. The SHARM code has several built-in models of the bidirectional reflectance of land and wind-ruffled water surfaces that are most widely used in research and satellite data processing. A modification of the SHARM code with the built-in Mie algorithm designed for calculations with spherical aerosols is also described.

Firstly, the definition of the BRDF kernels and equations embedded in the SHARM software needs to be confirmed with MODIS BRDF kernel parameters. To do so, we decided to isolate the surface by calculating the TOA reflectance using only a Raleigh atmosphere (i.e. zero aerosol optical depth assumption). Clearly, at long weavelengths (i.e. 2120 nm), the TOA signal is completely due to the surface reflection. Therefore, by calculating the TOA reflectance over a realistic set of angles, the BRDF kernels parameters and the SHARM processing can be checked for accuraccy. This calculation is done in solar zenith angles of 0, 30 and 60 degree with view zenith angles of -80 to 80 with 10 degree increment and relative azimuth angle is 0 degree.

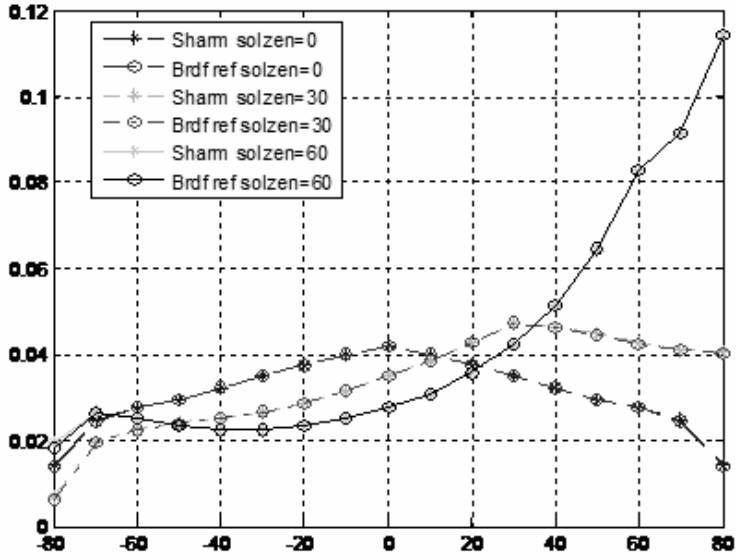

Figure 6.4 Comparison of MODIS BEDF effective surface reflectance with SHARM SWIR TOA reflectance while very clean atmospheric condition

In Fig 6.4, a comparison plot is given. . Clearly the two results are in very good agreement with each other. This result shows that MODIS and SHARM radiative transfer software use the same equation and definition of the BRDF parameters.

In addition, testing that the LUT from MODIS can be calculated by SHARM is critical if comparions to the earlier retrievals can be made. As this analysis is concentrated on fine mode aerosol model, comparison of the path reflectance of 3 fine mode aerosol models is plotted in Fig 6.5. The match up is in good agreement between SHARM radiative transfer model and MODIS LUT even though SHARM use a scalar model and MODIS LUT is calculated by vector model.

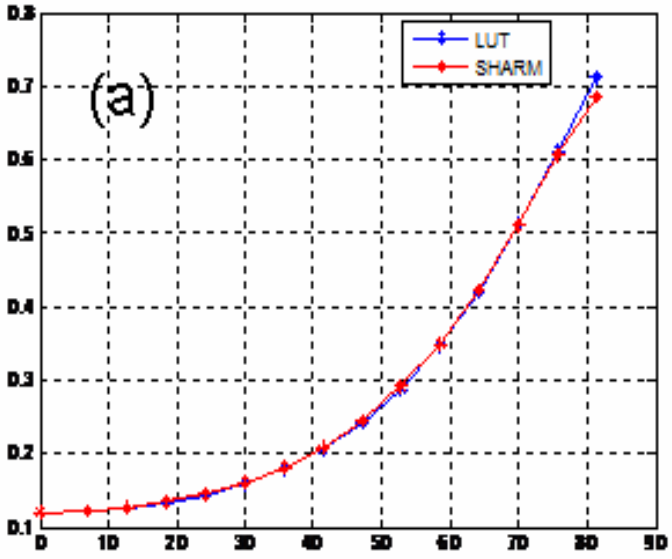
(a)
LUT
SHARM
0.8
0.7
0.6
0.5
0.4
0.3
0.2
0.1
0
10
20
30
40
50
60
70
80
90

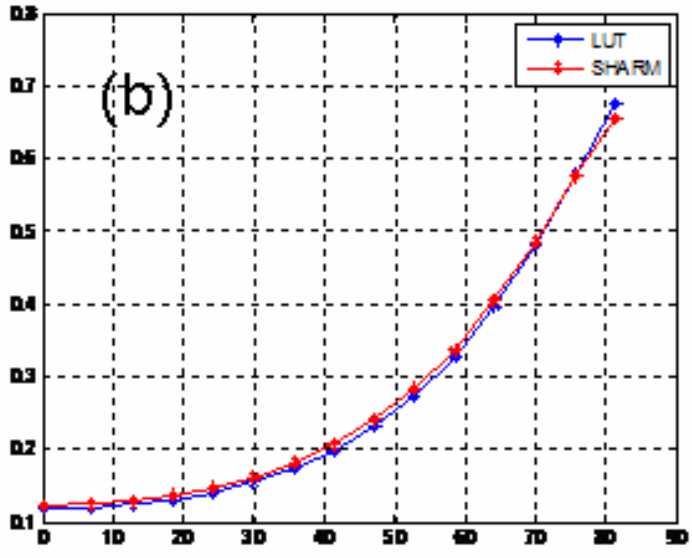
(b)
LUT
SHARM
0.8
0.7
0.6
0.5
0.4
0.3
0.2
0.1
0
10
20
30
40
50
60
70
80
90

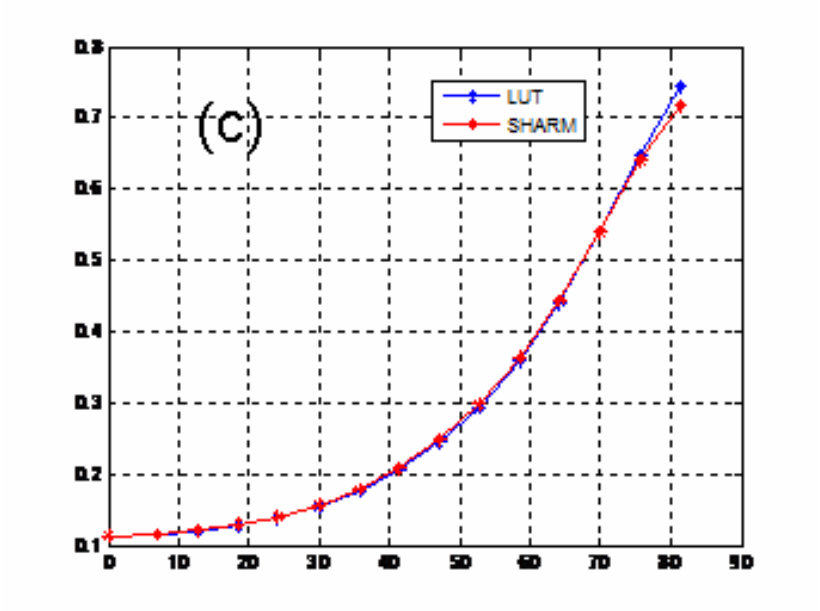

Figure 6.5 Atmospheric path reflectance at the top of atmosphere by MODIS look up table and SHARM simulation, (a) Natural /Generic Aerosol model, (b) Smoke aerosol model, (c) Urban aerosol model, for all three model, aerosol optical thickness= 1.0, wavelength = 553nm, solar zenith angle=48 deg and relative azimuth angle= 0 angle y-axis is reflectance and x-axis is view zenith

After confirmation of SHARM atmospheric and surface calculations with MODIS defined models, we can now calculate the deviations between the Lambertian and non Lambertian models for AOD retrieval.

6.5 Result of AOD retrieval in Lambertian Vs BRDF assumption

In this section, data from MODIS L3 BRDF dataset is used to calculate surface reflectance. Two particular days in the 16 days period of MODIS derived L3 BRDF parameters dataset are selected, (5-29-2006 and 06-01-2006) and the TOA signal is calculated in both the Lambertian and non-Lambertian models as the AOD at 0.550µm varies from 0 to 0.5. Comparison of these two results is shown

in Fig 6.6. Clearly, there are differences in TOA reflectance due two different assumptions in surface reflection model.

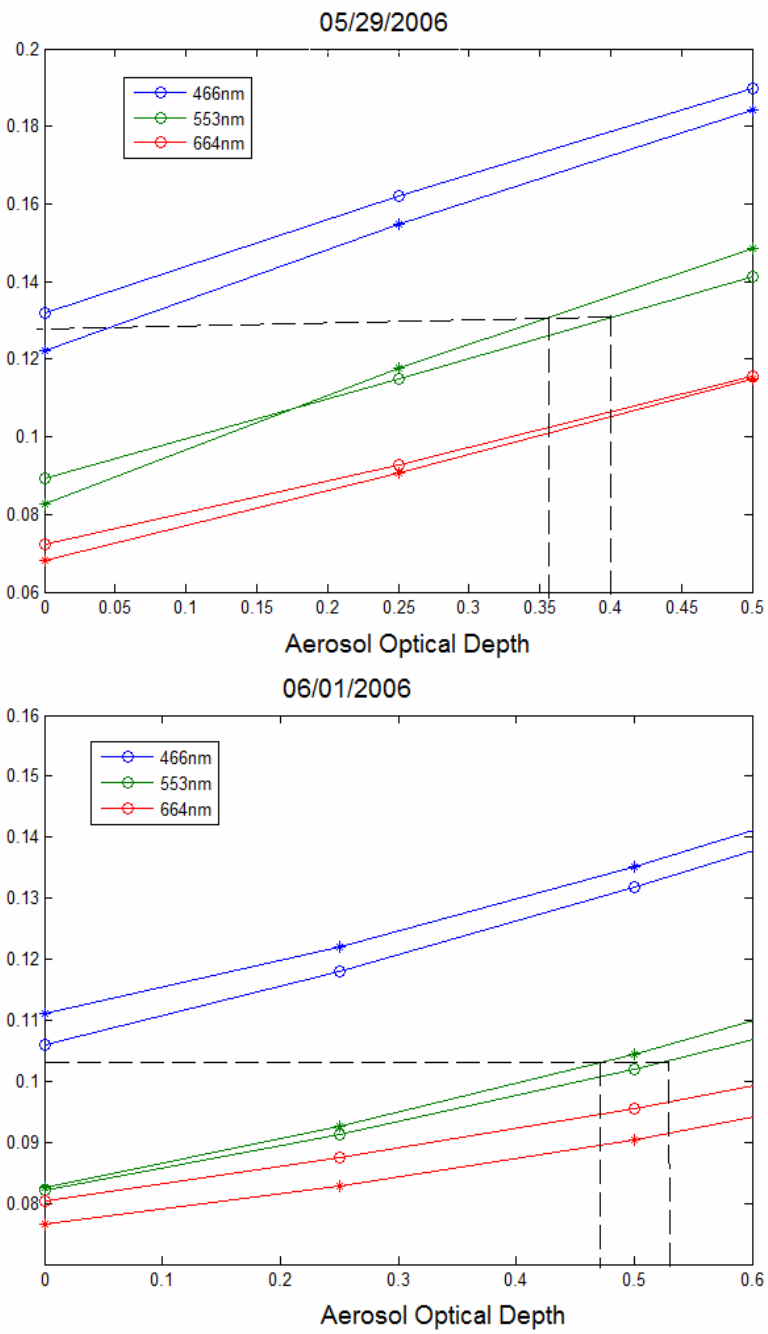

Figure 6.6 Comparison of TOA reflectance: Lambertian surface reflectance assumption is “o’ and BRDF surface reflectance assumption is “*” , y-axis: TOA reflectance (top) 05-29-2006 (bottom) 06-01-2006

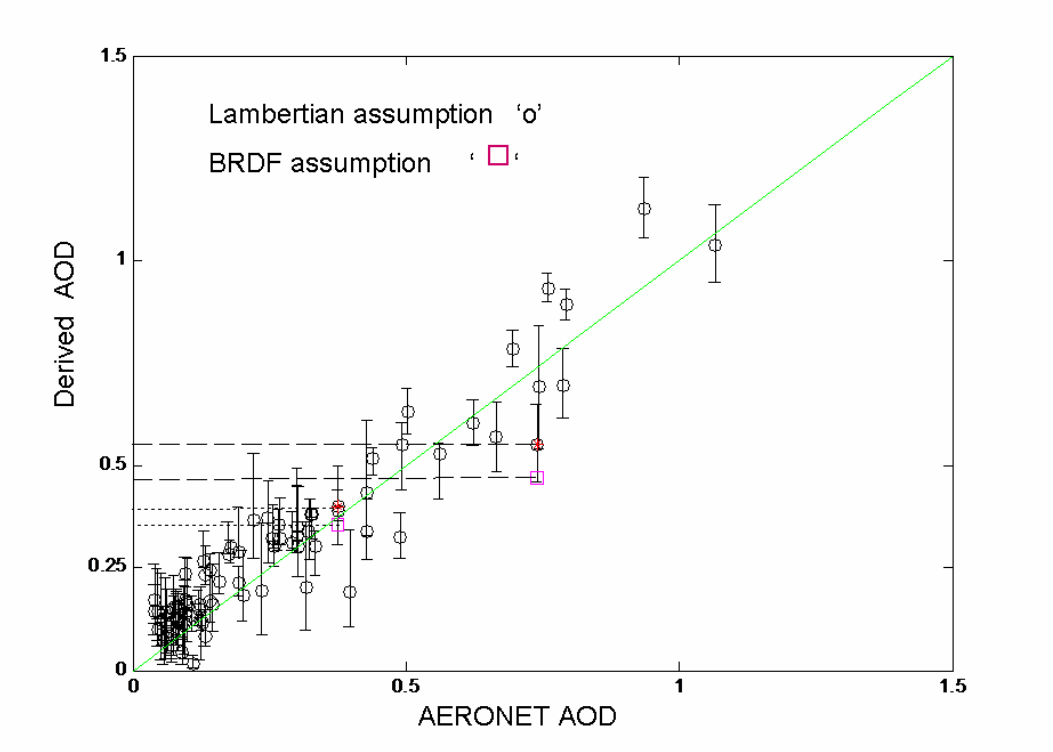

Figure 6.7 Retrieved AOD with mean (and standard deviation) of surface reflectance VIS/SWIR ratio in 1.5x1.5 km resolution plot against with AERONET AOD, two square marks are the retrieved AOD

AOD of the two (days) test cases can be retrieved from the above two TOA reflectance with urban surface reflectance ratios derived in section 5.2 and plotted in Fig 6.7. Preliminary result shows that error due to this source (Lambertian Vs BRDF model) is no bigger than the errors we observe due to the simple variation (standard deviation) in the correlation coefficient magnitude. Therefore the effect of BRDF will not be considered further.

References

[1] Ross, J.K. (1981). *The radiation regime and architecture of plant stands*. Dr W Junk, The Hague, **ISBN-13:** 978-9061936077

[2] Roujean, J.L., Latoy, M. and Deschamps, P.Y. (1992). A bidirectional reflectance model of the earth's surface for the correction of remote sensing data. *J. Geophys. Res*., 97, 20455-20468.

[3]Wanner, W., X. Li, and A. H. Strahler (1995). On the derivation of kernels for kernel-driven models of bidirectional reflectance, *J. Geophys. Res*., 21077-21090

[4] Strahler A. H., J.-P. Muller, MODIS Science Team Members, MODIS BRDF/Albedo Product: Algorithm Theoretical Basis Document, Version 5.0 , MODIS Product ID: MOD43, April 1999

[5] A. I. Lyapustin, "Radiative transfer code SHARM for atmospheric and terrestrial applications," Appl. Opt. **44**, 7764-7772 (2005)

[6] Lyapustin, A. I., and T. Z. Muldashev, Method of spherical harmonics in the radiative transfer problem with non-Lambertian surface, *J. Quant. Spectrosc. Radiat. Transfer,* **61** (4), 545-555, 1999.

[7] Muldashev, T. Z., A. I. Lyapustin, and U. M. Sultangazin, Spherical harmonics method in the problem of radiative transfer in the atmosphere-surface system, *J. Quant. Spectrosc. Radiat. Transfer,* **61** (3), 393-404,
1998.

[8] Marshak, R. E., Note on the spherical harmonics method as applied to the Milne problem for a sphere, *Phys.Rev*., **71**, 443-446, 1947.

CHAPTER 7

CONCLUSIONS

The need for a regionally based surface model has been demonstrated based on significant overestimation with respect to AERONET in the AOD retrieval using the current Collection (5) algorithm. This is due to the fact that the globally based model cannot retrieve the high VIS-SWIR correlation coefficients observed when regionally processing urban areas. In inverting the TOA reflectance data, simultaneous AOD measurements from MODIS and an AERONET CIMEL sky radiometer were used to retrieve regional surface properties where suitable filters on the aerosol loading and stability was used in building the analysis data set. These filters were put in place to ensure that the aerosol optical depth was small, and fine mode dominated and that the aerosol is fairly stable over the day. This ensured that good surface reflection data can be obtained at 0.47, 0.66 and 2.120 μm allowing us to retrieve accurate surface reflection VIS-SWIR correlation functions.

The resultant correlations were significantly higher than Collection (5) results and were shown to be in good agreement with surface reflectance ratio from Hyperion results. In addition, it is shown that significant differences between the Collection (5) relation between the correlation coefficients and MVI parameters including the fact that the urban correlations are significantly higher than vegetation. On the other hand, any meaningful trend behavior as a function of scattering angle was not detected and that allow using a Lambertian

approximation of the surface. However, water contamination is a serious problem, artificially increasing the surface correlation values for scenes in close proximity to water. To eliminate this problem, a simple water body mask on the 2120nm channel was used and these water contamination pixels were eliminated allowing for a much more homogeneous result. In validating the procedure, the correlation map over vegetation areas is consistent with values appropriate for vegetation dominated regions is shown.

Inter-comparisons of AOD between AERONET and MODIS processed using the regional surface model clearly show that the bias has been removed and if the water contamination is dealt with, there is only slight degradation in the retrieval even for spatial resolutions as high as 1.5km. As a demonstration, high spatial resolution AOD maps were retrieved for a case where the AOD is higher than the data used to derive the new VIS/SWIR ratios but small enough so that errors in the ground model are significant. In this case, the spatial distribution of aerosols was shown to be well approximated by a Gaussian distribution with much more accurate mean value then if the processing was done operationally. Most important, anomalously high AOD retrievals (i.e. hotspots) obtained using the Collection (5) algorithm due to significant underestimation of surface albedo were drastically reduced allowing for a much more accurate of aerosol loading within the city and thereby eliminating false EPA non attainment predictions.

In addition, complementary results for Mexico City urban area were obtained showing that the surface model obtained from NYC is quite similar. This is also in good agreement with surface albedo modeling obtained during the

MILARGO campaign. Ultimately, more urban cases should be explored to assess whether the VIS-SWIR albedo correlations and their relationship to the MVI parameters are more universal.

In addition, the MODIS AOD retrieval over highly vegetated area, Billerica Massachusetts is examined. The retrieved AOD result is within the MODIS land algorithm expected error bar. However, there is detectable error due to a poor MVI to VIS/SWIR relationship which we show can be somewhat compensated. Finally, error due to Lambertian surface assumption over BRDF surface is discussed. Clearly the magnitude of that error can be considered as the same amount of error due to STD variation in VIS/SWIR ratios.

Bibliography

Chapter 1

[1] NASA Earth Observatory http://earthobservatory.nasa.gov/

[2] NASA: TERRA(EOS AM-1) http://terra.nasa.gov/

[3] Intergovernmental Panel on Climate Change (IPCC), 2001 web site info at http://www.ipcc.ch/

[4] R. J. Charlson, S. E. Schwartz, J. M. Hales, R. D. Cess, J. A. Coakley Jr., J. E. Hansen, and D. J. Hofmann, "Climate forcing by anthropogenic aerosols", *Science* Vol. 255. no. 5043, pp. 423 – 430 (1992)

[5] Al-Saadi, J., J. Szykman, R. B. Pierce, C. Kittaka, D. Neil, D. A. Chu, L. Remer, L. Gumley, E. Prins, L.Weinstock, C. MacDonald, R. Wayland, F. Dimmick and J. Fishman. "Improving National Air Quality Forecasts with Satellite Aerosol Observations", Bull. Am. Met. Soc. 86, 1249-1261, (2005)

[6] Y. Liu, M. Franklin, R. Kahn, P. Koutrakis, "Using aerosol optical thickness to predict ground-level PM2.5 concentrations in the St. Louis area: A comparison between MISR and MODIS", Remote Sensing of Environment 107, 33-44 (.2007)

[7] Department of Environmental Conservation,"PM2.5 Monitoring" http://www.dec.ny.gov

[8] C. Kittaka, J. Szykman; B. Pierce; Al-Sadi, J.; D. Neil; A. Chu; L. Remer; E. Prins, and J. Holdzkom, "Utilizing MODIS satellite observations to monitor and analyze fine particulate matter, PM2.5, transport event**"**. Conference on Atmospheric Chemistry, 6th: Air Quality in Megacities, Seattle, WA, 11-15 January 2004 (preprints). Boston, MA, American Meteorological Society, Paper 1.3 , (2004)

[9] Doreen Neil, James J. Szykman, Jack Fishman, R. Bradley Pierce, Jassim A. Al-Saadi, Chieko Kittaka, "A good IDEA" (Infusing satellite Data into Environmental Applications), American Meteorological Society, 13the Conference on Satellite Meteorology, Society, Norfolk, VA Sept. 21, 2004.

[10] Levy, Robert C., Remer, Lorraine A., and Dubovik, Oleg " Global aerosol optical properties and application to Moderate Resolution Imaging Spectroradiometer aerosol retrieval over land", . *J. Geophys. Res*., 112, D13,210, 2007

[11] Holben, B.N., D. Tanre, A. Smirnov, et al., An emerging ground-based aerosol climatology: Aerosol optical depth from AERONET. *J. Geophys. Res.*, 106, 12,067- 12,097, 2001

[12] Level-2 MODIS atmosphere product,: http://modis-atmos.gsfc.nasa.gov

[13] Remer, L., A., R., Tanré, D., Kaufman, Y.,J., Levy, R., and Mattoo, S., "ALGORITHM FOR REMOTE SENSING OF TROPOSPHERIC AEROSOL FROM MODIS: Collection 005" ATBD document

[14] Kaufman, Y.J.; Tanre, D. "Algorithm for Remote Sensing of Tropospheric Aerosol from MODIS" Mod04 ATBD Document (1998)

[15] Castanho, A., A.D. de, Prinn, R., Martins, V., Herold, M., Ichoku, C. and Mollna, L. T., "Urban Visible/SWIR surface reflectance ratios from satellite and sun photometer measurements in Mexico City", Atmos. Chem. Phys, Discuss., 8113-8139, (2007)

[16] Levy, R. C., L. A. Remer, et al. (2005), Evaluation of the MODIS aerosol retrievals over ocean and land during CLAMS, *J. Atmos. Sci.,* 62(4), 974-992.

[17] Kaufman, Y. J. and C. Sendra,: 'Algorithm for atmospheric corrections', Int. J.Rem. Sens., 9 , 1357-1381 (1988)

[18] Kaufman, Y. J. and L. Remer: 'Remote Sensing of Vegetation in the mid-IR: the 3.75 µm channels', IEEE J. Geosc. and Rem. Sens. 32, 672-683 (1994)

[19] Martins, J., V., Tanre, D., Remer, L., Kaufman, Y.,J., Mattoo, S., Levy, R. , "MODIS cloud screening for remote sensing of aerosols over oceans using spatial variability "; Geophysical Research Letters .29, no.12 : MOD4-1-4, (2002)

[20] Kaufman, Y., J., Wald, A., E., Remer, L., A., Gao, B-C., Li, R-R., Flynn, L., "The MODIS 2.1- mu m channel-correlation with visible reflectance for use in remote sensing of aerosol"; IEEE Transactions on Geoscience and Remote Sensing 35 1286-98, (1997)

[21] Remer, L., A., Wald, A., E., Kaufman, Y., J., "Angular and seasonal variation of spectral surface reflectance ratios: implications for the remote sensing of aerosol over land" ; IEEE Transactions on Geoscience and Remote Sensing 39, 275-83, (2001)

[22] Wen, G., Tsay, S-C.; Calahan, R.F., Oreopoulos, L., "Path Radiance Technique for retrieving aerosol optical thickness over land", JGR 104 31321-31332 (1999).

[23] E. Drury, D. J. Jacob, J. Wang, R. J. D. Spurr, and K. Chance (2008), "Improved algorithm for MODIS satellite retrievals of aerosol optical depths over western North America", *J. Geophys. Res.*, 113, D16204, 2007JD009573

[24] A. Lyapustin and Y. Wang, "MAIAC: multi-angle implementation of atmospheric correction for MODIS" NASA, GFSC, ATBD (Feb, 2007)

Chapter 2

[1] Level-2 MODIS atmosphere product,: http://modis-atmos.gsfc.nasa.gov

[2] Holben, B.N., D. Tanre, A. Smirnov, et al., An emerging ground-based aerosol climatology: Aerosol optical depth from AERONET. *J. Geophys. Res.*, 106, 12,067- 12,097, 2001

[3] AERONET, Aerosol Robotic Network: http://aeronet.gsfc.nasa.gov/

[4] Kaufman, Y.,J., Tanre, D., "Algorithm for Remote Sensing of Tropospheric Aerosol from MODIS" Mod04 ATBD Document (1998)

[5] Levy, R. C., L. A. Remer, et al. (2004). "Effects of neglecting polarization on the MODIS aerosol retrieval over land." Ieee Transactions on Geoscience and Remote Sensing **42**(11): 2576-2583.

[6] Levy, R. C., L. A. Remer, et al. (2005). "Evaluation of the MODIS aerosol retrievals over ocean and land during CLAMS." Journal of the Atmospheric Sciences **62**(4): 974-992.

[7] Levy, R.C., L.A. Remer and O. Dubovik et al. (2006), Aerosol optical properties and lookup tables for the new MODIS aerosol retrieval over land,

[8] Levy, R.C., L.A. Remer, S. Mattoo, E. Vermote, Y.J. Kaufman, (2006), A new algorithm for retrieving aerosol properties over land from MODIS spectral reflectance, JGR.

[9] Remer, L., A., R., Tanré, D., Kaufman, Y.,J., Levy, R., and Mattoo, S., "ALGORITHM FOR REMOTE SENSING OF TROPOSPHERIC AEROSOL FROM MODIS: Collection 005" ATBD document

[9] Levy, Robert C., Remer, Lorraine A., and Dubovik, Oleg " Global aerosol optical properties and application to Moderate Resolution Imaging Spectroradiometer aerosol retrieval over land", . *J. Geophys. Res.*, 112, D13,210, 2007

[10] D'Almeida, G., P. Koepke, and E. P. Shettle, 1991: Atmospheric aerosols-global climatology and radiative characteristics. A Deepak ISBN 0-937194-22-0

[11] Gross, B., Ogunwuyi, O., Moshary, F., Ahmed, S.; Cairns, B. “Aerosol retrieval over urban areas using spatial regression between VIS/NIR and MIR Hyperion channels” Remote Sensing of Atmospheric Aerosols, IEEE Workshop, 43- 50 (2005)

Chapter 3

[1] Kaufman, Y.,J., Tanre, D., “Algorithm for Remote Sensing of Tropospheric Aerosol from MODIS” Mod04 ATBD Document (1998)

[2] Remer, L., A., R., Tanré, D., Kaufman, Y.,J., Levy, R., and Mattoo, S., “ALGORITHM FOR REMOTE SENSING OF TROPOSPHERIC AEROSOL FROM MODIS: Collection 005” ATBD document

[3] R. C. Levy, L. A. Remer, and Y. J. Kaufman “Effects of Neglecting Polarization on the MODIS Aerosol Retrieval Over Land” *IEEE Trans. Geos. Rem. Sens.,* vol 42 Pp 2576-2583, 2004

[4] Kaufman, Y., J., Wald, A., E., Remer, L., A., Gao, B-C., Li, R-R., Flynn, L., "The MODIS 2.1- mu m channel-correlation with visible reflectance for use in remote sensing of aerosol"; IEEE Transactions on Geoscience and Remote Sensing 35 1286-98, (1997)

[5] Gross, B., Ogunwuyi, O., Moshary, F., Ahmed, S.; Cairns, B. “Aerosol retrieval over urban areas using spatial regression between VIS/NIR and MIR Hyperion channels” Remote Sensing of Atmospheric Aerosols, IEEE Workshop, 43- 50 (2005)

[6] Castanho, A., A.D. de, Prinn, R., Martins, V., Herold, M., Ichoku, C. and Mollna, L. T., “Urban Visible/SWIR surface reflectance ratios from satellite and sun photometer measurements in Mexico City”, Atmos. Chem. Phys, Discuss., 7, 8113-8139, (2007)

[7] S. Platnick, M.D. King, S.A. Ackerman, W.P. Menzel, B.A Baum, J.C Riedi, R.A Frey, R.A. ,“The MODIS cloud products: algorithms and examples from Terra”, *IEEE Trans Geos. Rem. Sens.*, Vol 41, pp 459- 473, (2003)

[8] S. A. Ackerman, R. E. Holz, R. Frey, E. W. Eloranta, B. C. Maddux, and M. McGill “Cloud Detection with MODIS. Part II: Validation”, Journal of Atmospheric and Oceanic Technology, Volume 25, Issue 7 (July 2008)

[9] Wiscombe, W. J. (1981). "Improved Mie scattering algorithms." Appl. Opt. **19**: 1505-1509.

[10] Dubovik, O., B. Holben, et al. (2002). "Variability of absorption and optical properties of key aerosol types observed in worldwide locations." Journal of the Atmospheric Sciences **59**(3): 590-608.

[11] Dubovik, O., B. N. Holben, et al. (2002). "Non-spherical aerosol retrieval method employing light scattering by spheroids." Geophysical Research Letters **29**(10): art. no.-1415.

[12] Dubovik, O. and M. D. King (2000). "A flexible inversion algorithm for retrieval of aerosol optical properties from Sun and sky radiance measurements." Journal of Geophysical Research-Atmospheres **105**(D16): 20673-20696.

[13] Evans, K.F. and G. L. Stephens, 1991, A New Polarized Atmospheric Radiative Transfer Model, *J. Quant. Spectrosc. Radiat. Transfer,* **46**(5):413-423

Chapter 4

[1] Kaufman, Y.J.; Tanre, D. “Algorithm for Remote Sensing of Tropospheric Aerosol from MODIS” Mod04 ATBD Document (1998)

[2] L. A. Remer, D. Tanré, Y. J. Kaufman, R. Levy, and S. Mattoo, “ALGORITHM FOR REMOTE SENSING OF TROPOSPHERIC AEROSOL FROM MODIS: Collection 005” ATBD document

[4] Levy, R. C., L. A. Remer, et al. (2005). "Evaluation of the MODIS aerosol retrievals over ocean and land during CLAMS." Journal of the Atmospheric Sciences **62**(4): 974-992.

[4] R. C. Levy, L. A. Remer, and Y. J. Kaufman “Effects of Neglecting Polarization on the MODIS Aerosol Retrieval Over Land” *IEEE Trans. Geos. Rem. Sens.,* vol 42 Pp 2576-2583, 2004

Chapter 5

[1] R. C. Levy, L. A. Remer, and Y. J. Kaufman “Effects of Neglecting Polarization on the MODIS Aerosol Retrieval Over Land” *IEEE Trans. Geos. Rem. Sens.,* vol 42 Pp 2576-2583, 2004

[2] L. A. Remer, D. Tanré, Y. J. Kaufman, R. Levy, and S. Mattoo, “ALGORITHM FOR REMOTE SENSING OF TROPOSPHERIC AEROSOL FROM MODIS: Collection 005” ATBD document

[3] A. Lyapustin and Y. Wang, “MAIAC: multi-angle implementation of atmospheric correction for MODIS” NASA, GFSC, ATBD (Feb, 2007)

[4] Sensing of Vegetation: Reflectance spectra of ground vegetation, http://www.aai.ee/bgf/

[5] Levy, R. C., L. A. Remer, et al. (2005) "Evaluation of the MODIS aerosol retrievals over ocean and land during CLAMS." Journal of the Atmospheric Sciences **62**(4): 974-992.

Chapter 6

[1] Ross, J.K. (1981). *The radiation regime and architecture of plant stands*. Dr W Junk, The Hague, **ISBN-13:** 978-9061936077

[2] Roujean, J.L., Latoy, M. and Deschamps, P.Y. (1992). A bidirectional reflectance model of the earth's surface for the correction of remote sensing data. *J. Geophys. Res*., 97, 20455-20468.

[3]Wanner, W., X. Li, and A. H. Strahler (1995). On the derivation of kernels for kernel-driven models of bidirectional reflectance, *J. Geophys. Res*., 21077-21090

[4] Strahler A. H., J.-P. Muller, MODIS Science Team Members, MODIS BRDF/Albedo Product: Algorithm Theoretical Basis Document, Version 5.0 , MODIS Product ID: MOD43, April 1999

[5] A. I. Lyapustin, "Radiative transfer code SHARM for atmospheric and terrestrial applications," Appl. Opt. **44**, 7764-7772 (2005)

[6] Lyapustin, A. I., and T. Z. Muldashev, Method of spherical harmonics in the radiative transfer problem with non-Lambertian surface, *J. Quant. Spectrosc. Radiat. Transfer,* **61** (4), 545-555, 1999.

[7] Muldashev, T. Z., A. I. Lyapustin, and U. M. Sultangazin, Spherical harmonics method in the problem of radiative transfer in the atmosphere-surface system, *J. Quant. Spectrosc. Radiat. Transfer,* **61** (3), 393-404,
1998.

[8] Marshak, R. E., Note on the spherical harmonics method as applied to the Milne problem for a sphere, *Phys.Rev*., **71**, 443-446, 1947

PUBLICATIONS AND PRESENTATION:

1. Min M. Oo, M. Vargas, A. Gilerson, B. Gross, F. Moshary, and S. Ahmed, "Improving atmospheric correction for highly productive coastal waters using the short wave infrared retrieval algorithm with water-leaving reflectance constraints at 412 nm," Appl. Opt. 47, 3846-3859 (2008)

2. Min M. Oo, Eduardo Hernandez, Matthias Jerg, Barry M. Gross, Fred Moshary and Samir A. Ahmed "High-resolution surface correlation maps for improved resolution and retrieval of aerosols over urban scenes", SPIE EURO Remote Sensing (ERS08 Symposium), 2008

3. Min M. Oo, Matthias Jerg, Eduardo Hernandez, Julia He, Barry M. Gross Fred Moshary, Samir Ahmed "Aerosol retrieval and improved surface albedo over urban scenes using combine MODIS and sunphotometer measurement" Proceedings of IGARSS conference. July 6-11, 2008 | Boston, Massachusetts, U.S.A.

4. Min M. Oo, Eduardo Hernandez, Matthias Jerg, Barry M. Gross ,Fred Moshary and Samir A. Ahmed, "Improved MODIS Aerosol Retrieval Using Modified VIS/MIR Surface Albedo Ratio Over Urban Scenes" CoRP Science Symposium,August 12 - 13, 2008,Corvallis, OR

5. Min M. Oo, Eduardo Hernandez, Matthias Jerg, Barry M. Gross, Fred Moshary, and Samir A. Ahmed," Improved MODIS aerosol retrieval over urban scenes" Processing of. SPIE 6684, 66840Q (2007)

6. Min M. Oo, Eduardo Hernandez, Matthias Jerg, Barry M. Gross, Fred Moshary and Samir A. Ahmed "Improved MODIS Aerosol Retrieval Using Modified VIS/SWIR Surface Albedo Ratio Over Urban Scenes", *IEEE Trans Geos. Rem. Sens* (*submitted*)

7. Min M. Oo, Barry Gross, Fred Moshary and Sam Ahmed "The Effect of Calibration of Uncertainties on Cloud Height Retrievals from HIRS" NOAA/NESDIS Co-Operative Research Program, 2nd Annual Science Symposium, University of Wisconsin- Madison, Wisconsin. July 13-14, 2005

8. Min Min Oo, Barry Gross, Fred Moshary and Sam Ahmed "The Effect of SpectralUncertainty on Cloud Height Retrievals within the CO2 Slicing Method",National Einstein Conference, the City College of New York, April 11-12, 2005:

9. Barry Gross, Min Min Oo and Changyang Cao "The Effect of HIRS Spectral Uncertainty on Cloud Retrievals with CO2 Slicing", 2004 CALCON Technical Conference Logan Utah (Aug 2004).

10. Y. Hassebo, B. Gross, M. Oo, F. Moshary, and S. Ahmed “Polarization-discrimination technique to maximize the lidar signal-to-noise ratio for daylight operations”, Applied Optics, 45, No 22, pp. 5521-5531 (2006)

11. A Gilerson, .J Zhou, M. Oo, J. Chowdhary, B. Gross, F. Moshary, and S. Ahmed “Retrieval of fluorescence from reflectance spectra of algae in sea water through polarization discrimination: modeling and experiments”, Applied Optics, 45, No 22, pp. 5568-5581 (2006)

12. A Gilerson, J. Zhou, M. Oo, B. Gross, S. Ahmed, F. Moshary “Comparison of fluorescence retrieval algorithms using radiative transfer simulations and field measurements”. Proceedings of IGARSS conference. Denver, CO, July 31 – August 4 2006

13. A. Gilerson, M. Oo, J. Chowdhary, B. M. Gross, F. Moshary, S. A. Ahmed. “Polarization discrimination fluorescence retrieval from reflectance spectra of algae in seawater: comparison of multi-component Mie scattering and polarized radiative transfer models with laboratory and field tests”. Proceedings of SPIE, v.5977, September 2005, Bruges, Belgium

14. A. Gilerson, M. Oo, J. Chowdhary, B. M. Gross, F. Moshary, S. A. Ahmed. “Polarization characteristics of water-leaving radiance: application to separation of fluorescence and scattering components in coastal waters”. Proceedings of SPIE, v.5885, August 2005, San Diego